UNIVERSITY OF CALIFORNIA,
IRVINE

Passive Imaging of a Spherical Inclusion by Elastic Waves

DISSERTATION

submitted in partial satisfaction of the requirements
for the degree of

DOCTOR OF PHILOSOPHY

in Mathematics

by

Lingxiao Zhang

Dissertation Committee:
Professor Knut Sølna, Chair
Professor Hongkai Zhao
Professor Long Chen

2016

Dedication

To my father Shaohua Zhang, my mother Jing Zhao and my husband Penghang Yin.

Table of Contents

List of Figures

List of Tables

Acknowledgments

I would like to express my gratitude to Professor Knut Sølna. Your guidance and assistance on both my research and career was invaluable. I am especially grateful to you for introducing me to the field of inverse problems and providing me with opportunities to be exposed to this sector. Your patience and commitment as an advisor makes you a great mentor. Without your supervision and constant help, this dissertation would not have been possible.

A special thanks to my committee members Professor Hongkai Zhao and Professor Long Chen. I have learned a lot from Professor Zhao when I was teaching assistant of the probability class. In addition, I have learnt so much from Professor Chen's computational PDE course. My deepest appreciation goes to all my teachers, instructors and faculty members at University of California Irvine. You have either provided me with the knowledge and skills or other necessary supports to make this dissertation happen.

I would like to thank Penghang Yin and Xiaolong Long for your helpful discussions on my research project, and all my classmates and friends in the University. You have made my Ph.D. study productive and life colorful.

I am indebted to University of California Irvine for its generous offer of scholarship in the past five years. My dissertation would not exist without its full support.

Last but not least, my gratitude goes to my parents whose selfless support and understanding are always an encouragement to my efforts to make progress in this dissertation writing and my overall life.

Curriculum Vitae

Lingxiao Zhang

B.S. in Applied Mathematics, University of Science and Technology of China, 2010

M.S. in Statistics, University of California, Irvine, 2014

Ph.D. in Applied Mathematics, University of California, Irvine, 2016

Abstract of the Dissertation

Passive Imaging of a Spherical Inclusion by Elastic Waves

By

Lingxiao Zhang

Doctor of Philosophy in Mathematics

University of California, Irvine, 2016

Professor Knut Sølna, Chair

A method is proposed to detect and estimate the location of the spherical inclusion in the homogeneous isotopic elastic medium. The signals are emitted by ambient noise sources and recorded by a sensor array. The vector nature of elastic waves is exploited to find a proper imaging function to detect and locate the inclusion. We consider imaging of a spherical inclusion using seismic wave recordings.

Chapter 1

Introduction

Imaging with waves involves probing an unknown medium with waves and information from reflection. These waves can be acoustic, elastic or electro-magnetic. They can be generated by controlled sources or by unknown ambient noise sources. They are recorded by a set of sensors. Sensor imaging usually involves two steps. The first step is experimental, it consists in recording the waves generated by sources on a sensor array. The second step is numerical, it consists in processing the recorded data in order to estimate some relevant featrues of the medium. In [3, 4, 27], the analysis of passive imaging was proposed.

The theory of wave scattering, as developed in the fields of optics and acoustics, has been adapted to the case of elasitc waves. The full treatment of elastic wave scattering is not a simple task, and most seismological studies have employed various approximations in their use of scattering theory. One method of checking the validity of the approximations is to compare them with exact analytical solutions. In our study, we consider a spherical inclusion and exploit the explicit results available for the scattering off of such an object. The theory of wave scattering, as developed in the fields of optics and acoustics, has been adapted to the case of elasitc waves. The treatment of the canonical scattering problem for the spherical inclusion has a long history. Light scattering was analyzed in [18] in terms of a series of spherical harmonics, and a comprehensive discussion of this topic can be found in [19]. Elastic scattering by spherical obstacles has also been the subject of many publications [20, 21, 22, 23, 24]. Our study follows displacement approach in [23, 24]. Details of the analytical and numerical aspects of the scattering problem for P waves incident upon a

spherical inclusion can be found in [25, 26].

In our study, we consider the problem with an source that generate signals and the waves are recorded at the surface by the receivers. Then the recorded signals are time-reversed and sent back into the medium. There will be strong correlation between S waves and P waves around the inclusion. As a result, we can make use of the cross correlation between P waves and S waves to find the imaging function and then locate the inclusion. The idea of using the cross correlation of noisy signals to retrieve information was first proposed in helioseismology and seismology [6, 7, 8]. This idea has been widely applied to background velocity estimation from regional to local scales [9, 11, 10], petroleum prospecting [15], and volcano monitoring [12, 14, 13]. In [16], correlation methods for imaging in randomly layered media are analyzed. When the support of the random noise sources extends over all space and they are uncorrelated, [17] shows that the derivative of the cross correlation of the recorded signals is the symmetrized Greens function between the sensors.

The rest of the dissertation is structured as follows. In Chapter 2, we provide a reference on the important concepts, definitions and theories that we used in our work. In Chapter 3, we discussed the model configuration and imaging functions in different cases. In Chapter 4, we presented the resolution analysis with respect to different imaging functions in different cases. In Chapter 5, we analyzed the stability of imaging functions. In Chapter 6, we presented numerical results of all the cases in the previous chapters. In Chapter 7, we summarized our results in tables.

Chapter 2

Basic Definitions and Theories

In this chapter, we will discuss the basic definitions and theories that used through this work.

2.1 The Elastic Waves

Elastodynamics is the study of elastic waves and involves linear elasticity with variation in time. An elastic wave is a type of mechanical wave that propagates in elastic or viscoelastic materials. The elasticity of the material provides the restoring force of the wave. When they occur in the Earth as the result of an earthquake or other disturbance, elastic waves are usually called seismic waves.

P-wave is a type of elastic wave, called seismic waves in seismology, that can travel through a continuum. The continuum is made up of gases, liquids, or solids, including the Earth. P-waves can be produced by earthquakes and recorded by seismographs. The name P-wave is often said to stand either for primary wave, as it has the highest velocity and is therefore the first to be recorded; or pressure wave, as it is formed from alternating compressions and rarefactions. In isotropic and homogeneous solids, the mode of propagation of a P-wave is always longitudinal; thus, the particles in the solid have vibrations along or parallel to the travel direction of the wave energy.

S-wave is a type of elastic wave, called secondary wave, or shear wave, which is one of the two main types of elastic body waves, so named because they move through the body of an object, unlike surface waves. The S-wave moves as a shear or transverse wave, so motion is

perpendicular to the direction of wave propagation. The wave moves through elastic media, and the main restoring force comes from shear effects.

In our study, we will use the properties of P-waves and S-waves to find the imaging function, and then find the location of the inclusion.

2.2 The Elastic Wave Equation

The displacement field u must satisfy the equations of motion for a homogeneous isotropic elastic medium. Here, the displacement is the shortest distance from the initial to the final position of a point, and the displacement field is also called the vector field. The elastic wave equation (Appendix A) is as below:

$$\rho u_{tt} - \delta_{\lambda,\mu} = f(t,x)$$
$$\delta_{\lambda,\mu} = (\lambda+\mu)\nabla(\nabla\cdot u) + \mu\Delta u$$

where ρ is the density; u is the displacement fro the wave; $f(t,x)$ denotes the source term, and also we can treat it as the body force; λ,μ are Lame parameters: λ is also called Lame's first parameter and μ is the shear modulus or Lame's second parameter. In homogeneous and isotropic materials, Lame's parameters define Hooke's law in 3D: $\sigma = 2\mu\epsilon + \lambda tr(\epsilon)I$, where σ is the stress, ϵ the strain tensor, I the identity matrix and $tr(\cdot)$ the trace function.The two parameters together constitute a parameterization of the elastic moduli for homogeneous isotropic media.

Also, we can use the following Momentum equation (Appendix A.1) :

$$\rho\frac{\partial^2 u_i}{\partial t^2} = \frac{\partial \tau_{ij}}{\partial x_j} + f_i,$$

where the stress tensor τ_{ij} is the Cauchy stress tensor which is a second order tensor of a linear map with nine components τ_{ij} that completely define the state of stress at a point inside a material in the deformed placement or configuration. The tensor relates a unit-length direction vector $\mathbf{n}$ to the stress vector $\mathbf{T}^{(\mathbf{n})}$ across an imaginary surface perpendicular to $\mathbf{n}$ as Figure **??** in Appendix:

$$\tau = \begin{bmatrix} \tau_{11} & \tau_{12} & \tau_{13} \\ \tau_{21} & \tau_{22} & \tau_{23} \\ \tau_{31} & \tau_{32} & \tau_{33} \end{bmatrix} = \begin{bmatrix} \tau_{xx} & \tau_{xy} & \tau_{xz} \\ \tau_{yx} & \tau_{yy} & \tau_{yz} \\ \tau_{zx} & \tau_{zy} & \tau_{zz} \end{bmatrix}.$$

In isotropic medium, the linear stress-strain relaionship (Appendix A.2):

$$\tau_{ij} = \lambda \frac{\partial u_k}{\partial x_k} \delta_{ij} + \mu (\frac{\partial u_i}{\partial x_j} + \frac{\partial u_j}{\partial x_i}),$$

then it becomes

$$\rho \frac{\partial^2 u_i}{\partial t^2} = \frac{\partial}{\partial x_i}(\lambda div\ u) + \frac{\partial}{\partial x_i}(\mu \frac{\partial u_i}{\partial x_j} + \mu \frac{\partial u_j}{\partial x_i}).$$

Assume that p is the pressure, and ϵ_{kl} is a part of stess tensor, that is the second term of τ_{kl}, then:

$$\begin{aligned} p &= \lambda \nabla u \\ \varepsilon_{kl} &= \mu (\frac{\partial u_l}{\partial x_k} + \frac{\partial u_k}{\partial x_l}). \end{aligned}$$

Plugging in the stress tensor τ_{kl}, then:

$$\begin{aligned} \tau_{kl} &= p(t,x)\delta_{kl} + \varepsilon_{kl} \\ \epsilon_k &= \frac{\partial u_k}{\partial t}. \end{aligned}$$

Thus, we have a symmetric hyperbolic problem for $(\epsilon_i, \varepsilon_{ij}, p)$, here, $i, j = 1, 2, 3$ and it is a 10 dimesional system.

2.3 The Cross Correlation

In our study, we consider the problem with an source that generate signals and the waves are recorded at the surface by the receivers. Then the recorded signals are time-reversed and sent back into the medium. There will be strong correlation between S waves and P waves

around the inclusion. As a result, we can make use of the cross correlation between P waves and S waves to find the imaging function and then locate the inclusion.

In signal processing, cross-correlation is a measure of similarity of two waveforms as a function of a time-lag applied to one of them. This is also known as a sliding dot product or sliding inner-product. It is commonly used for searching a long signal for a shorter, known feature.

For continuous functions f and g, we define the cross-correlation by:

$$(f * g)(\tau) \stackrel{\text{def}}{=} \frac{1}{T} \int_{-\frac{T}{2}}^{\frac{T}{2}} \bar{f}(t)\ g(t+\tau)\, dt,$$

where $\bar{f}$ denotes the complex conjugate of f and τ is the time lag; T denotes the period that the correlation exists.

In our study, we assume that $u(t, \mathbf{x}_1)$ and $u(t, \mathbf{x}_2)$ denote the time- dependent wave fields recorded by two sensors at $\mathbf{x}_1$ and $\mathbf{x}_2$. Their cross correlation function over the time interval $[0, T]$ with time lag τ is given by:

$$C_T(\tau, \mathbf{x}_1, \mathbf{x}_2) = \frac{1}{T} \int_0^T u(t, \mathbf{x}_1) u(t+\tau, \mathbf{x}_2) dt.$$

In a homogeneous medium, if the source of the waves is a space-time stationary random field that is also delta correlated in space and time, it has been shown that

$$\frac{\partial}{\partial \tau} C_T(\tau, \mathbf{x}_1, \mathbf{x}_2) \sim -[G(\tau, \mathbf{x}_1, \mathbf{x}_2) - G(-\tau, \mathbf{x}_1, \mathbf{x}_2)],$$

where G is the Green's function. This approximate equality holds for T sufficiently large and provided some limiting absorption is introduced to regularize the integral. The main point here is that the time-symmetrized Green's function can be obtained from the cross correlation if there is enough source diversity. In this case the wave field at any sensor is equipartitioned, in the sense that it is a superposition of uncorrelated plane waves of all directions. We can recover in particular the travel time $\tau(\mathbf{x}_1, \mathbf{x}_2)$ from the singular support of the cross correlation.

Chapter 3

Passive Imaging

Consider a two-part isotropic medium(as Figure 3.1) consisting of a spherically symmetric inclusion V_1(part $\nu = 1$) with radius $r = R$ having elastic parameters λ_1, μ_1 and density ρ_1 which is embedded in a homogeneous elastic surrounding medium (part $\nu = 2$) having elastic parameters λ_2, μ_2 and density ρ_2. The inclusion V_1 may contain a number of internal shells which are bounded by spherical interfaces where the material properties or their spatial derivatives are radially discontinuous. Also, P waves and S waves pass through V_1 with different velocities. The boundary conditions on such interfaces as well as those at the surface $r = R$ are linear and homogeneous. Here, homogeneity and heterogeneity are concepts relating to the uniformity in a substance. A material that is homogeneous is uniform in composition or character; one that is heterogeneous is distinctly nonuniform in one of these qualities.

We assume that all elastic displacement fields under consideration have harmonic time dependence of the form $e^{i\omega t}$ where ω is the angular frequency. Joint Cartesian $\{x, y, z\}$ and spherical $\{r, \theta, \phi\}$ coordinate systems with the origin at the center of the inclusion will be used.

Incident from medium $\nu = 2$ is a harmonic disturbance with a displacement field given by

$$\tilde{U_0} = U_0(x, y, z)e^{i\omega t}.$$

The interaction of this incident wave with the inclusion gives rise to additional displacement

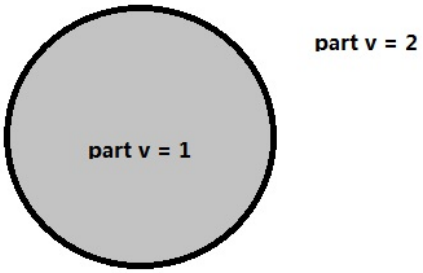

Figure 3.1: The Medium with Inclusion

fields both inside and outside the inclusion, and these are denoted by

$$U_\nu = U_\nu(x, y, z). \ (\nu = 1, 2)$$

Since we will be primarily interested in the properties of the additional disturbance outside the inclusion, this field with subscript 2 will be referred to as the scattered field $U_{sc} = U_2$. Thus, the total field U in the outer medium $\nu = 2$ is a sum of the incident wave and scattered field

$$U = U_0 + U_{sc}.$$

The field U, as well as both of its individual components, must satisfy the equation of motion for a homogeneous isotropic elastic medium:

$$(\lambda + \mu)\nabla(\nabla \cdot U) + \mu\Delta U + \rho\omega^2 U = 0.$$

We denote the velocities of the compressional and shear waves and their ratio by

$$v_p^{(\nu)} = \sqrt{\frac{\lambda_\nu + 2\mu_\nu}{\rho_\nu}}, \ v_s^{(\nu)} = \sqrt{\frac{\mu_\nu}{\rho_\nu}},$$

with the understanding that no superscript implies the surrounding medium, $v_p = v_p^{(2)}$,

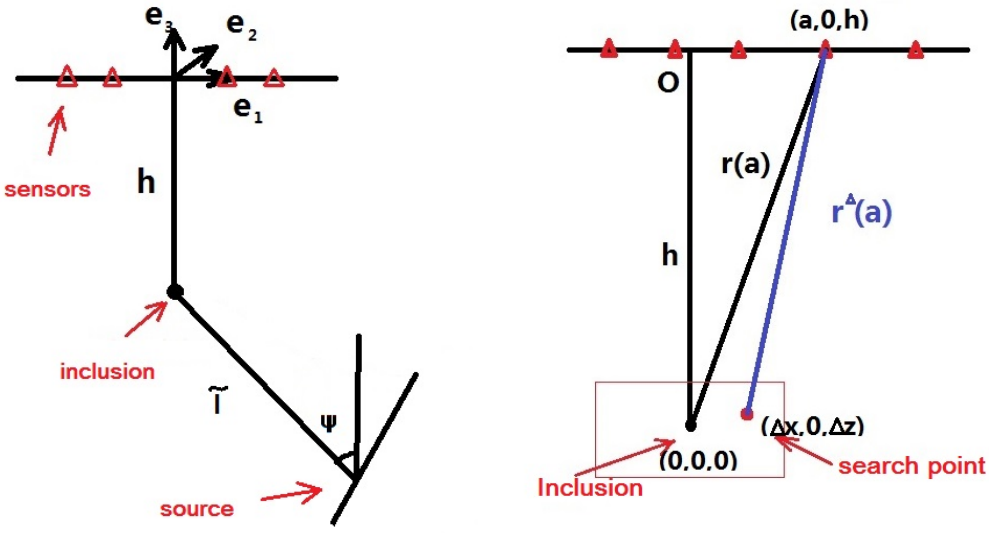

(a)Wave Propagation (b): Search Point

Figure 3.2: The Model Configuration

$v_s = v_s^{(2)}$. We require that the scattered field satisfy a radiation condition at large distances from the inclusion

$$U_{sc} \approx \frac{A_p(\theta,\phi)}{r} e^{-ik_p r} + \frac{A_s(\theta,\phi)}{r} e^{-ik_s r}, \ r \to \infty,$$

where the wavenumber $k_p = \omega/v_p^{(2)}$ and $k_s = \omega/v_s^{(2)}$. The functions $A_p(\theta,\phi)$ and $A_s(\theta,\phi)$ will be referred to as scattering diagrams of compressional and shear waves, respectly. The above formula shows that the sources must be sources, not sinks of energy; the energy which is radiated from the sources must scatter to infinity; no energy may be radiated from infinity into the field.

Figure 3.2(a) shows our model: There are several receivers on the x-axis. The inclusion with radius of R is in the homogeneous isotopic elastic medium. The source plane wave propagates in the direction $\vec{\mu}$. Our goal is to detect and estimate the location of the spherically symmetric inclusion by using the recorded data from receivers.

3.1 Modeling of the Source

We assume that the source field is:

$$\mathbf{U}_0 = e^{-ik_p(\vec{x}\cdot\vec{\mu}-l_0)}\hat{v}(\omega)\vec{\mu},$$

where $k_p = \omega/c_p$, and $\vec{\mu} = (-\sin(\phi), 0, \cos(\phi))$. Here, $v(t)$ is a stationary stochastic process. In our study, we suppose that $v(t) \sim N(0, C(0))$, where $C(h) = cov(v(t), v(t+h))$, with $C(\cdot)$ satisfies:$C(0) \geq 0$;$|C(h)| \leq C(0)$; $C(h) = C(-h)$. Actually, the harmonic disturbance of displacement field is:

$$\tilde{\mathbf{U}}_0 = \mathbf{U}_0 e^{i\omega t}.$$

3.2 Conversion at the Scatterer

From [2], scattering of an arbitrary elastic wave incident upon a spherically symmetric inclusion is considered and solutions are developed in terms of the spherical vector system of Petrashen, which produces results in terms of displacements rather than displacement potentials and in a form suitable for accurate numerical computations.

The two components of the scattered field $\mathbf{U}_P^P$ and $\mathbf{U}_S^P$ in the spherical $\{\hat{r}, \hat{\theta}, \hat{\phi}\}$ coordinate system are as below:

$$\mathbf{U}_P^P = A\left\{-\frac{1}{2}\frac{\frac{3}{2}(\lambda_1-\lambda_2)+\mu_1-\mu_2}{\frac{1}{2}(\frac{3}{2}\lambda_1+\mu_1)+\mu_2} + (\frac{\rho_1}{\rho_2}-1)\cos\phi + \frac{2}{3}(\frac{\mu_1}{\mu_2}-1)\frac{\gamma^2}{D}(1-3\cos^2\phi)\right\}\hat{r} \tag{3.1}$$

$$\mathbf{U}_S^P = B\left\{-(\frac{\rho_1}{\rho_2}-1)\sin\phi + (\frac{\mu_1}{\mu_2}-1)\frac{\gamma}{D}\sin 2\phi\right\}\hat{\theta}. \tag{3.2}$$

Here,

$$\begin{aligned} A =& k_p^2\frac{V}{4\pi h}e^{-ik_p(r+\tilde{l})}\hat{v}(\omega),\ B = k_s^2\frac{V}{4\pi h}e^{-i(k_s r+\tilde{l}k_p)}\hat{v}(\omega), \\ V =& \frac{4}{3}\pi R^3, D = 1+\frac{2}{15}(\frac{\mu_1}{\mu_2}-1)(3+2\gamma^2), \end{aligned}$$

where $\hat{v}(\omega)$ is the Fourier transform of the source term; R is the radius of the inclusion; V is

the volume of the inclusion; k_p and k_s are wave numbers for P waves and S waves: $k_p = \frac{\omega}{v_p}$ and $k_s = \frac{\omega}{v_s}$; $\tilde{l}$ is the distance between the source and the inclusion; r is the distance between the inclusion and the receiver; γ denotes the ratio of the velocity of P waves and the velocity of S waves, that is, $\gamma = \frac{v_s}{v_p} = \sqrt{\frac{\mu}{\lambda+2\mu}}$.

In the following sections, we will make use of the above equations to represent the scattering P waves and S waves, and show the correlation between them.

3.3 Imaging Function

In this section, we presented imaging functions for different cases with respect to different assumptions.

Before presenting imaging functions, we simplified the scattering components under some assumptions. The observed data $\mathbf{U} = \mathbf{U}_0 + \mathbf{U}_{sc}$, where $\mathbf{U}_{sc} = \mathbf{U}_P^P + \mathbf{U}_S^P$. See Figure 3.2(b), suppose that the coordinates of the inclusion is $(0, 0, 0)$, the coordinates of the search point is $(\Delta x, 0, \Delta z)$ and the coordinates of the receiver is $(a, 0, h)$. Under the scaling assumption: $a \ll h$, we can have the following approximation, and also, $a, \Delta x, \Delta z \ll 1$. Then the distance between inclusion and the receiver is:

$$r(a) = \sqrt{h^2 + a^2} \sim h + \frac{a^2}{2h},$$

where $a \in [-\frac{A}{2}, \frac{A}{2}]$. In Figure 3.2(b), suppose that the coordinates of the inclusion is $(0, 0, 0)$, the coordinates of the search point is $(\Delta x, 0, \Delta z)$ and the coordinates of the receiver is $(a, 0, h)$. Then the distance between inclusion and the receiver is:

$$r(a) = \sqrt{h^2 + a^2} \sim h + \frac{a^2}{2h}, \tag{3.3}$$

where $a \in [-\frac{A}{2}, \frac{A}{2}]$. In Figure 3.2(b), there is a search region which contains the location of

the inclusion. The distance between the search point and the receiver is defined as:

$$\begin{aligned} r^{\Delta}(a) = \sqrt{(h-\Delta z)^2 + (a-\Delta x)^2} &\sim (h-\Delta z) + (a-\Delta x)^2/2(h-\Delta z) \\ &\sim (h-\Delta z) + a^2/2h - a\Delta x/h + a^2\Delta z/2h^2 \\ &+ O(\Delta x^2, a\Delta x\Delta z, a^2\Delta z^2). \end{aligned}$$

Thus, by (3.3) we can approximately rewrite (3.1) and (3.2) into:

$$\begin{aligned} \mathbf{U}_P^P &\sim \omega^2 C_1(\phi) e^{-ik_p(\tilde{l}+h+\frac{a^2}{2h})} \hat{v}(\omega)\vec{e_3}, \\ \mathbf{U}_P^S &\sim \omega^2 C_2(\phi) e^{-ik_s(h+\frac{a^2}{2h})-ik_p\tilde{l}} \hat{v}(\omega)\vec{e_1}, \end{aligned} \tag{3.4}$$

where $C_i(\phi)$ are constant terms related to ϕ as below:

$$\begin{aligned} C_1(\phi) &= \frac{R^3}{3hv_p^2}\left\{-\frac{1}{2}\frac{\frac{3}{2}(\lambda_1-\lambda_2)+\mu_1-\mu_2}{\frac{1}{2}(\frac{3}{2}\lambda_1+\mu_1)+\mu_2} + (\frac{\rho_1}{\rho_2}-1)\cos\phi + \frac{2}{3}(\frac{\mu_1}{\mu_2}-1)\frac{\gamma^2}{D}(1-3\cos^2\phi)\right\} \\ C_2(\phi) &= \frac{R^3}{3hv_s^2}\left\{-(\frac{\rho_1}{\rho_2}-1)\sin\phi + (\frac{\mu_1}{\mu_2}-1)\frac{\gamma}{D}\sin 2\phi\right\}. \end{aligned}$$

In the following sections, we will utilize (3.4) to represent the scattering P waves and the scattering S waves, and they are important components in imaging functions.

3.3.1 With Known Sources

In Known Source Case, we suppose that the location and the properties of the source are known, then we can get the imaging function by computing the correlation between incident waves and the backpropagated scattering waves. In this section, there are two subsections: With One Sensor; With Many Sensors.

With One Sensor

Suppose we have one sensor only, then the incident waves (we consider P waves only) propagate to the inclusion and then are scattered by the inclusion, later, we receive the scattering P waves and S waves at the sensor. After that, we backpropagate the received signals, then

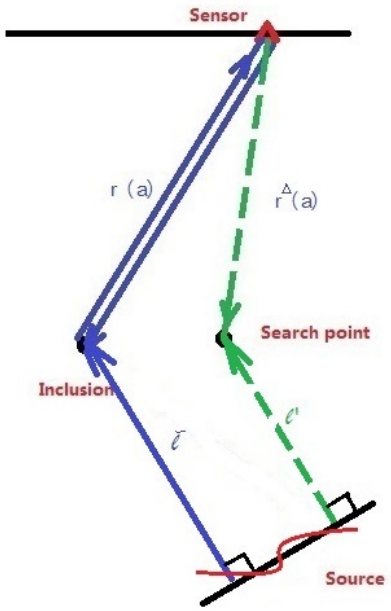

Figure 3.3: The Configuration for One Sensor

we should get the maximal correlation at inclusion, not other search points. Figure 4.5 shows the model configuration for this special case. In Figure 3.4, we compare the signals with received data at inclusion, at sensors and backpropagated scattering waves. The red line denotes the signal, and the blue line denotes the incident waves at inclusion in Figure 3.4a; the blue line denotes the received data at sensors in Figure 3.4b; the blue line denotes the backpropagated scattering waves at the search point in Figure 3.4c. To amplify the details in Figure 3.4, we can find the curve for scattering waves is the curve for soruce signals with several units of shift. See Figure 3.5.

Assume that $v(t)$ denotes the source signals, then $v(t+\frac{\tilde{l}}{c_p})$ denotes the incident waves at inclusion, where $\tilde{l}$ is the distance between the source and the inclusion. We can find that it is a time-lag beween the source signals and the incident waves at inclusion (Figure 3.5a). Similary,$v(t+\frac{l'}{c_p})$ denotes the incident waves at search point, where l' is the distance between the source and the search point. $v(t+\frac{\tilde{l}}{c_p}+\frac{r(a)}{c_p})$ denotes the received P component scattering waves at sensor (Figure 3.5b), where $r(a)$ is the distance between inclusion and the sensor. Also, $v(t+\frac{\tilde{l}}{c_p}+\frac{r(a)}{c_p}-\frac{r^{\Delta}(a)}{c_p})$ denotes the backpropagated scattering P waves at search point, where $r^{\Delta}(a)$ is the distance between the search point and the sensor.

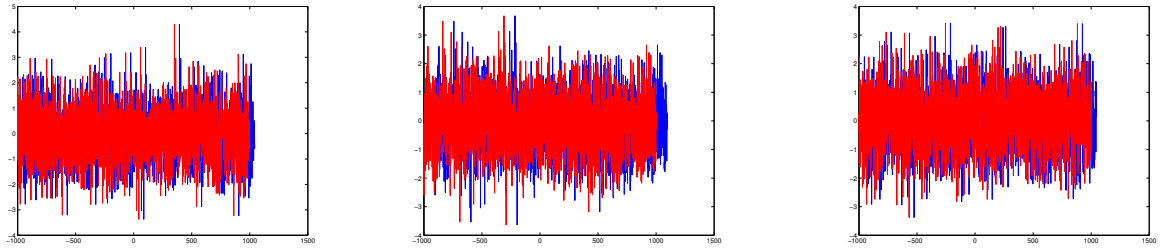

(a):incident waves(blue) (b): scattering waves(blue) (c):backpropagated waves(blue)

Figure 3.4: Comparing Signals with Received Data at Different Locations

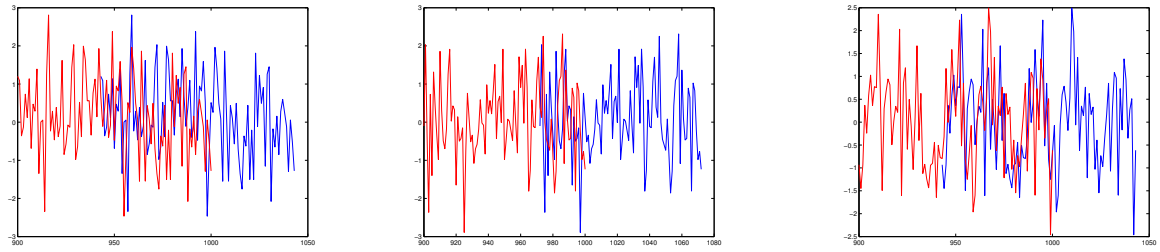

(a):incident waves(blue) (b): scattering waves(blue) (c):backpropagated waves(blue)

Figure 3.5: More Details for Comparing Signals with Received Data at Different Locations

In the frequency domain, at search point, by using the Fourier Transform,

$$\text{Incident Waves} \propto \hat{v}(\omega)e^{-ik_p l'}$$
$$\text{Backpropagated Waves} \propto \hat{v}(\omega)e^{-ik_p \tilde{l}}e^{-ik_p r(a)}e^{ik_p r^{\Delta}(a)}$$

If $e^{-ik_p l'} = e^{-ik_p \tilde{l}}e^{-ik_p r(a)}e^{ik_p r^{\Delta}(a)}$, then the incident waves and backpropagated waves will share same curve, and the correlation beween them will achieve the maximal values. Thus, when the above equation can be satisfied, we can achieve the maximal correlation between incident waves and backpropagated waves. To simplify the above equaion, we can get

$$k_p(l' - \tilde{l} - r(a) + r^{\Delta}(a)) = 2k\pi,$$

where k is an integer. We can find that the solution to this equation depends on the location of the sensor, i.e. when the location of the sensor differs, we will get the maximal values along different curves. It was showed in Figure 6.4.

Assume that the sensor is located at $(a, 0, h)$, the inclusion is at $(0, 0, 0)$ and the source is at $(\tilde{l}\sin\phi, 0, -\tilde{l}\cos\phi)$, then the solution to the above equation will be achieved on a ellipse. More details and figures will be in the Simulation Section. As a result, we can make use of the correlation between incident waves and backpropagated waves to find our imaging function. If we use P component scattering waves only, the imaging function for this case:

$$\begin{aligned} I(\Delta x, \Delta z) &= \int \bar{v}(t + \frac{l'}{c_p})v(t + \frac{\tilde{l}}{c_p} + \frac{r(a)}{c_p} - \frac{r^{\Delta}(a)}{c_p})dt \\ &= \int \mathcal{F}(\bar{v}(t + \frac{l'}{c_p}))\mathcal{F}(v(t + \frac{\tilde{l}}{c_p} + \frac{r(a)}{c_p} - \frac{r^{\Delta}(a)}{c_p}))d\omega, \end{aligned}$$

where $\mathcal{F}$ denotes the Fourier transform, and $\mathcal{F}(\bar{v}(t + \frac{l'}{c_p})) = \bar{\hat{v}}(\omega)e^{ik_p l'}$ and $\mathcal{F}(v(t + \frac{\tilde{l}}{c_p} + \frac{r(a)}{c_p} - \frac{r^{\Delta}(a)}{c_p})) = \hat{v}(\omega)e^{-ik_p \tilde{l}}\omega^2 e^{-ik_p r(a)}e^{ik_p r^{\Delta}(a)}$.

The above imaging function is as below:

$$
\begin{aligned}
I(\Delta x, \Delta z) &\sim \int \mathcal{F}(\bar{v}(t + \frac{l'}{c_p}))\mathcal{F}(v(t + \frac{\tilde{l}}{c_p} + \frac{r(a)}{c_p} - \frac{r^{\Delta}(a)}{c_p}))d\omega \\
&\sim \int \bar{\hat{v}}(\omega)e^{ik_p l'}\hat{v}(\omega)e^{-ik_p\tilde{l}}\omega^2 e^{-ik_p r(a)}e^{ik_p r^{\Delta}(a)}d\omega \\
&\sim \int \bar{\hat{v}}(\omega)\hat{v}(\omega)\omega^2 e^{ik_p l' - ik_p\tilde{l} - ik_p r(a) + ik_p r^{\Delta}(a)}d\omega.
\end{aligned}
$$

Here, $\bar{v}$ denotes the conjugate of v; $\hat{v}(\omega)e^{-ik_p\tilde{l}}$ denotes the received signals at inclusion; $\hat{v}(\omega)e^{-ik_p l'}$ denotes the received signals at search point; $\hat{v}(\omega)e^{-ik_p\tilde{l}}\omega^2 e^{-ik_p r(a)}$ denotes the received P component scattering waves at the sensor; $\hat{v}(\omega)e^{-ik_p\tilde{l}}\omega^2 e^{-ik_p r(a)}e^{ik_p r^{\Delta}(a)}$ denotes the backpropagated scattering P waves at search point. In Figure 4.5, it shows the model configuration for one sensor case.

Similarly, if we use S component scattering waves only, then the imaging function is:

$$
\begin{aligned}
I(\Delta x, \Delta z) &= \int \bar{v}(t + \frac{l'}{c_p})v(t + \frac{\tilde{l}}{c_p} + \frac{r(a)}{c_s} - \frac{r^{\Delta}(a)}{c_s})dt \\
&= \int \mathcal{F}(\bar{v}(t + \frac{l'}{c_p}))\mathcal{F}(v(t + \frac{\tilde{l}}{c_p} + \frac{r(a)}{c_s} - \frac{r^{\Delta}(a)}{c_s}))d\omega.
\end{aligned}
$$

With Many Sensors

Instead of one sensor only, we suppose that we have many sensors in an array. Then similarly, the incident waves propagate to the inclusion and then are scattered by the inclusion, later, we receive the scattering waves at the sensors. After that, we backpropagate the received signals from sensors, then we should get the maximal correlation at inclusion, where we have coherence from all sensors.

As a result, if we use P component scattering waves only, the imaging function for this case:

$$
\begin{aligned}
I(\Delta x, \Delta z) =& A^{-1}T^{-1}\iint \bar{v}(t + \frac{l'}{c_p})v(t + \frac{\tilde{l}}{c_p} + \frac{r(a)}{c_p} - \frac{r^{\Delta}(a)}{c_p})dtda \\
=& A^{-1}T^{-1}\iint \mathcal{F}(\bar{v}(t + \frac{l'}{c_p}))\mathcal{F}(v(t + \frac{\tilde{l}}{c_p} + \frac{r(a)}{c_p} - \frac{r^{\Delta}(a)}{c_p}))d\omega da.
\end{aligned}
$$

Similarly, if we use S component scattering waves only, then the imaging function is:

$$\begin{aligned} I(\Delta x, \Delta z) =& A^{-1}T^{-1} \iint \bar{v}(t + \frac{l'}{c_p}) v(t + \frac{\tilde{l}}{c_p} + \frac{r(a)}{c_s} - \frac{r^{\Delta}(a)}{c_s}) dt da \\ =& A^{-1}T^{-1} \iint \mathcal{F}(\bar{v}(t + \frac{l'}{c_p})) \mathcal{F}(v(t + \frac{\tilde{l}}{c_p} + \frac{r(a)}{c_s} - \frac{r^{\Delta}(a)}{c_s})) d\omega da. \end{aligned}$$

There is no big difference of the form of imaging function between One-sensor Case and Many-sensor case, but later, we can find they are totally different in the simulation. For One-sensor Case, we cannot find the unique maximum values, but for Many-Sensor case, we can find the unique maximum values for the imaging function.

3.3.2 With Unknown Sources

In Unknown Source Case, we suppose that the location and the properties of the source are unknown, then we can get the imaging function by computing the correlation between the backpropagated scattering P waves and S waves. In this case, we have to use the scattering P waves and S waves both. Without knowing the location of the source, we do not have information to derive the function to denote the incident waves at search points, as a result, we cannot achieve the correlation between the incident waves and the backpropagated scattering waves at search points. In this section, there are two subsections: With One Sensor; With Many Sensors.

One Sensor

Suppose we have one sensor only, then the incident waves (P waves only) propagate to the inclusion and then are scattered by the inclusion, later, we receive the scattering P waves and S waves at the sensor. The process of wave propagation is similar to the Known Source Case. After that, we backpropagate the received signals, then we should get the maximal correlation between the backpropagated scattering S waves and P waves at inclusion, not other search points.

Assume that $v(t)$ denotes the source signals, since the distance between the source and the inclusion $\tilde{l}$ is unknown, we cannot find the incident waves at inclusion. However, we

can receive the scattering S waves U_P^S and the scattering P waves U_P^P. In the time domain, $v(t+\frac{\tilde{l}}{c_p}+\frac{r(a)}{c_p}-\frac{r^\Delta(a)}{c_p})$ denotes the backpropagated scattering P waves at search point, where $r(a)$ is the distance between inclusion and the sensor and $r^\Delta(a)$ is the distance between the search point and the sensor. Similarly, $v(t+\frac{\tilde{l}}{c_p}+\frac{r(a)}{c_s}-\frac{r^\Delta(a)}{c_s})$ denotes the backpropagated scattering S waves at search point.

In the frequency domain, the backpropagated scattering P waves

$$\begin{aligned}\mathbf{U}_{sc}\cdot\vec{e_3}(t-r^\Delta(a)/c_p) &\sim \int U_P^P e^{-i\omega(t-r^\Delta(a)/c_p)}d\omega \\ &\sim \int \omega^2 C_p(\phi)e^{-ik_p(r(a)+\tilde{l})}\hat{v}(\omega)e^{-i\omega(t-r^\Delta(a)/c_p)}d\omega,\end{aligned}$$

where U_P^P denotes the scattering P waves as (3.1).

In the other hand, the backpropagated scattering S waves

$$\begin{aligned}\mathbf{U}_{sc}\cdot\vec{e_1}(t-r^\Delta(a)/c_s) &\sim \int U_P^S e^{-i\tilde{\omega}(t-r^\Delta(a)/c_s)}d\tilde{\omega} \\ &\sim \int \tilde{\omega}^2 C_s(\phi)e^{-i\tilde{k_s}r(a)-i\tilde{k_p}\tilde{l}}\hat{v}(\tilde{\omega})e^{-i\tilde{\omega}(t-r^\Delta(a)/c_s)}d\tilde{\omega},\end{aligned}$$

where U_P^S denotes the scattering S waves as (3.2).

By the definition of the cross correlation, we can untilize the correlation between the backpropagated scattering S waves and P waves to get the imaging function in the Unknown Source case with one sensor:

$$I(\Delta x,\Delta z)=T^{-1}\int_{-T/2}^{T/2}\mathbf{U}_{sc}\cdot\vec{e_3}(t-r^\Delta(a)/c_p)*\mathbf{U}_{sc}\cdot\vec{e_1}(t-r^\Delta(a)/c_s)dt,$$

where $\mathbf{U}_{sc}\cdot\vec{e_3}$ is the scattering P waves and $\mathbf{U}_{sc}\cdot\vec{e_1}$ is the scattering S waves; $\mathbf{U}_{sc}\cdot\vec{e_3}(t-r^\Delta(a)/c_p)$ and $\mathbf{U}_{sc}\cdot\vec{e_1}(t-r^\Delta(a)/c_s)$ are backpropagated scattering P waves and S waves as above.

Assuming that $\omega=\tilde{\omega}$, if $e^{-i\omega(t+\frac{\tilde{l}}{c_p}+\frac{r(a)}{c_s}-\frac{r^\Delta(a)}{c_s})}=e^{-i\omega(t+\frac{\tilde{l}}{c_p}+\frac{r(a)}{c_p}-\frac{r^\Delta(a)}{c_p})}$, then the backpropagated S waves and P waves will share same curve, and the correlation beween them will achieve the maximal values. Thus, when the above equation can be satisfied, we can achieve the maximal correlation between the backpropagated P waves and S waves.

To simplify the above equaion, we can get

$$(k_p - k_s)(r(a) - r^{\Delta}(a)) = 2k\pi,$$

where k is an integer. We can find that the solution to this equation depends on the location of the sensor, i.e. when the location of the sensor differs, we will get the maximal values along different curves. It was showed in Figure 6.9.

Assume that the sensor is located at $(a, 0, h)$ and the inclusion is at $(0, 0, 0)$, then the solution to the above equation will be achieved on a circle. More details and figures of simulations will be in Chapter 6. As a result, we can make use of the correlation between the backpropagated P waves and S waves to find our imaging function. Under the assumption $\omega = \tilde{\omega}$, the imaging function with one sensor only in the Unknown Source case:

$$\begin{aligned} I(\Delta x, \Delta z) &= \int \bar{v}(t + \frac{\tilde{l}}{c_p} + \frac{r(a)}{c_p} - \frac{r^{\Delta}(a)}{c_p}) v(t + \frac{\tilde{l}}{c_p} + \frac{r(a)}{c_s} - \frac{r^{\Delta}(a)}{c_s}) dt \\ &= \int \mathcal{F}(\bar{v}(t + \frac{\tilde{l}}{c_p} + \frac{r(a)}{c_p} - \frac{r^{\Delta}(a)}{c_p})) \mathcal{F}(v(t + \frac{\tilde{l}}{c_p} + \frac{r(a)}{c_s} - \frac{r^{\Delta}(a)}{c_s})) d\omega, \end{aligned}$$

where $\mathcal{F}$ denotes the Fourier transform, then $\mathcal{F}(\bar{v}(t + \frac{\tilde{l}}{c_p} + \frac{r(a)}{c_p} - \frac{r^{\Delta}(a)}{c_p})) = \bar{\hat{v}}(\omega) e^{ik_p \tilde{l}} \omega^2 e^{ik_p r(a)} e^{-ik_p r^{\Delta}(a)}$ and $\mathcal{F}(v(t + \frac{\tilde{l}}{c_p} + \frac{r(a)}{c_s} - \frac{r^{\Delta}(a)}{c_s})) = \hat{v}(\omega) e^{-ik_p \tilde{l}} \omega^2 e^{-ik_s r(a)} e^{ik_s r^{\Delta}(a)}$.

The above imaging function is as below:

$$\begin{aligned} I(\Delta x, \Delta z) &\sim \int \mathcal{F}(\bar{v}(t + \frac{\tilde{l}}{c_p} + \frac{r(a)}{c_p} - \frac{r^{\Delta}(a)}{c_p})) \mathcal{F}(v(t + \frac{\tilde{l}}{c_p} + \frac{r(a)}{c_s} - \frac{r^{\Delta}(a)}{c_s})) d\omega \\ &\sim \int \bar{\hat{v}}(\omega) e^{ik_p \tilde{l}} \omega^2 e^{ik_p r(a)} e^{-ik_p r^{\Delta}(a)} \hat{v}(\omega) e^{-ik_p \tilde{l}} \omega^2 e^{-ik_s r(a)} e^{ik_s r^{\Delta}(a)} d\omega. \end{aligned}$$

Here, $\bar{v}$ denotes the conjugate of v; $\hat{v}(\omega) e^{-ik_p l'}$ denotes the received signals at search point; $\hat{v}(\omega) e^{-ik_p \tilde{l}} \omega^2 e^{-ik_p r(a)}$ denotes the received P component scattering waves at the sensor; $\hat{v}(\omega) e^{-ik_p \tilde{l}} \omega^2 e^{-ik_p r(a)} e^{i}$ denotes the backpropagated scattering P waves at search point; $\hat{v}(\omega) e^{-ik_p \tilde{l}} \omega^2 e^{-ik_s r(a)} e^{ik_s r^{\Delta}(a)}$ denotes the backpropagated scattering S waves at search point.

With Many Sensors

Instead of one sensor only, we suppose that we have many sensors in an array. Then we have the similar wave propagation process. After that, we backpropagate the received signals from sensors, then we should get the maximal correlation at inclusion, where we have coherence from all sensors.

By using the above formulas and the definition of the cross correlation, we can get the imaging function:

$$I(\Delta x, \Delta z) = T^{-1}A^{-1}\int_{-T/2}^{T/2}\int_{-A/2}^{A/2}\mathbf{U}_{sc}\cdot\vec{e_3}(t-r^{\Delta}(a)/c_p) * \mathbf{U}_{sc}\cdot\vec{e_1}(t-r^{\Delta}(a)/c_s)dtda,$$

where $\mathbf{U}_{sc}\cdot\vec{e_3}$ is the scattering P waves and $\mathbf{U}_{sc}\cdot\vec{e_1}$ is the scattering S waves; $\mathbf{U}_{sc}\cdot\vec{e_3}(t-r^{\Delta}(a)/c_p)$ and $\mathbf{U}_{sc}\cdot\vec{e_1}(t-r^{\Delta}(a)/c_s)$ are backpropagated scattering P waves and S waves. Then, the imaging function can be written as

$$\begin{aligned} I(\Delta x, \Delta z) =& T^{-1}A^{-1}\iiiint \omega^2\tilde{\omega}^2 C_p(\phi)C_s(\phi)e^{-ik_p(r(a)+\tilde{l})} \\ & e^{i\tilde{k_s}r(a)+i\tilde{k_p}\tilde{l}}\hat{v}(\omega)\bar{\hat{v}}(\tilde{\omega})e^{ik_p r^{\Delta}(a)}e^{-i\tilde{k_s}r^{\Delta}(a)}e^{-i\omega t}e^{i\tilde{\omega}t}\ dtdad\omega d\tilde{\omega}. \end{aligned}$$

Suppose that $\omega = \omega_c = const$, by using the properties of the Fourier transform,

$$E[I(\Delta x, \Delta z)] \sim \omega_c^4 C_p(\phi)C_s(\phi)T^{-1}A^{-1}\int_{-A/2}^{A/2}da\int_{-T/2}^{T/2}E[v(t-\frac{r(a)-r^{\Delta}(a)}{c_p})v(t-\frac{r(a)-r^{\Delta}(a)}{c_s})]dt.$$

Assume that the correlation $C(\frac{\tau}{l}) = E[v(t)v(t+\tau)]$, where l is the correlation length and $l = \frac{1}{C(0)}\int_{-\infty}^{\infty}C(h)dh$. Then, by the property of the stationary stochastic process,

$$E[I(\Delta x, \Delta z)] \sim \omega_c^4 C_p(\phi)C_s(\phi)A^{-1}\int_{-A/2}^{A/2}C(\frac{\frac{r(a)-r^{\Delta}(a)}{c_p}-\frac{r(a)-r^{\Delta}(a)}{c_s}}{l})da.$$

After achieving the above function, we can do the resolution analysis in the following chapter.

3.3.3 Image Contribution of Incident Waves

In this section, we consider a new case. Assume that the source is unknown, however, when we received the scattering P waves and the scattering S waves in the sensors, actually, we can also receive incident P waves. Since the incident P waves and the scattering P waves are both P waves and they behave in the same way, it is impossible to seperate the scattering P waves and the incident P waves in the received data. As a result, we need to consider the image contribution of the directly transmitted waves, that is, the incident waves' contribution. To build the imaging funcion, we will have to use both the scattering P waves and the incident P waves, then the final imaging function in the simulation consist of two components: the correlation between backpropagated incident P waves and the backpropagated scattering S waves; the correlation between backpropagated scattering P waves and the backpropagated scattering S waves. By using the received data, our imaging function will be:

$$I_{sim} = I + I_{incident}.$$

Here, I is the imaging function we mentioned in the above sections; $I_{incident}$ is the correlation between backpropagated incident P waves and the backpropagated scattering S waves. In the simulation, the imaging function I_{sim} is the correlation between the backpropagated scattering S waves and the backpropagated P waves which includes backpropagated incident P waves and backpropagated scattering P waves because of the seperation issue.

In the above sections, we get some results without considering the incident wave term. In this section, we will do the similar simulation with considering the incident wave term.

Then, our imaging function with the incident wave component term is as below:

$$\begin{aligned} I_{sim}(\Delta x, \Delta z) =& T^{-1}A^{-1}\int_{-T/2}^{T/2}\int_{-A/2}^{A/2}\mathbf{U}_{sc}\cdot\vec{e_3}(t-r^{\Delta}(a)/c_p)*\mathbf{U}_{sc}\cdot\vec{e_1}(t-r^{\Delta}(a)/c_s) \\ &+\mathbf{U}_0\cdot\vec{e_3}(t-r^{\Delta}(a)/c_p)*\mathbf{U}_{sc}\cdot\vec{e_1}(t-r^{\Delta}(a)/c_s)dtda \\ =& T^{-1}A^{-1}\iiiint \omega^2\tilde{\omega}^2 C_p(\phi)C_s(\phi)e^{-ik_p(r(a)+\tilde{l})}e^{i\tilde{k_s}r(a)+i\tilde{k_p}\tilde{l}} \\ &\hat{v}(\omega)\bar{\hat{v}}(\tilde{\omega})e^{ik_pr^{\Delta}(a)-i\tilde{k_s}r^{\Delta}(a)-i\omega t+i\tilde{\omega}t} \\ &+\tilde{\omega}^2C_s(\phi)e^{-ik_p\hat{l}(a)}e^{i\tilde{k_s}r(a)+i\tilde{k_p}\tilde{l}} \\ &\hat{v}(\omega)\bar{\hat{v}}(\tilde{\omega})e^{ik_pr^{\Delta}(a)-i\tilde{k_s}r^{\Delta}(a)-i\omega t+i\tilde{\omega}t}dtdad\omega d\tilde{\omega}. \end{aligned} \tag{3.5}$$

3.3.4 With Unknown Pulse Source Case

In this case, the source is unknown but it is pulse source instead of gaussian source. Suppose that our source is a continuous pulse source:

$$\rho(t) = \cos(\omega_0 t) * e^{-(\frac{t}{t_0})^2/2}, \tag{3.6}$$

where ω_0 and t_0 are parameters and $\omega_0 \gg \frac{1}{t_0}$. The above pulse function is the product of the cosine function and the Gaussian kernal. The source gennerated a continuous pulse, and scattered at inclusion, then we can receive scattering P waves and S waves. Since our source is also unknown, based on the unknown source case, our imaging function in the continous pulse source case:

$$\begin{aligned} I(\Delta x, \Delta z) =& T^{-1}A^{-1}\iiiint \omega^2\tilde{\omega}^2 C_p(\phi)C_s(\phi)e^{-ik_p(r(a)+\tilde{l})} \\ &e^{i\tilde{k_s}r(a)+i\tilde{k_p}\tilde{l}}\hat{\rho}(\omega)\bar{\hat{\rho}}(\tilde{\omega})e^{ik_pr^{\Delta}(a)}e^{-i\tilde{k_s}r^{\Delta}(a)}e^{-i\omega t}e^{i\tilde{\omega}t}dtdad\omega d\tilde{\omega}. \end{aligned} \tag{3.7}$$

Similarly, if we have a rectangular pulse source, then we will have a similar imaging function.

Chapter 4

Resolution Analysis

To quantify the imaging resolution we compute the point spread function (PSF), which is the spatial profile of the imaging functional centered at a point reflector. The cross range resolution and the range resolution are the widths of PSF in the transverse and longitudinal directions, respectively. In our study, we need to use the analysis of PSF to find the region for search points.

4.1 With Known Sources Case

In this section, we will show the resolution analysis in the Known Source Case.

Proposition 4.1.1. *Suppose we have a known source which is a stationary stochastic process, based on the imaging function in the known source case, we have the following:*

1. *Considering P component scattering waves only, then*

$$\textbf{PSF} \sim \int_{\frac{-A/2}{A+h\sin\phi}}^{\frac{A/2}{A+h\sin\phi}} e^{-|\Delta\tilde{z}' + \Delta\tilde{x}' a'|} da',$$

where ϕ is the acute angle between z axis and the direction in which signals propagate from the source to the inclusion. In addition, the transverse radius of the focal spot is $\frac{\lambda_p}{\frac{A}{h}+\sin\phi}$ and the longitudinal radius of the focal spot is $\frac{\lambda_p}{\sqrt{2-2\cos\phi}}$.

2. Considering S component scattering waves only, then

$$\mathbf{PSF} \sim \int_{\frac{-Ac_p/2}{Ac_p+hc_s\sin\phi}}^{\frac{Ac_p/2}{Ac_p+hc_s\sin\phi}} e^{-|\Delta\tilde{z}'+\Delta\tilde{x}'a'|}da'.$$

In addition, the transverse radius of the focal spot is $\frac{1}{\frac{A}{\hbar\lambda_s}+\frac{\sin\phi}{\lambda_p}}$ *and the longitudinal radius of the focal spot is* $\frac{\sqrt{(\frac{\sin\phi}{\frac{A\lambda_p}{\hbar\lambda_s}+\sin\phi})^2+1}}{\frac{1}{\lambda_s}-\frac{\cos\phi}{\lambda_p}}$.

Proof. From the last section, if we use P component scattering waves only, the imaging function is:

$$\begin{aligned} I(\Delta x,\Delta z) &= \iint \bar{v}(t+\frac{l'}{c_p})v(t+\frac{\tilde{l}}{c_p}+\frac{r(a)}{c_p}-\frac{r^{\Delta}(a)}{c_p})dtda \\ &= \iint \mathcal{F}(\bar{v}(t+\frac{l'}{c_p}))\mathcal{F}(v(t+\frac{\tilde{l}}{c_p}+\frac{r(a)}{c_p}-\frac{r^{\Delta}(a)}{c_p}))d\omega da. \end{aligned}$$

Approximately, it is equivalent to

$$E[I(\Delta x,\Delta z)] \sim T^{-1}A^{-1}\int_{-A/2}^{A/2}da\int_{-T/2}^{T/2}E[v(t+\frac{l'}{c_p})v(t+\frac{\tilde{l}}{c_p}+\frac{r(a)-r^{\Delta}(a)}{c_p})]dt.$$

Suppose that $C(\frac{\tau}{l}) = E[v(t),v(t+\tau)]$, where l is the correlation length and $l = \frac{1}{C(0)}\int_{-\infty}^{\infty}C(h)dh$. Then,by the property of the stationary stochastic process,

$$E[I(\Delta x,\Delta z)] \sim A^{-1}\int_{-A/2}^{A/2}daC(\frac{\frac{l'-\tilde{l}}{c_p}-\frac{r(a)-r^{\Delta}(a)}{c_p}}{l}),$$

where $l' = \sqrt{(\tilde{l}\sin\phi-\Delta x)^2+(-\tilde{l}\cos\phi-\Delta z)^2}$; $r(a) = \sqrt{h^2+a^2}$; $r^{\Delta}(a) = \sqrt{(a-\Delta x)^2+(h-\Delta z)^2}$.

In Figure 4.5, the inclusion is at $(0,0,0)$, the sensors are located at $(a,0,h)$ $(a\in[-\frac{A}{2},\frac{A}{2}])$, the search point is at $(\Delta x,0,\Delta z)$, the source location is known, that is, $(\tilde{l}\sin\phi,0,-\tilde{l}\cos\phi)$, where ϕ is the acute angle between z axis and the direction in which signals propagate from the source to the inclusion. Since $\Delta x,\Delta z \ll a \ll h$, $l' \approx \tilde{l}-\Delta x\sin\phi+\Delta z\cos\phi$. Similarly, $r(a)\approx h+\frac{a^2}{2h}$ and $r^{\Delta}(a)\approx h-\Delta z+a^2/2h-a\Delta x/h+a^2\Delta z/2h^2 \approx h-\Delta z+a^2/2h-a\Delta x/h$.

Therefore, the imaging function is approximately equal to

$$\begin{aligned} E[I(\Delta x,\Delta z)] &\sim A^{-1}\int_{-A/2}^{A/2} daC(\frac{l'-\tilde{l}-r(a)+r^{\Delta}(a)}{lc_p}) \\ &\sim A^{-1}\int_{-A/2}^{A/2} daC(\frac{-\Delta x\sin\phi+\Delta z\cos\phi-(\Delta z+a\Delta x/h)}{lc_p}) \\ &= A^{-1}\int_{-A/2}^{A/2} daC(\frac{\Delta x(-\frac{a}{h}-\sin\phi)+\Delta z(\cos\phi-1)}{lc_p}). \end{aligned}$$

Assume that $\hat{C}=\mathcal{F}(e^{-B|t|})I_{[l,\infty)}$, support $\hat{C}=O(B)$, and $l\ll 1/B$, where B is the bandwidth. By the assumptions, we can change the above imaging function into:

$$E[I(\Delta x,\Delta z)]\sim A^{-1}\int_{-A/2}^{A/2} e^{-\frac{|\Delta x(-\frac{a}{h}-\sin\phi)+\Delta z(\cos\phi-1)|}{\lambda_p}}da,$$

where $\lambda_p=c_p/B$. Now let $\Delta\tilde{z}=\frac{\Delta z(\cos\phi-1)}{\lambda_p}$ and $\Delta\tilde{x}=\frac{\Delta x(-\frac{A}{h}-\sin\phi)}{\lambda_p}$, then we can get

$$E[\tilde{I}(\Delta\tilde{x},\Delta\tilde{z})]\sim A^{-1}\int_{-A/2}^{A/2} e^{-|\Delta\tilde{z}+\Delta\tilde{x}\frac{-\frac{a}{h}-\sin\phi}{-\frac{A}{h}-\sin\phi}|}da\sim\int_{\frac{A/2-h\sin\phi}{-A-h\sin\phi}}^{\frac{-A/2-h\sin\phi}{-A-h\sin\phi}} e^{-|\Delta\tilde{z}+\Delta\tilde{x}a'|}da'.$$

In Figure 4.1, it shows the surface and the contour of PSF with P waves by using the above formula.

Utilizing the transformation of coordinates, we can achieve a horizontal contour of PSF. Assume that $\Delta\tilde{z}'=\Delta\tilde{z}+\frac{h\sin\phi}{A+h\sin\phi}\Delta\tilde{x}$, $\Delta\tilde{x}'=\Delta\tilde{x}$, then the above formula can be changed into:

$$E[\tilde{I}'(\Delta\tilde{x}',\Delta\tilde{z}')]\sim\int_{\frac{-A/2}{A+h\sin\phi}}^{\frac{A/2}{A+h\sin\phi}} e^{-|\Delta\tilde{z}'+\Delta\tilde{x}'a'|}da'.$$

Thus, the transverse radius of the focal spot is $\frac{\lambda_p}{\frac{A}{h}+\sin\phi}$ and the longitudinal radius of the focal spot is $\frac{\lambda_p}{\sqrt{2-2\cos\phi}}$. In Figure 4.2, we can achieve the surface and the contour of PSF with P waves under the new coordinates, and it is the focal spot of the time-reversed focal spot in the time harmonic regime, where x in multiples of $\frac{\lambda_p}{\frac{A}{h}+\sin\phi}$ and z in multiples of $\frac{\lambda_p}{\sqrt{2-2\cos\phi}}$.

Similarly, if we use S component scattering waves only, then the imaging function is:

$$\begin{aligned} I(\Delta x, \Delta z) &= \iint \bar{v}(t + \frac{l'}{c_p}) v(t + \frac{\tilde{l}}{c_p} + \frac{r(a)}{c_s} - \frac{r^{\Delta}(a)}{c_s}) dt da \\ &= \iint \mathcal{F}(\bar{v}(t + \frac{l'}{c_p})) \mathcal{F}(v(t + \frac{\tilde{l}}{c_p} + \frac{r(a)}{c_s} - \frac{r^{\Delta}(a)}{c_s})) d\omega da. \end{aligned}$$

Then, we will have similar resolution analysis but better than P component scattering waves only since the velocity of P waves is faster than the velocity of S waves. The above function can be written as:

$$\begin{aligned} E[I(\Delta x, \Delta z)] &\sim A^{-1} \int_{-A/2}^{A/2} C(\frac{(l' - \tilde{l})/c_p - (r(a) - r^{\Delta}(a))/c_s}{l}) da \\ &\sim A^{-1} \int_{-A/2}^{A/2} C(\frac{(-\Delta x \sin\phi + \Delta z \cos\phi)/c_p - (\Delta z + a\Delta x/h)/c_s}{l}) da \\ &= A^{-1} \int_{-A/2}^{A/2} C(\frac{\Delta x(-\frac{a}{hc_s} - \frac{\sin\phi}{c_p}) + \Delta z(\frac{\cos\phi}{c_p} - \frac{1}{c_s})}{l}) da. \end{aligned}$$

Now let $\Delta\tilde{z} = \left(\frac{\cos\phi}{\lambda_p} - \frac{1}{\lambda_s}\right)\Delta z$ and $\Delta\tilde{x} = \left(-\frac{A}{h\lambda_s} - \frac{\sin\phi}{\lambda_p}\right)\Delta x$, then we can get

$$\begin{aligned} E[\tilde{I}(\Delta\tilde{x}, \Delta\tilde{z})] \sim & A^{-1} \int_{-A/2}^{A/2} e^{-|\Delta\tilde{z} + \Delta\tilde{x} \frac{\frac{a}{h\lambda_s} + \frac{\sin\phi}{\lambda_p}}{\frac{A}{h\lambda_s} + \frac{\sin\phi}{\lambda_p}}|} da \\ & \sim \int_{\frac{-A}{2}\frac{\lambda_p}{A\lambda_p + h\lambda_s \sin\phi}}^{\frac{A}{2}\frac{\lambda_p}{A\lambda_p + h\lambda_s \sin\phi}} e^{-|\Delta\tilde{z} + \Delta\tilde{x} a'|} da'. \end{aligned}$$

In Figure 4.3, it shows the surface and the contour of PSF with S waves by using the above formula. Utilizing the transformation of coordinates, we can achieve a horizontal contour of PSF. Assume that $\Delta\tilde{z}' = \Delta\tilde{z} + \frac{h\lambda_s \sin\phi}{A\lambda_p + h\lambda_s \sin\phi}\Delta\tilde{x}$, $\Delta\tilde{x}' = \Delta\tilde{x}$, then the above formula can be changed into:

$$E[\tilde{I}'(\Delta\tilde{x}', \Delta\tilde{z}')] \sim \int_{\frac{-A\lambda_p/2}{A\lambda_p + h\lambda_s \sin\phi}}^{\frac{A\lambda_p/2}{A\lambda_p + h\lambda_s \sin\phi}} e^{-|\Delta\tilde{z}' + \Delta\tilde{x}' a'|} da'.$$

Thus, the transverse radius of the focal spot is $\frac{1}{\frac{A}{h\lambda_s} + \frac{\sin\phi}{\lambda_p}}$ and the longitudinal radius of the focal spot is $\frac{\sqrt{\left(\frac{\sin\phi}{\frac{A\lambda_p}{h\lambda_s} + \sin\phi}\right)^2 + 1}}{\frac{1}{\lambda_s} - \frac{\cos\phi}{\lambda_p}}$. In Figure 4.3 and Figure 4.4, we can achieve the surface and

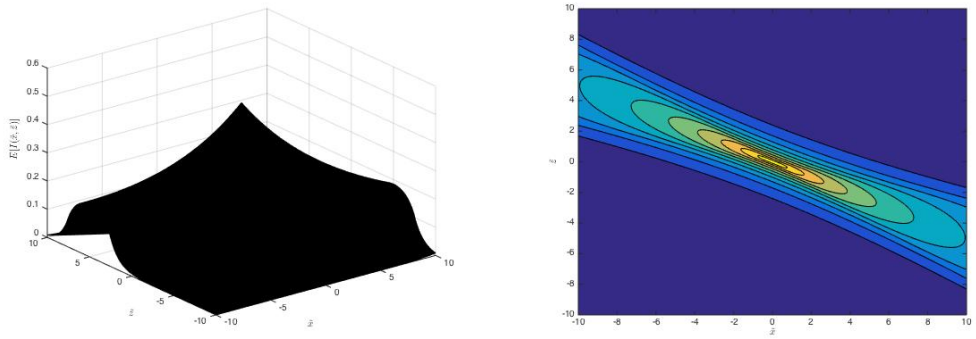

(a): The Surface of PSF (P waves) (b): The Contour of PSF (P waves)

Figure 4.1: PSF with P waves in the Original Coordinates

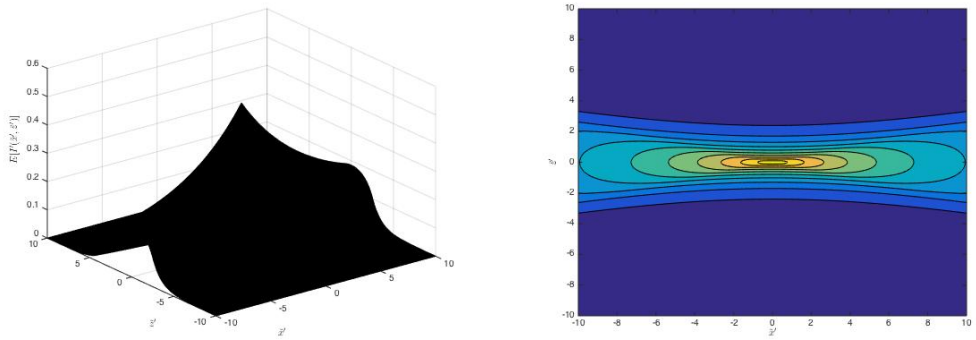

(a): The Surface of PSF (P waves) (b): The Contour of PSF (P waves)

Figure 4.2: PSF with P waves in the New Coordinates

the contour of PSF with S waves under the original coordinates and the new coordinates, and it is the focal spot of the time-reversed focal spot in the time harmonic regime, where x in multiples of $\frac{1}{\frac{A}{h\lambda_s}+\frac{\sin\phi}{\lambda_p}}$ and z in multiples of $\frac{\sqrt{\left(\frac{\sin\phi}{\frac{A\lambda_p}{h\lambda_s}+\sin\phi}\right)^2+1}}{\frac{1}{\lambda_s}-\frac{\cos\phi}{\lambda_p}}$.

□

If we change the location of the known source, the resolution changes too. As mentioned before, ϕ denotes the angle between z axis and the wave propagation direction from the source. When $\phi = 0$, the transverse radius of the focal spot is $\frac{\lambda_p h}{A}$ and the longitudinal radius of the focal spot is ∞, where $\frac{\lambda_p h}{A}$ is called Rayleigh resolution λ_R; When $\phi = \frac{\pi}{2}$, the transverse radius of the focal spot is $\frac{\lambda_p}{\frac{A}{h}+1}$ and the longitudinal radius of the focal spot

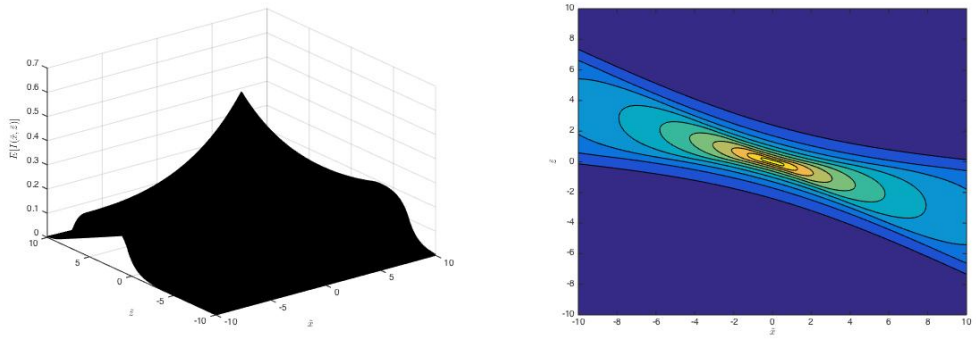

(a): The Surface of PSF (S waves) (b): The Contour of PSF (S waves)

Figure 4.3: PSF with S waves in the Original Coordinates

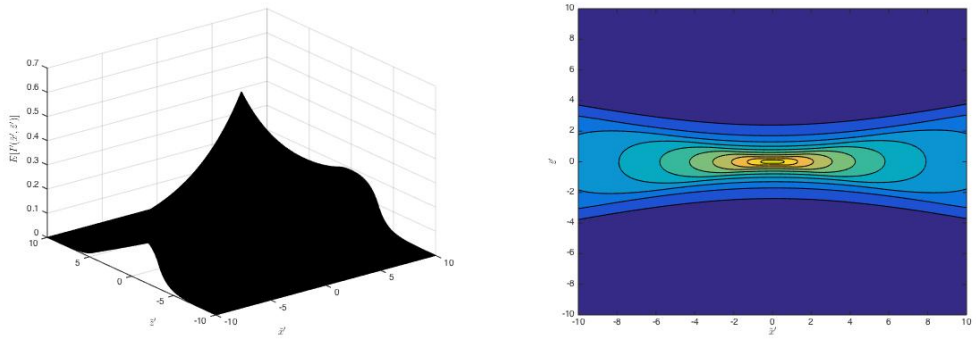

(a): The Surface of PSF (P waves) (b): The Contour of PSF (P waves)

Figure 4.4: PSF with S waves in the New Coordinates

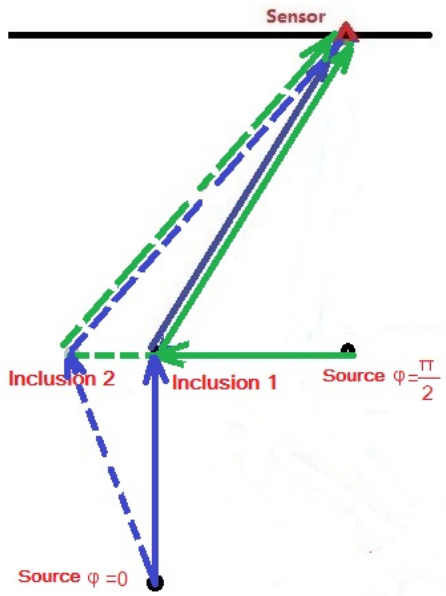

Figure 4.5: Compared PSF with different ϕ

is $\frac{\lambda_p}{\sqrt{2}}$, where λ_p is called broadband resolution; When $\phi = \pi$, the transverse radius of the focal spot is $\frac{\lambda_p h}{A}$ and the longitudinal radius of the focal spot is $\frac{\lambda_p}{2}$. As a result, when our source is in the same depth as the inclusion, the transverse radius and the longitudinal radius are less than the ones with a deeper source and our result will have better resolution. In Figure 4.5, changing the location of the inclusion, we compared different locations of the source and it shows that when the source is located at the same depth as the inclusion, the imaging function is more sensitive to the change of the location of inclusion, since our imaging function is related to the wave propagating path.

Similarly, with S scattering waves only, when $\phi = 0$, the transverse radius of the focal spot is $\frac{h\lambda_s}{A}$ which is Rayleigh resolution and the longitudinal radius of the focal spot is $\frac{1}{\frac{1}{\lambda_s}-\frac{1}{\lambda_p}}$, which is called harmonic difference resolution $\bar{\lambda}_{p,s}$; When $\phi = \frac{\pi}{2}$, the transverse radius of the focal spot is $\frac{h\lambda_s}{\frac{A}{h\lambda_s}+\frac{1}{\lambda_p}}$ which is called harmonic sum resolution and the longitudinal radius of the focal spot is $\frac{\sqrt{(\frac{1}{\frac{A\lambda_p}{h\lambda_s}+1})^2+1}}{\frac{1}{\lambda_s}}$; When $\phi = \pi$, the transverse radius of the focal spot is $\frac{h\lambda_s}{A}$ and the longitudinal radius of the focal spot is $\frac{1}{\frac{1}{\lambda_s}+\frac{1}{\lambda_p}}$. As a result, when our source is in the same depth as the inclusion, the transverse radius and the longitudinal radius are less than the ones with a deeper source and our result will have better resolution. It is similar to the

case with P component waves only.

4.2 With Unknown Sources Case

In this section, we will discuss the resolution analysis in Unknown Source Case.

Proposition 4.2.1. *Suppose we have an unknown source, based on the imaging function in the unknown source case, we have the following:*

$$\textbf{PSF} \sim \omega_c^4 C_p(\phi) C_s(\phi) A^{-1} \int_{-A/2}^{A/2} e^{-|\Delta\tilde{z}+\Delta\tilde{x}\frac{a}{A}|} da \sim \int_{-1/2}^{1/2} e^{-|\Delta\tilde{z}+\Delta\tilde{x}a'|} da'.$$

The transverse radius of the focal spot is $\frac{h\bar{\lambda}_{p,s}}{A}$ *and the longitudinal radius of the focal spot is* $\bar{\lambda}_{p,s}$*, where* $\bar{\lambda}_{p,s}$ *is harmonic difference resolution.*

Proof. From the last chapter, we can get

$$I(\Delta x, \Delta z) \sim$$
$$\omega_c^4 C_p(\phi) C_s(\phi) A^{-1} \int_{-A/2}^{A/2} C(\frac{\frac{r(a)-r^{\Delta}(a)}{c_p} - \frac{r(a)-r^{\Delta}(a)}{c_s}}{l}) da.$$

Since $r(a) - r^{\Delta}(a) \sim \Delta x(a/h) + \Delta z(1 - \frac{1}{2}(a/h)^2)$, then we can have the following formula:

(4.1)
$$E[I(\Delta x, \Delta z)] \sim \omega_c^4 C_p(\phi) C_s(\phi) A^{-1} \int_{-A/2}^{A/2} C([\Delta x(a/h) + \Delta z(1 - \frac{1}{2}(a/h)^2)](\frac{1}{c_s} - \frac{1}{c_p})/l) da.$$

Since $1 - \frac{1}{2}(a/h)^2$ is very close to 1 when $a \ll h$,

$$E[I(\Delta x, \Delta z)] \sim \omega_c^4 C_p(\phi) C_s(\phi) A^{-1} \int_{-A/2}^{A/2} C((\Delta x(a/h) + \Delta z)(\frac{1}{c_s} - \frac{1}{c_p})/l) da. \tag{4.2}$$

Consider a special case with assumption that $\hat{C} = \mathcal{F}(e^{-B|t|}) I_{[l,\infty)}$, support $\hat{C} = O(B)$, and $l \ll 1/B$. By the above assumptions, we can change (4.1) into:

$$E[I(\Delta x, \Delta z)] \sim \omega_c^4 C_p(\phi) C_s(\phi) A^{-1} \int_{-A/2}^{A/2} e^{-\frac{|\Delta z+\Delta x(a/h)|}{\bar{\lambda}_{p,s}}} da,$$

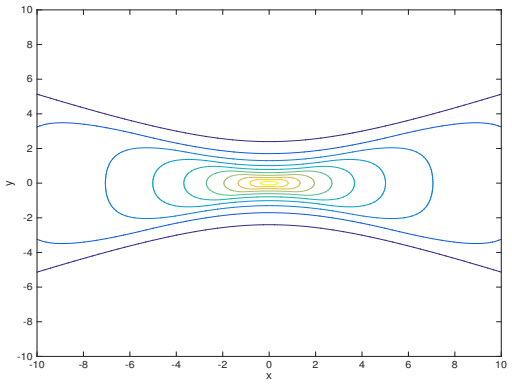

(a) The Contour of Point Spread Function

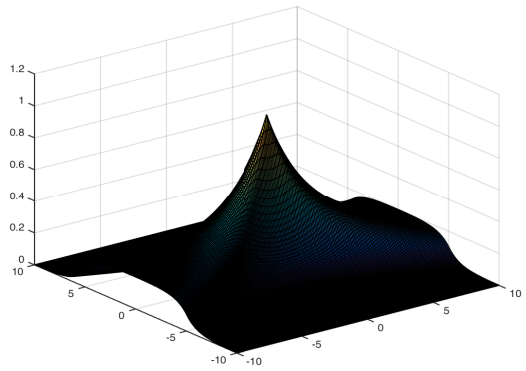

(b) The Surface of Point Spread Function

Figure 4.6: Point Spread Function with Unknown Source

where $\lambda_s = c_s/B; \lambda_p = c_p/B; \bar{\lambda}_{p,s} = \frac{\lambda_s \lambda_p}{\lambda_p - \lambda_s}$. Now let $\Delta\tilde{z} = \frac{\Delta z}{\bar{\lambda}_{p,s}}$ and $\Delta\tilde{x} = \frac{\Delta x}{\bar{\lambda}_{p,s}} \frac{A}{h}$, then we can get

$$E[\tilde{I}(\Delta\tilde{x}, \Delta\tilde{z})] \sim \omega_c^4 C_p(\phi) C_s(\phi) A^{-1} \int_{-A/2}^{A/2} e^{-|\Delta\tilde{z} + \Delta\tilde{x}\frac{a}{A}|} da \sim \int_{-1/2}^{1/2} e^{-|\Delta\tilde{z} + \Delta\tilde{x}a'|} da'.$$

Thus, the transverse radius of the focal spot is $\frac{h\bar{\lambda}_{p,s}}{A}$ and the longitudinal radius of the focal spot is $\bar{\lambda}_{p,s}$. In Figure 4.6, it is the time-reversed focal spot in the time harmonic regime, where x in multiples of $\frac{h\bar{\lambda}_{p,s}}{A}$ and z in multiples of $\bar{\lambda}_{p,s}$.

□

4.3 Image Contribution of Incident Waves

In this section, we will show the resolution analysis in Image Contribution of Incident Waves. Since we need to consider the contribution of the incident waves, our resolution analysis in the last two cases does not work in this section. Below is the resolution analysis on considering the incident waves' contribution.

Proposition 4.3.1. *Suppose we have an unknown source, based on the imaging function in the unknown source case with considering the contribution of incident waves' components,*

we have the following:

$$\textbf{PSF} \sim \omega_c^4 C_p(\phi) C_s(\phi) A^{-1} \int_{-A/2}^{A/2} e^{-|\Delta\tilde{z}+\Delta\tilde{x}\frac{a}{A}|} da \sim \int_{-1/2}^{1/2} e^{-|\Delta\tilde{z}+\Delta\tilde{x}a'|} da'.$$

In addition, the transverse radius of the focal spot is $\frac{h\bar{\lambda}_{p,s}}{A}$ *and the longitudinal radius of the focal spot is* $\bar{\lambda}_{p,s}$*. They are same as the values achieved in the unknown source case without considering the incident waves' component.*

Proof. From the last chapter, we get the imaging function in this case:

$$\begin{aligned}
I_{sim}(\Delta x, \Delta z) =& T^{-1}A^{-1} \int_{-T/2}^{T/2} \int_{-A/2}^{A/2} \mathbf{U}_{sc} \cdot \vec{e_3}(t - r^{\Delta}(a)/c_p) * \mathbf{U}_{sc} \cdot \vec{e_1}(t - r^{\Delta}(a)/c_s) \\
&+ \mathbf{U}_0 \cdot \vec{e_3}(t - r^{\Delta}(a)/c_p) * \mathbf{U}_{sc} \cdot \vec{e_1}(t - r^{\Delta}(a)/c_s) dt da \\
=& T^{-1}A^{-1} \iiiint \omega^2 \tilde{\omega}^2 C_p(\phi) C_s(\phi) e^{-ik_p(r(a)+\tilde{l})} e^{i\tilde{k_s} r(a) + i\tilde{k_p}\tilde{l}} \\
&\qquad \hat{v}(\omega)\bar{\hat{v}}(\tilde{\omega}) e^{ik_p r^{\Delta}(a) - i\tilde{k_s} r^{\Delta}(a) - i\omega t + i\tilde{\omega} t} \\
&+ \tilde{\omega}^2 C_s(\phi) e^{-ik_p \hat{l}(a)} e^{i\tilde{k_s} r(a) + i\tilde{k_p}\tilde{l}} \\
&\qquad \hat{v}(\omega)\bar{\hat{v}}(\tilde{\omega}) e^{ik_p r^{\Delta}(a) - i\tilde{k_s} r^{\Delta}(a) - i\omega t + i\tilde{\omega} t} dt da d\omega d\tilde{\omega}.
\end{aligned}$$

Then, it is similar to simplify the above function as below:

$$E[I_{sim}(\Delta x, \Delta z)] \sim \omega_c^4 C_p(\phi) C_s(\phi) A^{-1} \int_{-A/2}^{A/2} C(\frac{\frac{r(a)-r^{\Delta}(a)}{c_p} - \frac{r(a)-r^{\Delta}(a)}{c_s}}{l}) + C(\frac{\frac{\hat{l}-r^{\Delta}(a)-\tilde{l}}{c_p} - \frac{r(a)-r^{\Delta}(a)}{c_s}}{l}) da.$$

Here, $\hat{l}$ is the distance between the source and the sensor:

$$\begin{aligned}
\hat{l} =& \sqrt{(\tilde{l} - a)^2 + (-\tilde{l} - h)^2} \\
\sim& \tilde{l} + h\cos\phi - a\cos\phi + \frac{h^2}{2\tilde{l}} + \frac{a^2}{2\tilde{l}},
\end{aligned}$$

with the assumption that $a \ll h \ll \tilde{l}$.

Similarly, we have $r(a) - r^{\Delta}(a) \sim \Delta x(a/h) + \Delta z$, and from the above assumption, we

can have the following formula:

$$\begin{aligned}\hat{l} - r^{\Delta}(a) - \tilde{l} &\sim \tilde{l} + h\cos\phi - a\cos\phi + \frac{h^2}{2\tilde{l}} + \frac{a^2}{2\tilde{l}} - (h - \Delta z - \frac{a\Delta x}{h} + \frac{a^2}{h}) - \tilde{l} \\ &\sim h\cos\phi - h + \frac{h^2}{2\tilde{l}} \gg r(a) - r^{\Delta}(a).\end{aligned}$$

Then, we can simiplify the expectation of the imaging function:

$$\begin{aligned}(4.3)\quad & E[I_{sim}(\Delta x, \Delta z)] \sim \\ & \omega_c^4 C_p(\phi) C_s(\phi) A^{-1} \int_{-A/2}^{A/2} C([\Delta x(a/h) + \Delta z](\frac{1}{c_s} - \frac{1}{c_p})/l) + C(\frac{h\cos\phi - h + \frac{h^2}{2\tilde{l}}}{lc_p}) da.\end{aligned}$$

Consider a special case with assumption that $\hat{C} = \mathcal{F}(e^{-B|t|}) I_{[l,\infty)}$, support $\hat{C} = O(B)$, and $l \ll 1/B$. By the above assumptions, we can change (4.3) into:

$$E[I_{sim}(\Delta x, \Delta z)] \sim \omega_c^4 C_p(\phi) C_s(\phi) A^{-1} \int_{-A/2}^{A/2} e^{-\frac{|\Delta z + \Delta x(a/h)|}{\bar{\lambda}_{p,s}}} + e^{-\frac{|h\cos\phi - h + \frac{h^2}{2\tilde{l}}|}{l\lambda_p}} da,$$

where $\lambda_s = c_s/B$; $\lambda_p = c_p/B$; $\bar{\lambda}_{p,s} = \frac{\lambda_s \lambda_p}{\lambda_p - \lambda_s}$.

Assume that

$$\begin{aligned}l_1 =& \omega_c^4 C_p(\phi) C_s(\phi) A^{-1} \int_{-A/2}^{A/2} e^{-\frac{|\Delta z + \Delta x(a/h)|}{\bar{\lambda}_{p,s}}} da \\ l_2 =& \omega_c^4 C_p(\phi) C_s(\phi) A^{-1} \int_{-A/2}^{A/2} e^{-\frac{|h\cos\phi - h + \frac{h^2}{2\tilde{l}}|}{l\lambda_p}} da,\end{aligned}$$

where l_1 is the expection of the original imaging function; l_2 is the incident waves' contribution and l_2 is a constant which is much smaller than l_1, as a result,

$$\begin{aligned}E[I_{sim}(\Delta x, \Delta z)] =& l_1 + l_2 \\ =& E[I(\Delta x, \Delta z)] + constant \\ \sim& E[I(\Delta x, \Delta z)].\end{aligned}$$

As a result, the incident waves' component will not influence the image a lot, so the resolution

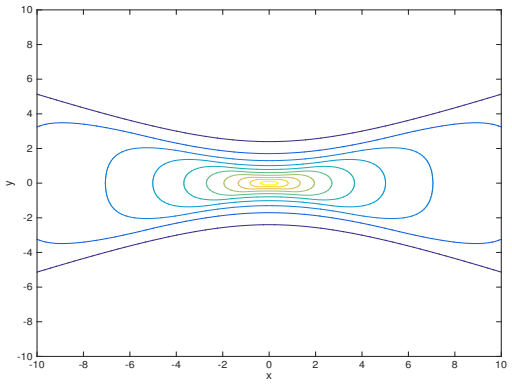

(a) The Contour of PSF

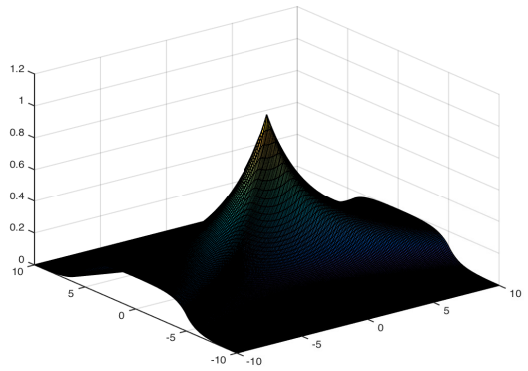

(b) The Surface of PSF

Figure 4.7: PSF with Incident Waves' Contribution

analysis of this case can follow the above section.

Now let $\Delta\tilde{z} = \frac{\Delta z}{\bar{\lambda}_{p,s}}$ and $\Delta\tilde{x} = \frac{\Delta x}{\bar{\lambda}_{p,s}}\frac{A}{h}$, then we can get

$$E[\tilde{I}_{sim}(\Delta\tilde{x}, \Delta\tilde{z})] \sim \omega_c^4 C_p(\phi) C_s(\phi) A^{-1} \int_{-A/2}^{A/2} e^{-|\Delta\tilde{z}+\Delta\tilde{x}\frac{a}{A}|} da + \epsilon \sim \int_{-1/2}^{1/2} e^{-|\Delta\tilde{z}+\Delta\tilde{x}a'|} da' + \epsilon,$$

where ϵ denotes a small constant.

Thus, similarly, the transverse radius of the focal spot is $\frac{h\bar{\lambda}_{p,s}}{A}$ and the longitudinal radius of the focal spot is $\bar{\lambda}_{p,s}$. They are same as the values achieved in the last section. Since SNR is much larger than 1, the incident waves' component influences the image only a little, therefore, it will not change the radius of the focal spot. Also, we can achieve almost the same figure of Point Spread Function. See Figure 4.7, it is the time-reversed focal spot in the time harmonic regime, where x in multiples of $\frac{h\bar{\lambda}_{p,s}}{A}$ and z in multiples of $\bar{\lambda}_{p,s}$. Figure 4.7 and Figure 4.6 are almost same.

□

4.4 With Unknown Pulse Source Case

In this section, we will present the resolution anlysis in Unknown Pulse Source Case.

4.4.1 With Rectangular Pulse Source Case

In this subsection, we assume that we have a rectangular pulse source, but we do not know the location of the source.

Proposition 4.4.1. *Suppose we have a rectangular pulse source and the location of the source is unknown, then*

$$\begin{aligned}\textbf{PSF} \sim & \omega_c^4 C_p(\phi) C_s(\phi) A^{-1} \int_{-A/2}^{A/2} (2\tau - |\Delta\tilde{z} + \Delta\tilde{x}\frac{a}{A}|) da \\ \sim & \int_{-1/2}^{1/2} -|\Delta\tilde{z} + \Delta\tilde{x}a^{'}| da^{'}.\end{aligned}$$

In addition, the transverse radius of the focal spot is $\frac{h\bar{\lambda}_{p,s}}{A}$ *and the longitudinal radius of the focal spot is* $\bar{\lambda}_{p,s}$*, where* $\bar{\lambda}_{p,s}$ *is harmonic difference resolution.*

Proof. From the Unknown Source Case section, we can get

$$I(\Delta x, \Delta z) \sim \omega_c^4 C_p(\phi) C_s(\phi) A^{-1} \int_{-A/2}^{A/2} C(\frac{\frac{r(a)-r^{\Delta}(a)}{c_p} - \frac{r(a)-r^{\Delta}(a)}{c_s}}{l}) da.$$

Since $r(a) - r^{\Delta}(a) \sim \Delta x(a/h) + \Delta z(1 - \frac{1}{2}(a/h)^2)$, then we can have the following formula (4.1) as before. Similarly, since $1 - \frac{1}{2}(a/h)^2$ is very close to 1 when $a \ll h$,

$$E[I(\Delta x, \Delta z)] \sim \omega_c^4 C_p(\phi) C_s(\phi) A^{-1} \int_{-A/2}^{A/2} C((\Delta x(a/h) + \Delta z)(\frac{1}{c_s} - \frac{1}{c_p})/l) da.$$

Suppose the rectangular pulse source is defined as:

$$\rho_\tau(t) = \begin{cases} 1 & -\tau \le t \le \tau \\ 0 & \text{otherwise.} \end{cases} \tag{4.4}$$

At the end of Chapter 2, we introduce the definition of the correlation function: $C(\frac{\Delta t}{l}) = E[v(t)v(t + \Delta t)]$, where l is the correlation length and $l = \frac{1}{C(0)} \int_{-\infty}^{\infty} C(h) dh$. In this section,

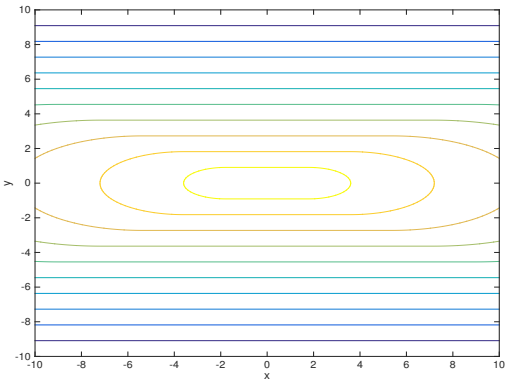

(a) The Contour of Point Spread Function

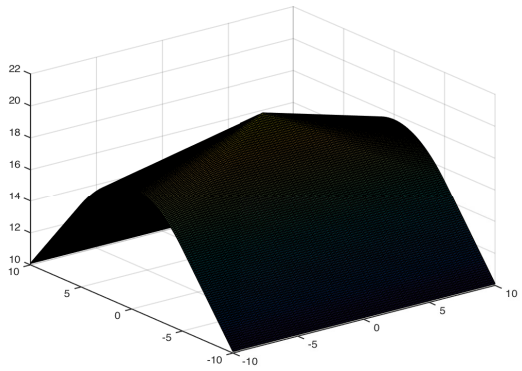

(b) The Surface of Point Spread Function

Figure 4.8: Point Spread Function with Rectangular Pulse Source

$v(t) = \rho_\tau(t)$, as a result,

$$C(t) = \begin{cases} 2\tau - t & t > 0 \\ 2\tau + t & t \leq 0. \end{cases} \tag{4.5}$$

By the above assumptions, we can change (4.1) into:

$$\begin{aligned} E[I(\Delta x, \Delta z)] \sim & \omega_c^4 C_p(\phi) C_s(\phi) A^{-1} \int_{-A/2}^{A/2} (2\tau - |\frac{r(a) - r^\Delta(a)}{c_p} - \frac{r(a) - r^\Delta(a)}{c_s}|) da \\ \sim & \omega_c^4 C_p(\phi) C_s(\phi) A^{-1} \int_{-A/2}^{A/2} (2\tau - |(\Delta x(a/h) + \Delta z)(\frac{1}{c_s} - \frac{1}{c_p})|) da. \end{aligned}$$

Assume that $\bar{\lambda}_{p,s} = \frac{\lambda_p \lambda_s}{\lambda_p - \lambda_s}$, if we let $\Delta\tilde{z} = \frac{\Delta z}{\bar{\lambda}_{p,s}}$ and $\Delta\tilde{x} = \frac{\Delta x}{\bar{\lambda}_{p,s}} \frac{A}{h}$, then we can get

$$E[\tilde{I}(\Delta\tilde{x}, \Delta\tilde{z})] \sim \omega_c^4 C_p(\phi) C_s(\phi) A^{-1} \int_{-A/2}^{A/2} (2\tau - |\Delta\tilde{z} + \Delta\tilde{x}\frac{a}{A}|) da \sim \int_{-1/2}^{1/2} -|\Delta\tilde{z} + \Delta\tilde{x} a'| da'.$$

Thus, the transverse radius of the focal spot is $\frac{h\bar{\lambda}_{p,s}}{A}$ and the longitudinal radius of the focal spot is $\bar{\lambda}_{p,s}$. In Figure 4.8, it is the time-reversed focal spot in the time harmonic regime, where x in multiples of $\frac{h\bar{\lambda}_{p,s}}{A}$ and z in multiples of $\bar{\lambda}_{p,s}$.

□

4.4.2 With Continous Pulse Source Case

In this section, we assume that we have a continous pulse source, and the resolution analysis in this case will be presented later in this section.

Proposition 4.4.2. *Suppose we have a continous pulse source and the location of the source is unknown, then*

$$\begin{aligned}\textbf{PSF} \sim & \omega_c^4 C_p(\phi) C_s(\phi) A^{-1} \int_{-A/2}^{A/2} \cos(\omega_0(\Delta\tilde{z} + \Delta\tilde{x}\frac{a}{A})) e^{-(\Delta\tilde{z}+\Delta\tilde{x}\frac{a}{A})^2/4t_0^2} da \\ \sim & \int_{-1/2}^{1/2} \cos(\omega_0(\Delta\tilde{z} + \Delta\tilde{x}a^{'})) e^{-(\Delta\tilde{z}+\Delta\tilde{x}a^{'})^2/4t_0^2} da^{'}.\end{aligned}$$

In addition, the transverse radius of the focal spot is $\frac{h\bar{\lambda}_{p,s}}{A}$ *and the longitudinal radius of the focal spot is* $\bar{\lambda}_{p,s}$*, where* $\bar{\lambda}_{p,s}$ *is harmonic difference resolution.*

Proof. From the Unknown Source Case section, we can get

$$I(\Delta x, \Delta z) \sim \omega_c^4 C_p(\phi) C_s(\phi) A^{-1} \int_{-A/2}^{A/2} C(\frac{\frac{r(a)-r^{\Delta}(a)}{c_p} - \frac{r(a)-r^{\Delta}(a)}{c_s}}{l}) da.$$

Similarly,

$$E[I(\Delta x, \Delta z)] \sim \omega_c^4 C_p(\phi) C_s(\phi) A^{-1} \int_{-A/2}^{A/2} C((\Delta x(a/h) + \Delta z)(\frac{1}{c_s} - \frac{1}{c_p})/l) da.$$

Assume that our source is a continuous pulse source:

$$\rho(t) = \cos(\omega_0 t) e^{-(\frac{t}{t_0})^2/2},$$

where ω_0 and t_0 are parameters and $\omega_0 \gg \frac{1}{t_0}$. By the definition of the correlation function: $C(\frac{\Delta t}{l}) = E[v(t)v(t+\Delta t)]$, where l is the correlation length and $l = \frac{1}{C(0)} \int_{-\infty}^{\infty} C(h) dh$. Assume

that the source$v(t) = \rho(t)$, as a result,

$$\begin{aligned}
C(\Delta t) &\sim \int \rho(\frac{t}{\tau})\rho(\frac{t+\Delta t}{\tau})dt \\
&\sim \int \rho(t)\rho(t+\frac{\Delta t}{\tau})dt \\
&\sim \int (\cos(\omega_0 t)e^{-(\frac{t}{t_0})^2/2})(\cos(\omega_0(t+\frac{\Delta t}{\tau}))e^{-(\frac{t+\frac{\Delta t}{\tau}}{t_0})^2/2})dt \\
&\sim (\cos(\omega_0 t)\cos(\omega_0(t+\frac{\Delta t}{\tau})))e^{-(\frac{t}{t_0})^2/2-(\frac{t+\Delta t/\tau}{t_0})^2/2}dt \\
&\sim e^{-\left(\frac{\Delta t/\tau}{2t_0}\right)^2}\int (\cos(2\omega_0 t+\omega_0\Delta t/\tau)+\cos(\omega_0\Delta t/\tau))e^{-\frac{(t+\Delta t/(2\tau))^2}{t_0^2}}dt \\
&\sim e^{-\left(\frac{\Delta t/\tau}{2t_0}\right)^2}\int (\cos(2\omega_0 s)+\cos(\omega_0\Delta t/\tau))e^{-\frac{s^2}{t_0^2}}ds \\
&\sim I_1 + I_2,
\end{aligned}$$

where C is the correlation function, τ is the duration time of the pulse, $I_1 = \int \cos(2\omega_0 s)e^{-\frac{s^2}{t_0^2}}ds$, and $I_2 = \int \cos(\omega_0\Delta t/\tau)e^{-\frac{s^2}{t_0^2}}ds$.

Since $I_1 = o(t_0)$ and $I_2 = O(t_0)$,

$$C(\Delta t) \sim \cos(\omega_0\Delta t/\tau)e^{-\left(\frac{\Delta t/\tau}{2t_0}\right)^2}.$$

By the above assumptions, we can change (4.2) into:

$$\begin{aligned}
E[I(\Delta x,\Delta z)] &\sim \omega_c^4 C_p(\phi)C_s(\phi)A^{-1}\int_{-A/2}^{A/2}\cos(\omega_0(r(a)-r^{\Delta}(a))(\frac{1}{c_p}-\frac{1}{c_s})/\tau)e^{-\left(\frac{r(a)-r^{\Delta}(a)}{2t_0c_p\tau}-\frac{r(a)-r^{\Delta}(a)}{2t_0c_s\tau}\right)^2}da \\
&\sim \omega_c^4 C_p(\phi)C_s(\phi)A^{-1}\int_{-A/2}^{A/2}\cos(\omega_0(\Delta x(a/h)+\Delta z)(\frac{1}{c_s}-\frac{1}{c_p}))e^{-(\Delta x(a/h)+\Delta z)^2(\frac{1}{2t_0c_s}-\frac{1}{2t_0c_p})^2}da.
\end{aligned}$$

Since $\lambda_p = c_p/\tau$, $\lambda_s = c_s/\tau$ and $\bar{\lambda}_{p,s} = \frac{\lambda_p\lambda_s}{\lambda_p-\lambda_s}$, if we let $\Delta\tilde{z} = \frac{\Delta z}{\bar{\lambda}_{p,s}}$ and $\Delta\tilde{x} = \frac{\Delta x}{\bar{\lambda}_{p,s}}\frac{A}{h}$, then we can get

$$\begin{aligned}
E[\tilde{I}(\Delta\tilde{x},\Delta\tilde{z})] &\sim \omega_c^4 C_p(\phi)C_s(\phi)A^{-1}\int_{-A/2}^{A/2}\cos(\omega_0(\Delta\tilde{z}+\Delta\tilde{x}\frac{a}{A}))e^{-(\Delta\tilde{z}+\Delta\tilde{x}\frac{a}{A})^2/4t_0^2}da \\
&\sim \int_{-1/2}^{1/2}\cos(\omega_0(\Delta\tilde{z}+\Delta\tilde{x}a'))e^{-(\Delta\tilde{z}+\Delta\tilde{x}a')^2/4t_0^2}da'.
\end{aligned}$$

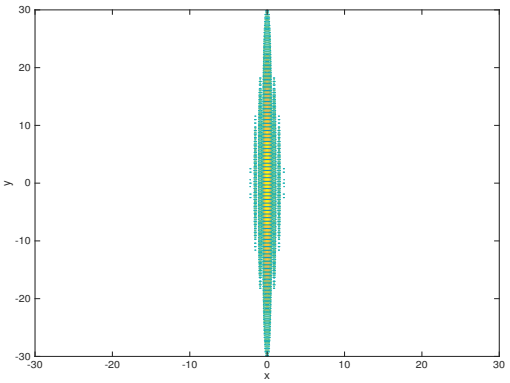

(a) The Contour of Point Spread Function

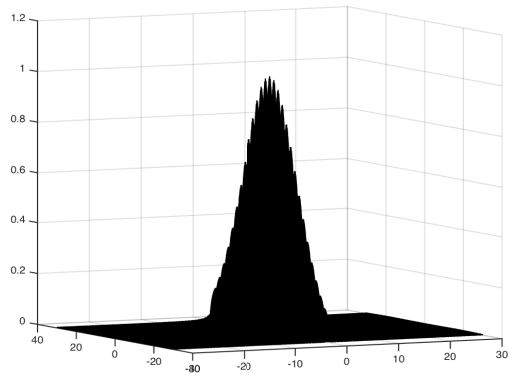

(b) The Surface of Point Spread Function

Figure 4.9: Point Spread Function with Continuous Pulse Source

Thus, the transverse radius of the focal spot is $\frac{h\bar{\lambda}_{p,s}}{A}$ and the longitudinal radius of the focal spot is $\bar{\lambda}_{p,s}$. In Figure 4.9, it is the time-reversed focal spot in the time harmonic regime, where x in multiples of $\frac{h\bar{\lambda}_{p,s}}{A}$ and z in multiples of $\bar{\lambda}_{p,s}$.

□

Chapter 5

Stability Analysis

Elastic imaging involves how measurement and medium noises are modeled and how the imaging process handles them-that is, whether they are suppressed or amplified. Measurememt and medium noises affect the stability of the imaging functionals in very different ways. The principle objective of this chapter is to carry out a detailed stability analysis of the topological derivative based imaging functionals with respect to noises.

5.1 Fundamental Results

Before analyzing the stability of the imaging functions, we need to introduce the important results in [5].

Proposition 5.1.1 ([5]). *Suppose $z_n = z(t_n)$ for $(n = 1, 2, \ldots, N)$ are samples from zero-mean, complex Gaussian video process $z(t)$.*

a). If $s \neq t$, then

$$E_{\bar{z}_{m_1}\bar{z}_{m_2}\ldots\bar{z}_{m_s}z_{n_1}z_{n_2}\ldots z_{n_t}} = 0$$

where m_k and n_i are integers from set $\{1, 2, 3, \ldots, N\}$.

b). If $s = t$, then

$$\begin{aligned} &E_{\bar{z}_{m_1}\bar{z}_{m_2}\ldots\bar{z}_{m_s}z_{n_1}z_{n_2}\ldots z_{n_t}} \\ =&\sum_{\pi}(E\bar{z}_{m_{\pi(1)}}z_{n_1})(E\bar{z}_{m_{\pi(2)}}z_{n_2})\ldots(E\bar{z}_{m_{\pi(t)}}z_{n_t}), \end{aligned}$$

where π is a permutation of the set of integers $\{1, 2, 3, \ldots, t\}$.

Corollary 5.1.1 ([5]). *Suppose that $v(z)$ is a complex, circulary symmetric Gaussian process, then*

$$\begin{aligned} &E[\bar{v}(z_1)\bar{v}(z_2)v(z_3)v(z_4)] \\ =&E[\bar{v}(z_1)v(z_3)]E[\bar{v}(z_2)v(z_4)] + E[\bar{v}(z_2)v(z_3)]E[\bar{v}(z_1)v(z_4)]. \end{aligned}$$

Proposition 5.1.2 (Moment Theorem for Circular Symmetric Complex Gaussian Variables [5]). *Suppose that $z_j^{'}s$ are complex circular symmetric Gaussian random vectors, then*

$$E[z_1z_2z_3z_4] = E[z_1z_2]E[z_3z_4] + E[z_1z_3]E[z_2z_4] + E[z_1z_4]E[z_2z_3].$$

5.2 Stability Analysis based on Imaging Functions

5.2.1 Stability Analysis in Known Source Case

In this section, we will utilize Signal-to-noise ratio(SNR) to analyze the stability in Known Source Case.

SNR is defined as the ratio of the power of a signal (meaningful information) and the power of background noise (unwanted signal):

$$\textbf{SNR} = \frac{|E[I(0,0)]|^2}{\mathrm{Var}[I(0,0)]}.$$

Proposition 5.2.1. *Suppose we have a known source which is a stationary stochastic process. Then the signal-to-noise ratio in the known source case either with only P component*

scattering waves or with only S component scattering waves is as below:

$$\begin{aligned}\textbf{SNR} \geq & \frac{(\int_R \omega^2 \hat{C}(\omega)\, d\omega)^2}{(\int_R \hat{C}(\omega)\, d\omega)\sup_\omega(\omega^4 \hat{C}(\omega))} \frac{T}{4\int_R \mathrm{sinc}^2(s)\, ds} \\ \geq & \left(\frac{T}{\tau}\right)\frac{2\pi}{\sqrt{2\pi}}\frac{1}{16} \\ \approx & \frac{0.157T}{\tau},\end{aligned}$$

where C is the correlation function and the correlation time is τ. In addition, **SNR** *in the P component scattering case is the same as that in the S component case.*

Proof. Recall the form of our imaging function in the known source case with respect to P waves only from the above chapters:

$$\begin{aligned}I(\Delta x, \Delta z) \sim & \iiiint \mathcal{F}(\bar{v}(t + \frac{l'}{c_p}))\mathcal{F}(v(t + \frac{\tilde{l}}{c_p} + \frac{r(a)}{c_p} - \frac{r^\Delta(a)}{c_p}))d\omega d\tilde{\omega} dt da \\ \sim & \iiiint \bar{\hat{v}}(\tilde{\omega}) e^{i\tilde{\omega}l'/c_p} \hat{v}(\omega) e^{-i\omega\tilde{l}/c_p} \omega^2 e^{-i\omega r(a)/c_p} e^{i\omega r^\Delta(a)/c_p} e^{-i(\omega-\tilde{\omega})t} d\omega d\tilde{\omega} dt da \\ \sim & T^{-1}\int_R d\omega \int_R d\tilde{\omega} \int_{-\frac{T}{2}}^{\frac{T}{2}} \chi_A(\omega, \tilde{\omega}) e^{i(\tilde{\omega}-\omega)t} \hat{v}(\omega)\bar{\hat{v}}(\tilde{\omega}) dt.\end{aligned}$$

Here,

$$\begin{aligned}\chi_A(\omega, \tilde{\omega}) = & \chi_A(\omega, \tilde{\omega}; \Delta x, \Delta z) \\ = & A^{-1}\int_{-A/2}^{A/2} \omega^2 C_p(\phi) e^{i\tilde{\omega}l'/c_p} e^{-i\omega\tilde{l}/c_p} e^{-i\omega r(a)/c_p} e^{i\omega r^\Delta(a)/c_p} da.\end{aligned}$$

Then,

$$\begin{aligned}E[I(\Delta x, \Delta z)] = & T^{-1}\int_R d\omega \int_R d\tilde{\omega} \int_{-T/2}^{T/2} \chi_A(\omega, \tilde{\omega}) e^{i(\tilde{\omega}-\omega)t} \hat{C}(\omega)\delta(\omega - \tilde{\omega}) dt \\ = & \int_R \chi_A(\omega, \omega)\hat{C}(\omega) d\omega.\end{aligned}$$

The variance of the imaging function is:

$$\begin{aligned}Var[I(\Delta x,\Delta z)] =& E[|I^2(\Delta x,\Delta z)|]-|E[I(\Delta x,\Delta z)]|^2\\ =&\int_R d\omega\int_R d\tilde{\omega}\int_R d\omega'\int_R d\tilde{\omega}' T^{-2}\int_{-T/2}^{T/2}dt\int_{-T/2}^{T/2}dt'\\ &\chi_A(\omega,\tilde{\omega})\bar{\chi}_A(\omega',\tilde{\omega}')e^{i(\tilde{\omega}-\omega)t}e^{-i(\tilde{\omega}'-\omega')t'}\\ &(E[\bar{\hat{v}}(\tilde{\omega})\hat{v}(\omega)\hat{v}(\tilde{\omega}')\bar{\hat{v}}(\omega')]-E[\bar{\hat{v}}(\tilde{\omega})\hat{v}(\omega)]E[\hat{v}(\tilde{\omega}')\bar{\hat{v}}(\omega')]).\end{aligned}$$

Using Theorem 2, then

$$\begin{aligned}Var[I(\Delta x,\Delta z)] =&\int_R d\omega\int_R d\tilde{\omega}\int_R d\omega'\int_R d\tilde{\omega}' T^{-2}\int_{-T/2}^{T/2}dt\int_{-T/2}^{T/2}dt'\\ &\chi_A(\omega,\tilde{\omega})\bar{\chi}_A(\omega',\tilde{\omega}')e^{i(\tilde{\omega}-\omega)t}e^{-i(\tilde{\omega}'-\omega')t'}\\ &(E[\bar{\hat{v}}(\tilde{\omega})\hat{v}(\tilde{\omega}')]E[\hat{v}(\omega)\bar{\hat{v}}(\omega')]+E[\bar{\hat{v}}(\tilde{\omega})\bar{\hat{v}}(\omega')]E[\hat{v}(\omega)\hat{v}(\tilde{\omega}')])\\ =&\int_R d\omega\int_R d\tilde{\omega}\int_R d\omega'\int_R d\tilde{\omega}' T^{-2}\int_{-T/2}^{T/2}dt\int_{-T/2}^{T/2}dt'\\ &\chi_A(\omega,\tilde{\omega})\bar{\chi}_A(\omega',\tilde{\omega}')e^{i(\tilde{\omega}-\omega)t}e^{-i(\tilde{\omega}'-\omega')t'}\\ &(\hat{C}(\tilde{\omega})\delta(\tilde{\omega}-\tilde{\omega}')\bar{\hat{C}}(\omega)\delta(\omega-\omega')+\hat{C}(\tilde{\omega})\delta(\tilde{\omega}+\omega')\bar{\hat{C}}(\omega)\delta(\omega+\tilde{\omega}')).\end{aligned}$$

We can simplify the above function:

$$\begin{aligned}Var[I(\Delta x,\Delta z)] =&\int_R d\omega\int_R d\tilde{\omega}T^{-2}\int_{-T/2}^{T/2}dt\int_{-T/2}^{T/2}dt'\\ &\chi_A(\omega,\tilde{\omega})\bar{\chi}_A(\omega,\tilde{\omega})\hat{C}(\tilde{\omega})\bar{\hat{C}}(\omega)e^{i(\tilde{\omega}-\omega)t}e^{-i(\tilde{\omega}-\omega)t'}\\ &+\int_R d\omega\int_R d\tilde{\omega}T^{-2}\int_{-T/2}^{T/2}dt\int_{-T/2}^{T/2}dt'\\ &\chi_A(\omega,\tilde{\omega})\bar{\chi}_A(-\tilde{\omega},-\omega)\hat{C}(\tilde{\omega})\bar{\hat{C}}(\omega)e^{i(\tilde{\omega}-\omega)t}e^{-i(\tilde{\omega}-\omega)t'}\\ =&2\int_R d\omega\int_R d\tilde{\omega}\ \chi_A(\omega,\tilde{\omega})\bar{\chi}_A(\omega,\tilde{\omega})\hat{C}(\tilde{\omega})\bar{\hat{C}}(\omega)\mathrm{sinc}^2(\frac{(\tilde{\omega}-\omega)T}{2}).\end{aligned}$$

Consider $(\Delta x,\Delta z)=(0,0)$, then

$$E[I(0,0)]=C_p(\phi)\int_R\omega^2\hat{C}(\omega)d\omega.$$

Note that

$$|\chi_A(\omega,\tilde{\omega})| \leq C_p(\phi)\omega^2,$$

then,

$$Var[I(0,0)] \leq 2\int_R d\omega \int_R d\tilde{\omega}\ \omega^4 \hat{C}(\tilde{\omega})\hat{C}(\omega)\mathrm{sinc}^2(\frac{(\tilde{\omega}-\omega)T}{2})(C_p(\phi))^2,$$

where $\hat{C}$ is real and positive.

Assume that v is smooth and

$$\sup_{\omega}(\hat{C}(\omega)) \leq \mathcal{C} < \infty,$$

then

$$Var[I(0,0)] \leq 2\mathcal{C}\frac{2}{T}(\int_R \mathrm{sinc}^2(s)ds)(\int_R \omega^4\hat{C}(\omega)d\omega)(C_p(\phi))^2.$$

Then,

$$\begin{aligned}\textbf{SNR} =& \frac{|E[I(0,0)]|^2}{Var[I(0,0)]} \\ \geq& \frac{(\int_R \omega^2\hat{C}(\omega)d\omega)^2}{(\int_R \omega^4\hat{C}(\omega)d\omega)\sup_\omega(\omega^4\hat{C}(\omega))}\frac{T}{4\int_R \mathrm{sinc}^2(s)ds}.\end{aligned}$$

Suppose that the correlation time is τ, then $\hat{C}(\omega) = \tau\hat{\tilde{C}}(\tau\omega)$, with $\tilde{C}$ non-dimensionalized and $O(1)$ support. Thus,

$$\textbf{SNR} \geq \frac{(\int_R s^2\hat{\tilde{C}}(s)ds)^2}{(\int_R s^4\hat{\tilde{C}}(s)ds)\sup_s(s^4\hat{\tilde{C}}(s))}\frac{1}{4\int_R \mathrm{sinc}^2(s)ds}\frac{T}{\tau}.$$

WLOG, we assume that $\tilde{C}(s)$ is Gaussian, then

$$\int_R \hat{\tilde{C}}(s)\,ds = 2\int_0^\infty e^{-\frac{s^2}{2}}\,ds = \sqrt{2\pi}.$$

Moreover,

$$\int_R s^2\hat{\tilde{C}}(s)\,ds = 2\int_0^\infty s^2 e^{-\frac{s^2}{2}}\,ds = \sqrt{2\pi}.$$

Under the same assumption, to achieve the maximum of $\hat{\tilde{C}}(s)$, we only need to make

$$\frac{d}{ds}e^{-\frac{s^2}{2}} = 0.$$

After solving the above equation, we can get $s = 0$. Thus,

$$\sup_s(\hat{\tilde{C}}(s)) = 1.$$

In addition, we know that

$$\int_R \mathrm{sinc}^2(s)\, ds \leq 2\left(1 + \int_1^\infty x^{-2}\, dx\right) \leq 4.$$

Therefore,

$$\mathbf{SNR} \geq (\frac{T}{\tau})\frac{2\pi}{3\sqrt{2\pi}}\frac{1}{16} \approx \frac{0.83T}{\tau}.$$

In conlusion, considering P scattering waves, SNR depends on the correlation time and the time domain only: the longer the time domain is, the better quality of the image is; the shorter the correlation time is, the better quality of the image is.

Similarly, considering the S component scattering waves, our imaging function in the known source case is as below:

$$\begin{aligned} I(\Delta x, \Delta z) &\sim \iiiint \mathcal{F}(\bar{v}(t + \frac{l'}{c_p}))\mathcal{F}(v(t + \frac{\tilde{l}}{c_p} + \frac{r(a)}{c_p} - \frac{r^\Delta(a)}{c_p}))d\omega d\tilde{\omega} dt da \\ &\sim \iiiint \bar{\hat{v}}(\tilde{\omega})e^{i\tilde{\omega}l'/c_p}\hat{v}(\omega)e^{-i\omega\tilde{l}/c_p}\omega^2 e^{-i\omega r(a)/c_s}e^{i\omega r^\Delta(a)/c_s}e^{-i(\omega-\tilde{\omega})t}d\omega d\tilde{\omega} dt da \\ &\sim T^{-1}\int_R d\omega \int_R d\tilde{\omega} \int_{-\frac{T}{2}}^{\frac{T}{2}} \chi_A(\omega, \tilde{\omega})e^{i(\tilde{\omega}-\omega)t}\hat{v}(\omega)\bar{\hat{v}}(\tilde{\omega})dt. \end{aligned}$$

Here,

$$\begin{aligned} \chi_A(\omega, \tilde{\omega}) =& \chi_A(\omega, \tilde{\omega}; \Delta x, \Delta z) \\ =& A^{-1}\int_{-A/2}^{A/2} \omega^2 C_s(\phi)e^{i\tilde{\omega}l'/c_p}e^{-i\omega\tilde{l}/c_p}e^{-i\omega r(a)/c_s}e^{i\omega r^\Delta(a)/c_s}da. \end{aligned}$$

Similarly,

$$\mathbf{SNR} \geq (\frac{T}{\tau})\frac{2\pi}{\sqrt{2\pi}}\frac{1}{16} \approx \frac{0.157T}{\tau}.$$

We will hold the same conclusion as above. In the following section, we will analyse stability in the unknown source case. □

5.2.2 Stability Analysis in Unknown Source Case

In this section, we analyze the stability in Unknown Source Case.

Proposition 5.2.2. *Suppose we have an unknown source, based on the imaging function in the unknown source case, we have the signal-to-noise ratio(SNR) in the unknown source case:*

$$\begin{aligned}\mathbf{SNR} =&\frac{|E[I(0,0)]|^2}{\mathrm{Var}[I(0,0)]}\\ \geq&\frac{\int_R \omega^4\hat{C}(\omega)d\omega}{\sup_\omega(\omega^4\hat{C}(\omega))}\frac{T}{4\int_R \mathrm{sinc}^2(s)ds}\\ \geq&(\frac{T}{\tau})\frac{3\sqrt{2\pi}}{16e^{-2}}\frac{1}{16} \approx \frac{T}{5\tau},\end{aligned}$$

where C is the correlation function, and the correlation time is τ, then $\hat{C}(\omega) = \tau\hat{\tilde{C}}(\tau\omega)$, with $\tilde{C}$ non-dimensionalized and $O(1)$ support.

Proof. Recall the form of our imaging function in the unknown source case from the above chapters:

$$\begin{aligned}I(\Delta x,\Delta z) =&T^{-1}A^{-1}\int_{-T/2}^{T/2}\int_{-A/2}^{A/2}\mathbf{U}_{sc}\cdot\vec{e_3}(t-r^\Delta(a)/c_p)*\mathbf{U}_{sc}\cdot\vec{e_1}(t-r^\Delta(a)/c_s)dtda\\ =&T^{-1}A^{-1}\iiiint \omega^2\tilde{\omega}^2C_p(\phi)C_s(\phi)e^{-ik_p(r(a)+\tilde{l})}e^{i\tilde{k_s}r(a)+i\tilde{k_p}\tilde{l}}\\ &\hat{v}(\omega)\bar{\hat{v}}(\tilde{\omega})e^{ik_pr^\Delta(a)-i\tilde{k_s}r^\Delta(a)-i\omega t+i\tilde{\omega}t}\,dtdad\omega d\tilde{\omega}\\ =&T^{-1}\int_R d\omega\int_R d\tilde{\omega}\int_{-T/2}^{T/2}\chi_A(\omega,\tilde{\omega})e^{i(\tilde{\omega}-\omega)t}\hat{v}(\omega)\bar{\hat{v}}(\tilde{\omega})dt.\end{aligned}$$

Here,

$$\begin{aligned}\chi_A(\omega,\tilde{\omega}) =&\chi_A(\omega,\tilde{\omega};\Delta x,\Delta z)\\ =&A^{-1}\int_{-A/2}^{A/2}\omega^2\tilde{\omega}^2C_p(\phi)C_s(\phi)e^{-ik_p(r(a)+\tilde{l})}e^{i\tilde{k_s}r(a)+i\tilde{k_p}\tilde{l}}e^{ik_pr^{\Delta}(a)-i\tilde{k_s}r^{\Delta}(a)}da\\ =&A^{-1}\int_{-A/2}^{A/2}\omega^2\tilde{\omega}^2C_p(\phi)C_s(\phi)e^{i\tilde{l}(\tilde{\omega}-\omega)/c_p+i(\tilde{\omega}/c_s-\omega/c_p)(r(a)-r^{\Delta}(a))}da.\end{aligned}$$

Then,

$$\begin{aligned}E[I(\Delta x,\Delta z)] =&T^{-1}\int_R d\omega\int_R d\tilde{\omega}\int_{-T/2}^{T/2}\chi_A(\omega,\tilde{\omega})e^{i(\tilde{\omega}-\omega)t}\hat{C}(\omega)\delta(\omega-\tilde{\omega})dt\\ =&\int_R\chi_A(\omega,\omega)\hat{C}(\omega)d\omega.\end{aligned}$$

The variance of the imaging function is:

$$\begin{aligned}Var[I(\Delta x,\Delta z)] =&E[|I^2(\Delta x,\Delta z)|]-|E[I(\Delta x,\Delta z)]|^2\\ =&\int_R d\omega\int_R d\tilde{\omega}\int_R d\omega'\int_R d\tilde{\omega'}\int_{-T/2}^{T/2}dt\int_{-T/2}^{T/2}dt'\\ &T^{-2}\chi_A(\omega,\tilde{\omega})\bar{\chi}_A(\omega',\tilde{\omega'})e^{i(\tilde{\omega}-\omega)t}e^{-i(\tilde{\omega'}-\omega')t'}\\ &(E[\bar{\hat{v}}(\tilde{\omega})\hat{v}(\omega)\hat{v}(\tilde{\omega'})\bar{\hat{v}}(\omega')]-E[\bar{\hat{v}}(\tilde{\omega})\hat{v}(\omega)]E[\hat{v}(\tilde{\omega'})\bar{\hat{v}}(\omega')]).\end{aligned}$$

Using Theorem 2, then

$$\begin{aligned}Var[I(\Delta x,\Delta z)] =&\int_R d\omega\int_R d\tilde{\omega}\int_R d\omega'\int_R d\tilde{\omega'}\int_{-T/2}^{T/2}dt\int_{-T/2}^{T/2}dt'\\ &T^{-2}\chi_A(\omega,\tilde{\omega})\bar{\chi}_A(\omega',\tilde{\omega'})e^{i(\tilde{\omega}-\omega)t}e^{-i(\tilde{\omega'}-\omega')t'}\\ &(E[\bar{\hat{v}}(\tilde{\omega})\hat{v}(\tilde{\omega'})]E[\hat{v}(\omega)\bar{\hat{v}}(\omega')]+E[\bar{\hat{v}}(\tilde{\omega})\bar{\hat{v}}(\omega')]E[\hat{v}(\omega)\hat{v}(\tilde{\omega'})])\\ =&\int_R d\omega\int_R d\tilde{\omega}\int_R d\omega'\int_R d\tilde{\omega'}\int_{-T/2}^{T/2}dt\int_{-T/2}^{T/2}dt'\\ &T^{-2}\chi_A(\omega,\tilde{\omega})\bar{\chi}_A(\omega',\tilde{\omega'})e^{i(\tilde{\omega}-\omega)t}e^{-i(\tilde{\omega'}-\omega')t'}\\ &(\hat{C}(\tilde{\omega})\delta(\tilde{\omega}-\tilde{\omega'})\bar{\hat{C}}(\omega)\delta(\omega-\omega')+\hat{C}(\tilde{\omega})\delta(\tilde{\omega}+\omega')\bar{\hat{C}}(\omega)\delta(\omega+\tilde{\omega'})).\end{aligned}$$

We can simplify the above function:

$$\begin{aligned}
Var[I(\Delta x, \Delta z)] = &\int_R d\omega \int_R d\tilde{\omega} T^{-2} \int_{-T/2}^{T/2} dt \int_{-T/2}^{T/2} dt' \\
&\chi_A(\omega, \tilde{\omega}) \bar{\chi}_A(\omega, \tilde{\omega}) \hat{C}(\tilde{\omega}) \bar{\hat{C}}(\omega) e^{i(\tilde{\omega}-\omega)t} e^{-i(\tilde{\omega}-\omega)t'} \\
&+ \int_R d\omega \int_R d\tilde{\omega} T^{-2} \int_{-T/2}^{T/2} dt \int_{-T/2}^{T/2} dt' \\
&\chi_A(\omega, \tilde{\omega}) \bar{\chi}_A(-\tilde{\omega}, -\omega) \hat{C}(\tilde{\omega}) \bar{\hat{C}}(\omega) e^{i(\tilde{\omega}-\omega)t} e^{-i(\tilde{\omega}-\omega)t'} \\
=&2 \int_R d\omega \int_R d\tilde{\omega} \ \chi_A(\omega, \tilde{\omega}) \bar{\chi}_A(\omega, \tilde{\omega}) \hat{C}(\tilde{\omega}) \bar{\hat{C}}(\omega) \mathrm{sinc}^2(\frac{(\tilde{\omega}-\omega)T}{2}).
\end{aligned}$$

Consider $(\Delta x, \Delta z) = (0, 0)$, then

$$E[I(0,0)] = C_p(\phi) C_s(\phi) \int_R \omega^4 \hat{C}(\omega) d\omega.$$

Note that

$$|\chi_A(\omega, \tilde{\omega})| \leq C_p(\phi) C_s(\phi) \omega^2 \tilde{\omega}^2,$$

then,

$$Var[I(0,0)] \leq 2 \int_R d\omega \int_R d\tilde{\omega} \ \omega^4 \tilde{\omega}^4 \hat{C}(\tilde{\omega}) \hat{C}(\omega) \mathrm{sinc}^2(\frac{(\tilde{\omega}-\omega)T}{2}) (C_p(\phi) C_s(\phi))^2,$$

where $\hat{C}$ is real and positive.

Assume that v is smooth and

$$\sup_{\omega} (\omega^4 \hat{C}(\omega)) \leq \mathcal{C} < \infty,$$

then

$$Var[I(0,0)] \leq 2\mathcal{C} \frac{2}{T} (\int_R \mathrm{sinc}^2(s) ds) (\int_R \omega^4 \hat{C}(\omega) d\omega) (C_p(\phi) C_s(\phi))^2.$$

Then,

$$\begin{aligned}\textbf{SNR} =& \frac{|E[I(0,0)]|^2}{Var[I(0,0)]} \\ \geq& \frac{\int_R \omega^4 \hat{C}(\omega) d\omega}{\sup_\omega(\omega^4 \hat{C}(\omega))} \frac{T}{4\int_R \text{sinc}^2(s) ds}.\end{aligned}$$

Suppose that the correlation time is τ, then $\hat{C}(\omega) = \tau\hat{\tilde{C}}(\tau\omega)$, with $\tilde{C}$ non-dimensionalized and $O(1)$ support. Thus,

$$\textbf{SNR} \geq \frac{\int_R s^4 \hat{\tilde{C}}(s) ds}{\sup_s(s^4 \hat{\tilde{C}}(s))} \frac{1}{4\int_R \text{sinc}^2(s) ds} \frac{T}{\tau}.$$

WLOG, we assume that $\tilde{C}(s)$ is Gaussian, then

$$\int_R s^4 \hat{\tilde{C}}(s)\, ds = 2\int_0^\infty s^4 e^{-\frac{s^2}{2}}\, ds = 3\sqrt{2\pi}.$$

Under the same assumption, to achieve the maximum of $s^4\hat{\tilde{C}}(s)$, we only need to make

$$\frac{d}{ds} s^4 e^{-\frac{s^2}{2}} = 0.$$

After solving the above equation, we can get $s = \pm 2$. Thus,

$$\sup_s(s^4 \hat{\tilde{C}}(s)) = 16e^{-2}.$$

In addition, we know that

$$\int_R \text{sinc}^2(s)\, ds \leq 2\left(1 + \int_1^\infty x^{-2}\, dx\right) \leq 4.$$

Therefore,

$$\textbf{SNR} \geq (\frac{T}{\tau})\frac{3\sqrt{2\pi}}{16e^{-2}}\frac{1}{16} \approx \frac{T}{5\tau}.$$

In conlusion, in Unknown Source Case, SNR depends on the correlation time and the time domain only: the longer the time domain is, the better quality of the image is; the

shorter the correlation time is, the better quality of the image is.

□

5.2.3 Stability Analysis in Image Contribution of Incident Waves

In Known Source Case and Unknown Source Case, we ulitized SNR to anlalyze the stability of the imaging function. Now we introduce a new way to define SNR as the ratio of the level of a desired signal to the level of background noise:

$$\mathbf{SNR} = \frac{|E[I]|}{|E[I_{incident}]|}, \tag{5.1}$$

where I is the original imaging function related to the correlation between the backpropagated P waves and S waves; $I_{incident}$ is the incident waves' contribution. In this section, we will utilize the new definition of SNR to analyze the stability in Image Contribution of Incident Waves Case.

Proposition 5.2.3. *Suppose we have an unknown source which is a stationary stochastic process, based on the imaging function considering the contribution of the incident waves, we have the following:*

$$\begin{aligned}\mathbf{SNR} =& \frac{\int_{-A/2}^{A/2} C([\Delta x(a/h)+\Delta z](\frac{1}{c_s}-\frac{1}{c_p})/l)da}{\int_{-A/2}^{A/2} C(\frac{h\cos\phi - h + \frac{h^2}{2\tilde{l}}}{lc_p})da} \\ \sim& \frac{\int_{-A/2}^{A/2} e^{-\frac{|\Delta z+\Delta x(a/h)|}{\lambda_{p,s}}}da}{\int_{-A/2}^{A/2} e^{-\frac{|h\cos\phi - h + \frac{h^2}{2\tilde{l}}|}{\lambda_p}}da} \gg 1,\end{aligned}$$

where C is the correlation function.

When $\phi = 0$, $SNR \sim e^{\frac{h^2}{2\tilde{l}\lambda_p}} H(\Delta x, \Delta z)$, where $H(\Delta x, \Delta z) = A^{-1}\int_{-A/2}^{A/2} e^{-\frac{|\Delta z+\Delta x(a/h)|}{\lambda_{p,s}}}da$; When $\phi = \frac{\pi}{2}$, $SNR \sim e^{\frac{h}{\lambda_p}} H(\Delta x, \Delta z)$; When $\phi = \pi$, $SNR \sim e^{\frac{2h}{\lambda_p}} H(\Delta x, \Delta z)$. In addition, when $\phi = \frac{\pi}{2}$ or $\phi = \pi$, SNR is much larger than that when $\phi = 0$.

Proof. From the above sections, we know that

$$I(\Delta x, \Delta z) \sim T^{-1}A^{-1}\int_{-T/2}^{T/2}\int_{-A/2}^{A/2}\mathbf{U}_{sc}\cdot\vec{e_3}(t-r^{\Delta}(a)/c_p) * \mathbf{U}_{sc}\cdot\vec{e_1}(t-r^{\Delta}(a)/c_s)dtda. \tag{5.2}$$

Then,

$$\begin{aligned} E[I(\Delta x, \Delta z)] \sim & \omega_c^4 C_p(\phi)C_s(\phi)A^{-1}\int_{-A/2}^{A/2} C(\frac{\frac{r(a)-r^{\Delta}(a)}{c_p} - \frac{r(a)-r^{\Delta}(a)}{c_s}}{l})da \\ \sim & \omega_c^4 C_p(\phi)C_s(\phi)A^{-1}\int_{-A/2}^{A/2} e^{-\frac{|\Delta z+\Delta x(a/h)|}{\lambda_{p,s}}}da. \end{aligned}$$

In addition,

$$I_{incident} \sim T^{-1}A^{-1}\int_{-T/2}^{T/2}\int_{-A/2}^{A/2}\mathbf{U}_{0}\cdot\vec{e_3}(t-r^{\Delta}(a)/c_p) * \mathbf{U}_{sc}\cdot\vec{e_1}(t-r^{\Delta}(a)/c_s)dtda. \tag{5.3}$$

Then,

$$\begin{aligned} E[I_{incident}(\Delta x, \Delta z)] \sim & \omega_c^4 C_p(\phi)C_s(\phi)A^{-1}\int_{-A/2}^{A/2} C(\frac{\frac{\hat{l}-r^{\Delta}(a)-\tilde{l}}{c_p} - \frac{r(a)-r^{\Delta}(a)}{c_s}}{l})da \\ \sim & \omega_c^4 C_p(\phi)C_s(\phi)A^{-1}\int_{-A/2}^{A/2} e^{-\frac{|h\cos\phi-h+\frac{h^2}{2\tilde{l}}|}{\lambda_p}}da. \end{aligned}$$

Since $\frac{|h\cos\phi-h+\frac{h^2}{2\tilde{l}}|}{\lambda_p}$ is a contant which is much larger than $\frac{|\Delta z+\Delta x(a/h)|}{\lambda_{p,s}}$, then

$$e^{-\frac{|\Delta z+\Delta x(a/h)|}{\lambda_{p,s}}} \gg e^{-\frac{|h\cos\phi-h+\frac{h^2}{2\tilde{l}}|}{\lambda_p}}.$$

As a result,

$$|E[I(\Delta x, \Delta z)]| \gg |E[I_{incident}(\Delta x, \Delta z)]|.$$

That is,

$$\mathbf{SNR} = \frac{|E[I]|}{|E[I_{incident}]|} \gg 1. \tag{5.4}$$

□

5.2.4 Stability Analysis in Pulse Source Case

Suppose we have a pulse source, and we utilize $I_{sim} = I + I_{incident}$ as our imaging function. From the last section, similarly, we can get

$$\begin{aligned} I_{sim}(\Delta x, \Delta z) =& T^{-1}A^{-1}\int_{-T/2}^{T/2}\int_{-A/2}^{A/2} \mathbf{U}_{sc}\cdot\vec{e_3}(t-r^{\Delta}(a)/c_p) * \mathbf{U}_{sc}\cdot\vec{e_1}(t-r^{\Delta}(a)/c_s) \\ &+ \mathbf{U}_0\cdot\vec{e_3}(t-r^{\Delta}(a)/c_p) * \mathbf{U}_{sc}\cdot\vec{e_1}(t-r^{\Delta}(a)/c_s)dtda \\ =& T^{-1}A^{-1}\iiiint \omega^2\tilde{\omega}^2 C_p(\phi)C_s(\phi)e^{-ik_p(r(a)+\tilde{l})}e^{i\tilde{k_s}r(a)+i\tilde{k_p}\tilde{l}} \\ &\qquad \hat{v}(\omega)\bar{\hat{v}}(\tilde{\omega})e^{ik_p r^{\Delta}(a)-i\tilde{k_s}r^{\Delta}(a)-i\omega t+i\tilde{\omega}t} \\ &\quad + \tilde{\omega}^2 C_s(\phi)e^{-ik_p\hat{l}(a)}e^{i\tilde{k_s}r(a)+i\tilde{k_p}\tilde{l}} \\ &\qquad \hat{v}(\omega)\bar{\hat{v}}(\tilde{\omega})e^{ik_p r^{\Delta}(a)-i\tilde{k_s}r^{\Delta}(a)-i\omega t+i\tilde{\omega}t}dtdad\omega d\tilde{\omega}. \end{aligned}$$

In this section, we will utilize the latter definition of SNR to analyze the stability in Unknown Pulse Source Case.

Proposition 5.2.4. *Suppose we have an unknown source which is a continuous pulse source(3.6), based on the imaging function considering the contribution of the incident waves, we have the following:*

$$\mathbf{SNR} = \frac{\int_{-A/2}^{A/2} C([\Delta x(a/h)+\Delta z](\frac{1}{c_s}-\frac{1}{c_p})/l)da}{\int_{-A/2}^{A/2} C(\frac{h\cos\phi - h + \frac{h^2}{2\tilde{l}}}{lc_p})da} \gg 1, \tag{5.5}$$

where the correlation function $C(\Delta t) \sim \cos(\omega_0\Delta t/\tau)e^{-\left(\frac{\Delta t/\tau}{2t_0}\right)^2}$.

When $\phi = 0$, $SNR \sim A^{-1}C^{-1}(\frac{h^2}{2\tilde{l}lc_p})E[I]$, *where* $E[I] = \int_{-A/2}^{A/2} C([\Delta x(a/h)+\Delta z](\frac{1}{c_s}-\frac{1}{c_p})/l)da$; *When* $\phi = \frac{\pi}{2}$, $SNR \sim A^{-1}C^{-1}(\frac{-h}{lc_p})E[I]$; *When* $\phi = \pi$, $SNR \sim A^{-1}C^{-1}(\frac{-2h}{lc_p})E[I]$. *In addition, when* $\phi = \frac{\pi}{2}$ *or* $\phi = \pi$, *SNR is much larger than that when* $\phi = 0$.

Proof. From Resolution Analysis Chapter, we know that the expectation of the imaging

function with a continous pulse source is:

$$E[I(\Delta x,\Delta z)] \sim \omega_c^4 C_p(\phi)C_s(\phi)A^{-1}\int_{-A/2}^{A/2} C(\frac{\frac{r(a)-r^{\Delta}(a)}{c_p}-\frac{r(a)-r^{\Delta}(a)}{c_s}}{l})da$$
$$\sim \omega_c^4 C_p(\phi)C_s(\phi)A^{-1}\int_{-A/2}^{A/2} \cos(\omega_0(\Delta x(a/h)+\Delta z)(\frac{1}{c_s}-\frac{1}{c_p}))$$
$$e^{-(\Delta x(a/h)+\Delta z)^2(\frac{1}{2t_0c_s}-\frac{1}{2t_0c_p})^2}da,$$

by utilizing the correlation function $C(\Delta t)\sim\cos(\omega_0\Delta t)e^{-\left(\frac{\Delta t}{2t_0}\right)^2}$. In addition,

$$E[I_{incident}(\Delta x,\Delta z)] \sim \omega_c^4 C_p(\phi)C_s(\phi)A^{-1}\int_{-A/2}^{A/2} C(\frac{\frac{\hat{l}-r^{\Delta}(a)-\tilde{l}}{c_p}-\frac{r(a)-r^{\Delta}(a)}{c_s}}{l})da$$
$$\sim \omega_c^4 C_p(\phi)C_s(\phi)A^{-1}\int_{-A/2}^{A/2} \cos(\omega_0\frac{|h\cos\phi-h+\frac{h^2}{2\tilde{l}}|}{\lambda_p})e^{-(\frac{|h\cos\phi-h+\frac{h^2}{2\tilde{l}}|}{\lambda_p})^2}da.$$

Since $\frac{|h\cos\phi-h+\frac{h^2}{2\tilde{l}}|}{\lambda_p}$ is a contant which is much larger than $\frac{|\Delta z+\Delta x(a/h)|}{\tilde{\lambda}_{p,s}}$, then

$$e^{-(\Delta x(a/h)+\Delta z)^2(\frac{1}{2t_0c_s}-\frac{1}{2t_0c_p})^2} \gg e^{-(\frac{|h\cos\phi-h+\frac{h^2}{2\tilde{l}}|}{\lambda_p})^2}.$$

Additionally, for $\cos(\omega_0(\Delta x(a/h)+\Delta z)(\frac{1}{c_s}-\frac{1}{c_p}))$ and $\cos(\omega_0\frac{|h\cos\phi-h+\frac{h^2}{2\tilde{l}}|}{\lambda_p})$, they have bouned values. As a result,

$$|E[I(\Delta x,\Delta z)]| \gg |E[I_{incident}(\Delta x,\Delta z)]|$$

That is,

$$\textbf{SNR} = \frac{|E[I]|}{|E[I_{incident}]|} \gg 1. \tag{5.6}$$

Similary, if our source is a unknown rectangular pulse source, SNR $\gg 1$ holds too. □

Chapter 6

Simulations

6.1 With Known Sources

Suppose that the location and the properties of the source are known, then we can get the imaging function by computing the correlation between incident waves and the backpropagate scattering waves.

6.1.1 With One Sensor

Suppose that we have one sensor only, then from last several sections, we know that the imaging function is :

$$\begin{aligned} I(\Delta x, \Delta z) &= \int \bar{v}(t + \frac{l'}{c_p}) v(t + \frac{l}{c_p} + \frac{r(a)}{c_p} - \frac{r^{\Delta}(a)}{c_p}) dt \\ &= \int \mathcal{F}(\bar{v}(t + \frac{l'}{c_p})) \mathcal{F}(v(t + \frac{l}{c_p} + \frac{r(a)}{c_p} - \frac{r^{\Delta}(a)}{c_p})) d\omega. \end{aligned}$$

In the simulation, assume that our sensor is located at $(\frac{A}{2}, 0, h)$, the inclusion is located at $(0, 0, 0)$, and the source is at $(\tilde{l}\sin\phi, 0, -\tilde{l}\cos\phi)$, with the assumption $\phi = \frac{\pi}{6}$, just like Figure 4.5.

In Figure 6.1a, for one dimensional offset ($\Delta x \neq 0$, $\Delta z \equiv 0$), we can get the maximum value for the imaging function when $\Delta x = 0$. In Figure 6.1b, it shows the surface of the imaging function in two dimensional offset, and we can find that the maximum values can

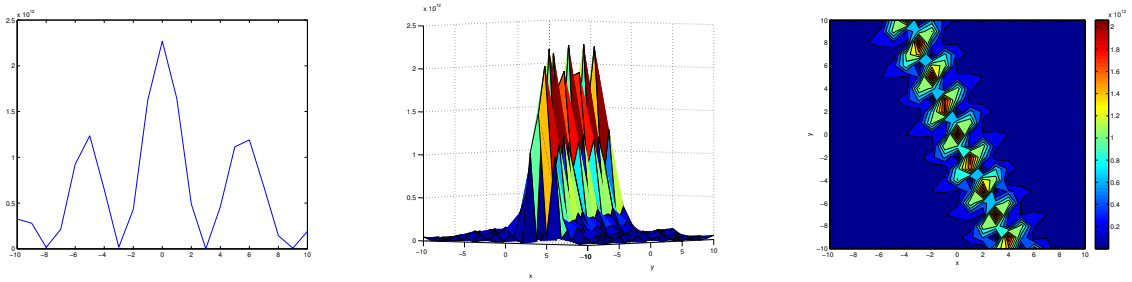

(a): 1D offset (b): 2D offset(Surface) (c): 2D offset(Contour)

Figure 6.1: Imaging Function in One-Sensor Case with P waves

be achieved along a line. In Figure 6.1c, it shows the contour of the imaging function in two dimensional offset, and also, we can find that the maximum values can be achieved along a curve. The location of the curve depends on the location of the sensor. If we extend the range of the search points, in Figure 6.2, more clearly, we can find that the maximum values can be achieved along a curve. The curve function satisfies

$$l' - l - r(a) + r^{\Delta}(a) = 0,$$

which is a function for ellipse. Similarly, if I relocate the sensor at $(0, 0, h)$, instead of $(\frac{A}{2}, 0, h)$, then we can get similar figure (Figure 6.3). They have similar shape but different curve functions. Therefore, different locations of the sensor will give us different curves where the maximum imaging function values can be achieved. See Figure 6.4, it shows that we can achieve maximum values along different ellipses when the location of the sensor is different, but they have one intersection point that is $(0, 0, 0)$ where $\Delta x = 0$, $\Delta z = 0$. We call this kind of curves Maximizer Curves.

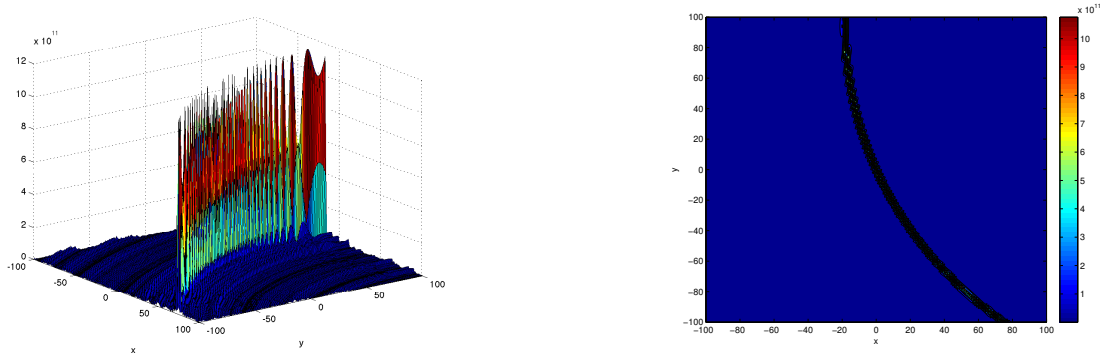

(a): Imaging Function with 2D Offset(Surface) (b):Imaging Function with 2D Offset(Contour)

Figure 6.2: Known Source with One-Sensor Case (P waves) (The N th sensor)

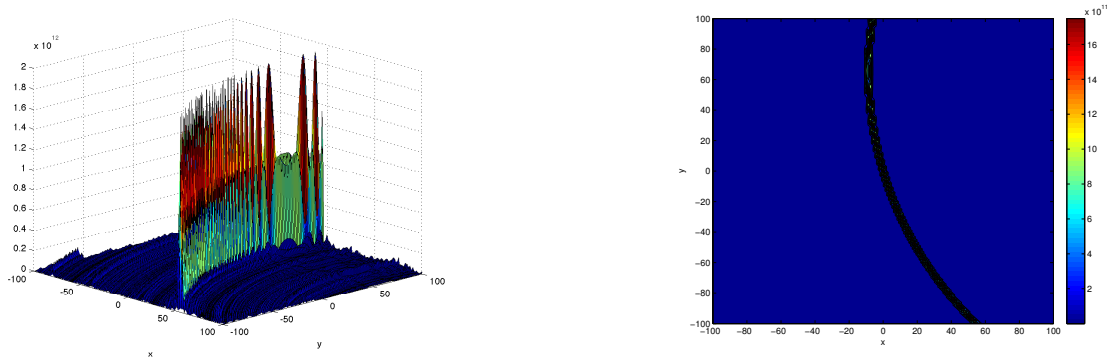

(a): Imaging Function with 2D Offset(Surface) (b): Imaging Function with 2D Offset(Contour)

Figure 6.3: Known Source with One-Sensor Case (P waves) (The $N/2$ th sensor)

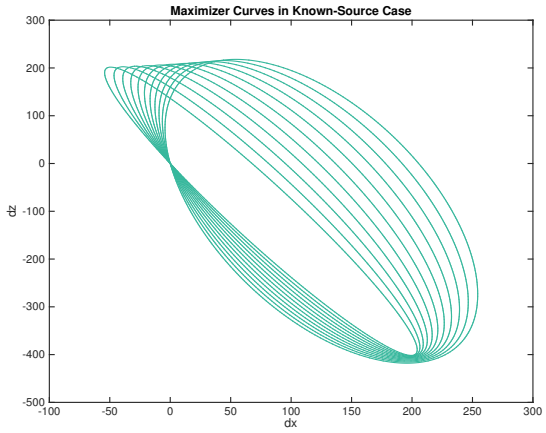

Figure 6.4: Maximizer Curves with Different Sensor Locations (Known Source)

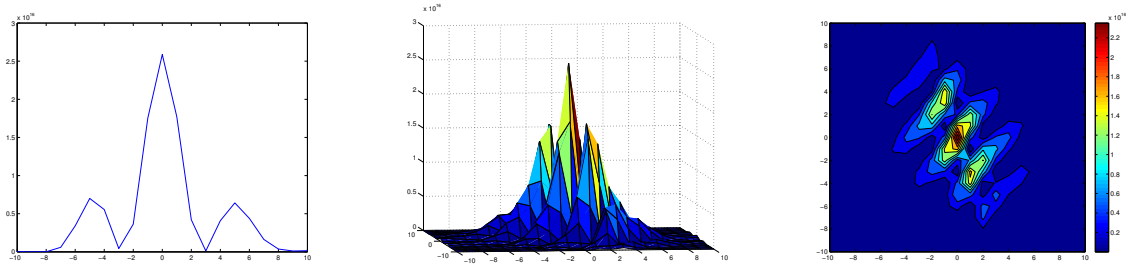

(a): 1D Offset (b): 2D Offset(Surface) (c): 2D Offset(Contour)

Figure 6.5: Imaging Function in Known Source with Many-Sensor Case (P waves)

6.1.2 With Many Sensors

Suppose that we have many sensors, then from last several sections, if we use P component scattering waves only, we know that the imaging function is :

$$\begin{aligned} I(\Delta x, \Delta z) &= \iint \bar{v}(t + \frac{l'}{c_p}) v(t + \frac{l}{c_p} + \frac{r(a)}{c_p} - \frac{r^{\Delta}(a)}{c_p}) dt da \\ &= \iint \mathcal{F}(\bar{v}(t + \frac{l'}{c_p})) \mathcal{F}(v(t + \frac{l}{c_p} + \frac{r(a)}{c_p} - \frac{r^{\Delta}(a)}{c_p})) d\omega da. \end{aligned}$$

In Figure 6.5a, for one dimensional offset ($\Delta x \neq 0$, $\Delta z \equiv 0$), we can get the maximum value for the imaging function when $\Delta x = 0$. In Figure 6.5b, it shows the surface of the imaging function in two dimensional offset, and we can find that the maximum values can be achieved when $\Delta x = 0$ and $\Delta z = 0$. In Figure 6.5c, it shows the contour of the imaging function in two dimensional offset, and also, we can find that the maximum values can be achieved when $\Delta x = 0$ and $\Delta z = 0$.

Similarly, if we use S component scattering waves only, then the imaging function is:

$$\begin{aligned} I(\Delta x, \Delta z) &= \iint \bar{v}(t + \frac{l'}{c_p}) v(t + \frac{l}{c_p} + \frac{r(a)}{c_s} - \frac{r^{\Delta}(a)}{c_s}) dt da \\ &= \iint \mathcal{F}(\bar{v}(t + \frac{l'}{c_p})) \mathcal{F}(v(t + \frac{l}{c_p} + \frac{r(a)}{c_s} - \frac{r^{\Delta}(a)}{c_s})) d\omega da. \end{aligned}$$

Similarly, we can get Figure 6.6.

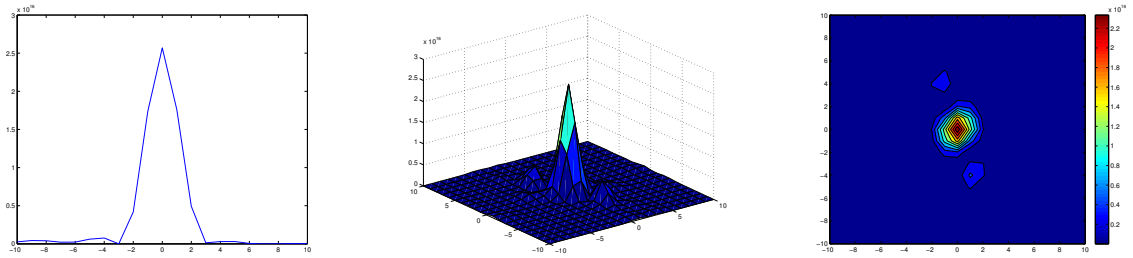

(a): 1D Offset (b): 2D Offset(Surface) (c): 2D Offset(Contour)

Figure 6.6: Imaging Function in Known Source with Many-Sensor Case (S waves)

6.2 With Unknown Sources

Suppose that the location and the properties of the source are unknown, then we can get the imaging function by computing the correlation between the backpropagated scattering P waves and S waves.

6.2.1 With One Sensor

Suppose that we have one sensor only, then from last several sections, we know that the imaging function in the unknown-source case with one sensor is :

$$\begin{aligned} I(\Delta x, \Delta z) &= \int \bar{v}(t + \frac{\tilde{l}}{c_p} + \frac{r(a)}{c_p} - \frac{r^{\Delta}(a)}{c_p}) v(t + \frac{\tilde{l}}{c_p} + \frac{r(a)}{c_s} - \frac{r^{\Delta}(a)}{c_s}) dt \\ &= \int \mathcal{F}(\bar{v}(t + \frac{\tilde{l}}{c_p} + \frac{r(a)}{c_p} - \frac{r^{\Delta}(a)}{c_p})) \mathcal{F}(v(t + \frac{\tilde{l}}{c_p} + \frac{r(a)}{c_s} - \frac{r^{\Delta}(a)}{c_s})) d\omega. \end{aligned}$$

In the simulation, assume that our sensor is located at $(\frac{A}{2}, 0, h)$, the inclusion is located at $(0, 0, 0)$.

In Figure 6.7a, it shows the surface of the imaging function in the unknown-source case with one sensor and two dimensional offset, and we can find that the maximum values can be achieved along a curve. In Figure 6.7b, it shows the contour of the imaging function in two dimensional offset, and also, we can find that the maximum values can be achieved along a curve. The location of the curve depends on the location of the sensor. If we extend the range of the search points, in Figure 6.7b, more clearly, we can find that the maximum

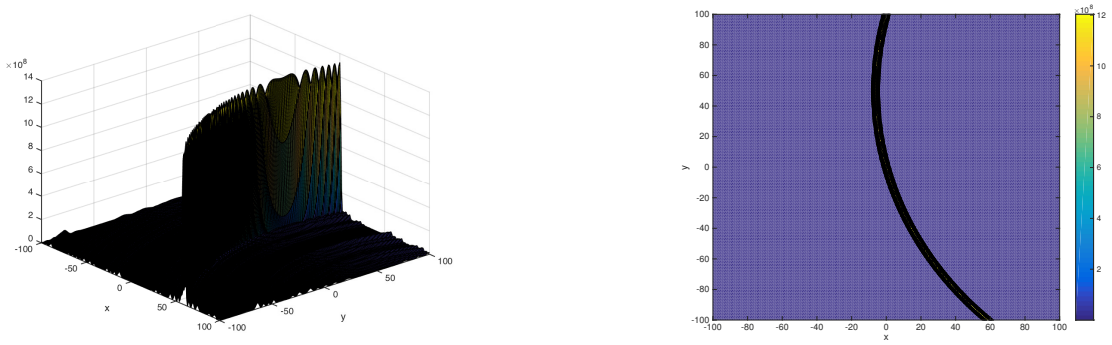

(a): Imaging Function with 2D Offset(Surface) (b): Imaging Function with 2D Offset(Contour)

Figure 6.7: Unknown Source with One-Sensor Case (The Nth Sensor)

values can be achieved along a curve. The curve function satisfies

$$r(a) - r^{\Delta}(a) = 0,$$

which is a function for a circle. Similarly, if I relocate the sensor at $(0, 0, h)$, instead of $(\frac{A}{2}, 0, h)$, then we can get similar figure (Figure 6.8). They have similar shape but different curve functions. Therefore, different locations of the sensor will give us different curves where the maximum imaging function values can be achieved. See Figure 6.9, it shows that, in the unknown-source case, we can achieve maximum values along different circles when the location of the sensor is different, but they have one intersection point in the search region that is $(0, 0, 0)$ where $\Delta x = 0$, $\Delta z = 0$. We call this kind of curves Maximizer Curves. In Figure 6.9, also, we can find two intersection points in total, but one of them is far away from the search region, so it will not influence our final result.

6.2.2 With Many Sensors

Assume that we have many sensors on x-axis, the source is at $(h, 0, -h\cot\phi)$, but we cannot use the location of the source to find the imaging function, since in this section our study focuses on the unknown sources. The source gennerated incident P waves, and scattered at inclusion, then we can receive scattering P waves and S waves. Our imaging function is from

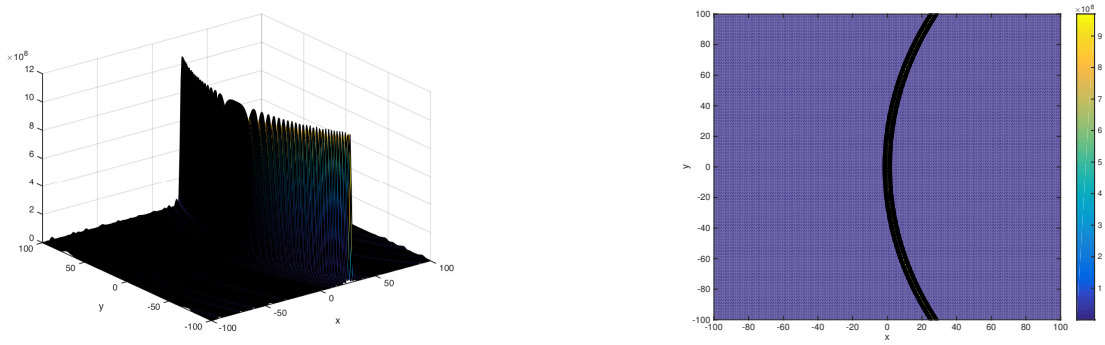

(a): Imaging Function with 2D Offset(Surface) (b): Imaging Function with 2D Offset(Contour)

Figure 6.8: Unknown Source with One-Sensor Case (The $N/2$th Sensor)

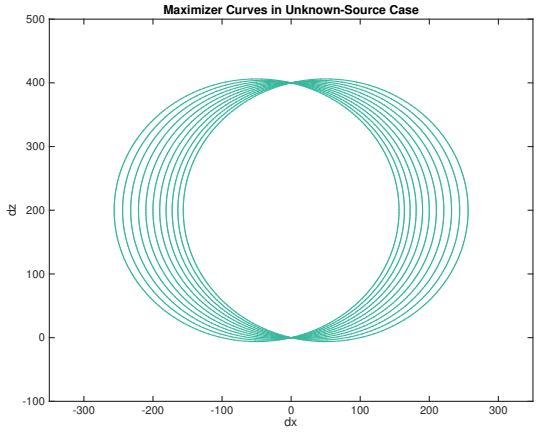

Figure 6.9: Maximizer Curves with Different Sensor Locations (Unknown Source)

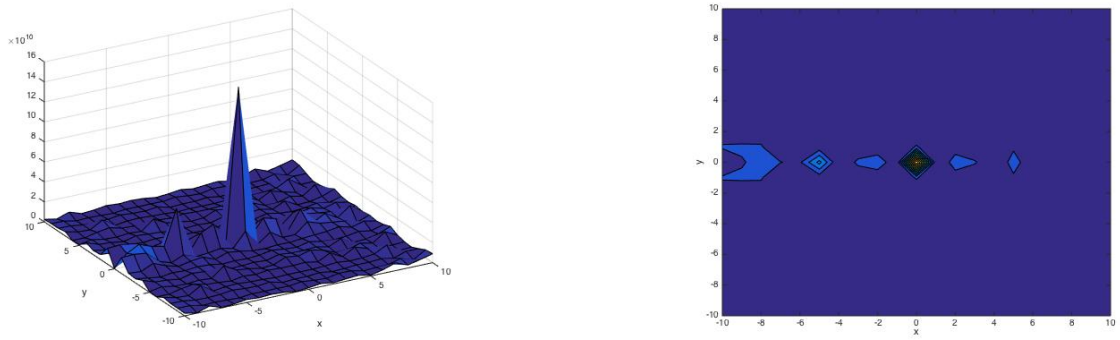

(a): Imaging Function with 2D Offset(Surface) (b): Imaging Function with 2D Offset(Contour)

Figure 6.10: Unknown Source Case with Many Sensors

the correlation between backpropagated scattering P waves and S waves as below:

$$I(\Delta x, \Delta z) = T^{-1}A^{-1} \iiiint \omega^2 \tilde{\omega}^2 C_p(\phi) C_s(\phi) e^{-ik_p(r(a)+\tilde{l})} e^{i\tilde{k_s} r(a) + i\tilde{k_p}\tilde{l}} \hat{v}(\omega)\bar{\hat{v}}(\tilde{\omega}) e^{ik_p r^{\Delta}(a)} e^{-i\tilde{k_s} r^{\Delta}(a)} e^{-i\omega t} e^{i\tilde{\omega}t} dt da d\omega d\tilde{\omega}.$$

In Figure 6.10a, it shows the surface of the imaging function in the unknown-source case with many sensors and two dimensional offset, and we can find that the maximum values can be achieved when $\Delta x = 0$ and $\Delta z = 0$. In Figure 6.10b, it shows the contour of the imaging function in the unknown-source case with many sensors and two dimensional offset, and also, we can find that the maximum values can be achieved when $\Delta x = 0$ and $\Delta z = 0$.

6.3 Image Contribution of Incident Waves

As mensioned before, when we received the scattering P waves and the scattering S waves in the sensors, actually, we can also receive incident P waves. By using the received data, our imaging function will be:

$$I_{sim} = I + I_{incident}.$$

Here, I is the imaging function we mentioned in the above sections; $I_{incident}$ is the correlation between backpropagated incident P waves and the backpropagated scattering S waves. In the simulation, the imaging function I_{sim} is the correlation between the backpropagated

scattering S waves and the backpropagated P waves which includes backpropagated incident P waves and backpropagated scattering P waves because of the seperation issue.

In the above two sections, we get some results without considering the incident wave term. In this section, we will do the similar simulation with considering the incident wave term.

6.3.1 With One Sensor

Suppose that we have one sensor only, we know that the imaging function with considering the incident waves' contribution is as below:

$$\begin{aligned}
I_{sim}(\Delta x, \Delta z) &= \int \bar{v}(t + \frac{\tilde{l}}{c_p} + \frac{r(a)}{c_p} - \frac{r^{\Delta}(a)}{c_p}) v(t + \frac{\tilde{l}}{c_p} + \frac{r(a)}{c_s} - \frac{r^{\Delta}(a)}{c_s}) \\
&\quad + \bar{v}(t + \frac{\hat{l}}{c_p} - \frac{r^{\Delta}(a)}{c_p}) v(t + \frac{\tilde{l}}{c_p} + \frac{r(a)}{c_s} - \frac{r^{\Delta}(a)}{c_s}) dt \\
&= \int \mathcal{F}(\bar{v}(t + \frac{\tilde{l}}{c_p} + \frac{r(a)}{c_p} - \frac{r^{\Delta}(a)}{c_p})) \mathcal{F}(v(t + \frac{\tilde{l}}{c_p} + \frac{r(a)}{c_s} - \frac{r^{\Delta}(a)}{c_s})) \\
&\quad + \mathcal{F}(\bar{v}(t + \frac{\hat{l}}{c_p} - \frac{r^{\Delta}(a)}{c_p})) \mathcal{F}(v(t + \frac{\tilde{l}}{c_p} + \frac{r(a)}{c_s} - \frac{r^{\Delta}(a)}{c_s})) d\omega \\
&\sim \int \bar{\hat{v}}(\omega) e^{ik_p \tilde{l}} \omega^2 e^{ik_p r(a)} e^{-ik_p r^{\Delta}(a)} \hat{v}(\omega) e^{-ik_p \tilde{l}} \omega^2 e^{-ik_s r(a)} e^{ik_s r^{\Delta}(a)} \\
&\quad + \bar{\hat{v}}(\omega) e^{ik_p \hat{l}} e^{-ik_p r^{\Delta}(a)} \hat{v}(\omega) e^{-ik_p \tilde{l}} \omega^2 e^{-ik_s r(a)} e^{ik_s r^{\Delta}(a)} d\omega,
\end{aligned}$$

where $\hat{l}$ is the distance between the source and the sensor.

In the simulation, assume that our sensor is located at $(\frac{A}{2}, 0, h)$, the inclusion is located at $(0, 0, 0)$. In Figure 6.11 a, considering the incident waves' contribution, it shows the surface of the imaging function in the unknown-source case with one sensor and two dimensional offset, and we can find that the maximum values can be achieved along two curves instead of one curve in the above sections. In Figure 6.11 b, considering the incident waves, it shows the contour of the imaging function in two dimensional offset, and also, we can find that the maximum values can be achieved along two curves. Also, we can find that the location of the curve depends on the location of the sensor. In the simulation, if we changed the location of the sensor, then the curves above will change a little bit. Compared with Figure 6.7, after

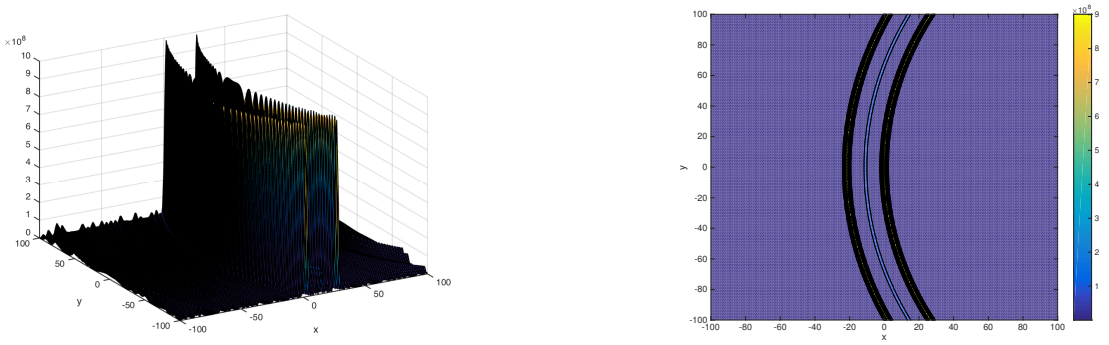

(a): Imaging Function with 2D Offset(Surface) (b): Imaging Function with 2D Offset(Contour)

Figure 6.11: One-Sensor Unknown Source Case with Incident Waves' Contribution

considering the incident waves' contribution, we can get two maximizer curves: one is the 'true' maximizer curve; the other one is a 'dummy' maximizer curve which was generated because of the incident waves' contribution. Now our results get much worse than before. The 'true' maximizer curve satifies the equation as before:

$$r(a) - r^{\Delta}(a) = 0.$$

The 'dummy' maximizer curve satisfies the new equation as below:

$$k_s(r(a) - r^{\Delta}(a)) - k_p(\hat{l}(a) - \tilde{l}(a) - r^{\Delta}(a)) = 0,$$

where $\hat{l}(a)$ denotes the distance between the sensor and the source; $\tilde{l}(a)$ denotes the distance between the sensor and the source; $r(a)$ denotes the distance between the sensor and the inclusion; $r^{\Delta}(a)$ denotes the distance between the sensor and the search point.

6.3.2 With Many Sensors

Assume that we have many sensors on x-axis, the source is at $(h, 0, -h\cot\phi)$, but we cannot use the location of the source to find the imaging function, since in this section our study focuses on the unknown sources. The source gennerated incident P waves, and scattered at inclusion, then we can receive the incident P waves, the scattering P waves and the scattering

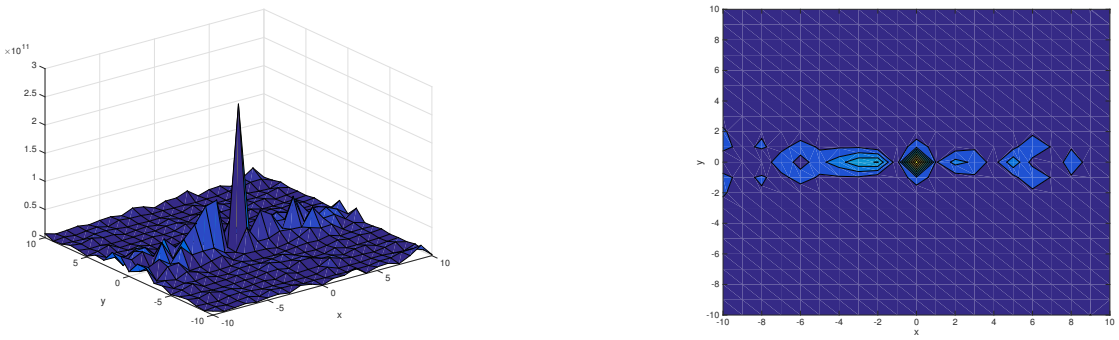

(a): Imaging Function with 2D Offset(Surface) (b): Imaging Function with 2D Offset(Contour)

Figure 6.12: Many-Sensor Unknown Source Case with Incident Waves' Contribution

S waves. Our imaging function with the incident waves' contribution is as below:

$$
\begin{aligned}
I_{sim}(\Delta x, \Delta z) =& T^{-1}A^{-1}\int_{-T/2}^{T/2}\int_{-A/2}^{A/2}\mathbf{U}_{sc}\cdot\vec{e_3}(t-r^{\Delta}(a)/c_p)*\mathbf{U}_{sc}\cdot\vec{e_1}(t-r^{\Delta}(a)/c_s)\\
&+\mathbf{U}_0\cdot\vec{e_3}(t-r^{\Delta}(a)/c_p)*\mathbf{U}_{sc}\cdot\vec{e_1}(t-r^{\Delta}(a)/c_s)dtda\\
=& T^{-1}A^{-1}\iiiint \omega^2\tilde{\omega}^2 C_p(\phi)C_s(\phi)e^{-ik_p(r(a)+\tilde{l})}e^{i\tilde{k_s}r(a)+i\tilde{k_p}\tilde{l}}\\
&\hat{v}(\omega)\bar{\hat{v}}(\tilde{\omega})e^{ik_p r^{\Delta}(a)-i\tilde{k_s}r^{\Delta}(a)-i\omega t+i\tilde{\omega}t}\\
&+\tilde{\omega}^2 C_s(\phi)e^{-ik_p\hat{l}(a)}e^{i\tilde{k_s}r(a)+i\tilde{k_p}\tilde{l}}\\
&\hat{v}(\omega)\bar{\hat{v}}(\tilde{\omega})e^{ik_p r^{\Delta}(a)-i\tilde{k_s}r^{\Delta}(a)-i\omega t+i\tilde{\omega}t}dtdad\omega d\tilde{\omega}.
\end{aligned}
$$

In Figure 6.12a, it shows that the surface of the imaging function in the unknown-source case with many sensors and two dimensional offset after considering the incident waves' contribution, and we can find that the maximum values can be achieved when $\Delta x = 0$ and $\Delta z = 0$. In Figure 6.12b, it shows the contour of the imaging function in the unknown-source case with many sensors and two dimensional offset after considering the incident wave term, and also, we can find that the maximum values can be achieved when $\Delta x = 0$ and $\Delta z = 0$. Compared with Figure 6.10, we can find that the resolution becomes worse after considering the incident waves' contribution, but we can find the maximum value of the imaging function at the same location.

6.4 With Pulse Sources

Suppose that the location of the source is unknown, however, the source is a pulse instead of random sources, then we can get the imaging function by computing the correlation between the backpropagated scattering P waves and S waves as before.

6.4.1 With Rectangular Pulse Source

Suppose that our source is a rectangular pulse defined as:

$$\rho_\tau(t) = \begin{cases} 1 & -\tau \le t \le \tau \\ 0 & \text{otherwise.} \end{cases} \tag{6.1}$$

The Fourier transform of the rectangular pulse is aclculated as follows:

$$\begin{aligned} \hat{\rho}_\tau(\omega) =& \mathcal{F}(\rho_\tau(t)) = \int \rho_\tau(t) e^{i\omega t} dt \\ =& \int_{-\tau}^{\tau} e^{i\omega t} dt \propto \frac{\sin(\omega\tau)}{\omega} \propto \operatorname{sinc}(\frac{\omega\tau}{\pi}). \end{aligned}$$

Suppose that we have many sensors, then the imaging function is same as before:

$$\begin{aligned} I(\Delta x, \Delta z) =& T^{-1} A^{-1} \iiiint \omega^2 \tilde{\omega}^2 C_p(\phi) C_s(\phi) e^{-ik_p(r(a)+\tilde{l})} \\ & e^{i\tilde{k_s} r(a) + i\tilde{k_p} \tilde{l}} \hat{v}(\omega) \bar{\hat{v}}(\tilde{\omega}) e^{ik_p r^{\Delta}(a)} e^{-i\tilde{k_s} r^{\Delta}(a)} e^{-i\omega t} e^{i\tilde{\omega} t} dt da d\omega d\tilde{\omega}. \end{aligned}$$

In this section, our source is a rectangular pulse, so $\hat{v}(\omega)$ can be replaced by $\operatorname{sinc}(\frac{\omega\tau}{\pi})$:

$$\begin{aligned} I(\Delta x, \Delta z) =& T^{-1} A^{-1} \iiiint \omega^2 \tilde{\omega}^2 C_p(\phi) C_s(\phi) e^{-ik_p(r(a)+\tilde{l})} \\ & e^{i\tilde{k_s} r(a) + i\tilde{k_p} \tilde{l}} \operatorname{sinc}(\frac{\omega\tau}{\pi}) \bar{\operatorname{sinc}}(\frac{\tilde{\omega}\tau}{\pi}) e^{ik_p r^{\Delta}(a)} e^{-i\tilde{k_s} r^{\Delta}(a)} e^{-i\omega t} e^{i\tilde{\omega} t} dt da d\omega d\tilde{\omega}. \end{aligned}$$

In Figure 6.13a, it shows the surface of the imaging function in the rectangular pulse source case with many sensors and two dimensional offset, and we can find that the maximum values can be achieved when $\Delta x = 0$ and $\Delta z = 0$. In Figure 6.13b, it shows the contour

of the imaging function in the rectangular pulse source case with many sensors and two dimensional offset, and also, we can find that the maximum values can be achieved when $\Delta x = 0$ and $\Delta z = 0$. In Figure 6.13, we used different values of τ. τ denotes the width of the rectangular pulse source. From these figures, we can find that the smaller τ is, the better resolution there will be.

6.4.2 With Continuous Pulse Source

Assume that we have many sensors on x-axis, the source is at $(h, 0, -h\cot\phi)$, but we cannot use the location of the source to find the imaging function. In this section, our source is a continuous pulse source:

$$\rho(t) = \cos(\omega_0 t) e^{-(\frac{t}{t_0})^2/2},$$

where ω_0 and t_0 are parameters and $\omega_0 \gg \frac{1}{t_0}$. The figures of the continuour pulse source are Figure 6.14 and Figure 6.15. They show that different parameter values will influence the width of the pulse.

The above pulse function is the product of the cosine function and the Gaussian kernal. The source gennerated a continuous pulse, and scattered at inclusion, then we can receive scattering P waves and S waves. Our imaging function is same as before:

$$\begin{aligned} I(\Delta x, \Delta z) =& T^{-1}A^{-1} \iiiint \omega^2 \tilde{\omega}^2 C_p(\phi) C_s(\phi) e^{-ik_p(r(a)+\tilde{l})} \\ & e^{i\tilde{k_s} r(a) + i\tilde{k_p}\tilde{l}} \hat{v}(\omega) \bar{\hat{v}}(\tilde{\omega}) e^{ik_p r^{\Delta}(a)} e^{-i\tilde{k_s} r^{\Delta}(a)} e^{-i\omega t} e^{i\tilde{\omega} t} dt da d\omega d\tilde{\omega}. \end{aligned}$$

In Figure 6.16a, it shows the surface of the imaging function in the continuous-pulse case with many sensors and two dimensional offset, and we can find that the maximum values can be achieved when $\Delta x = 0$ and $\Delta z = 0$. In Figure 6.16b, it shows the contour of the imaging function in the continuous-pulse case with many sensors and two dimensional offset, and also, we can find that the maximum values can be achieved when $\Delta x = 0$ and $\Delta z = 0$. In Figure 6.16, we can find that when we fix ω_0, the smaller t_0 is, the better resolution there will be.

If we fix $t_0 = 10$, then, as Figure 6.17, the resolution is not as good as before and there

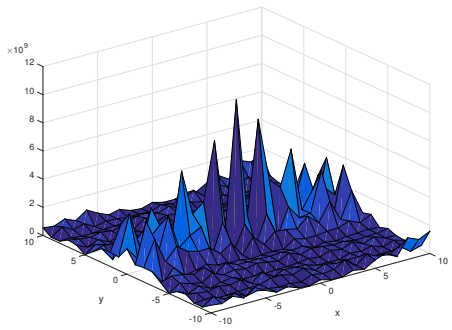

(a): 2D offset(Surface($\tau = 100$)

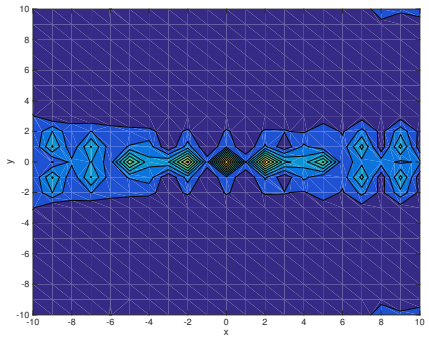

(b): 2D offset(Contour)($\tau = 100$)

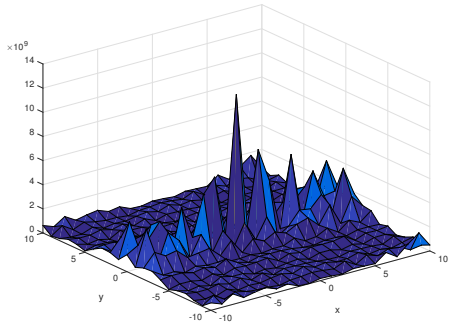

(c): 2D offset(Surface)($\tau = 10$)

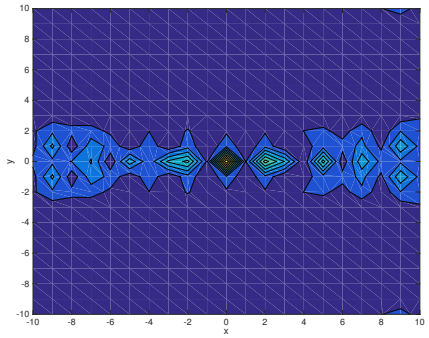

(d): 2D offset(Contour)($\tau = 10$)

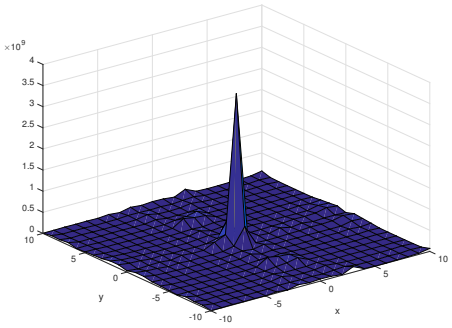

(e): 2D offset(Surface)($\tau = 1$)

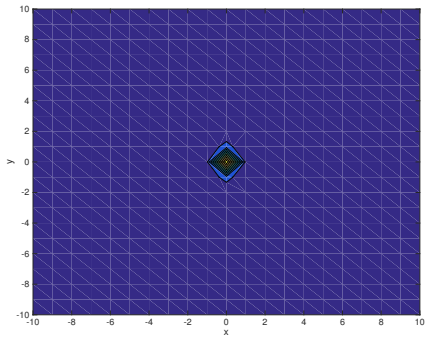

(f): 2D offset(Contour)($\tau = 1$)

Figure 6.13: Imaging Function with Rectangular Pulse Source with Different τ

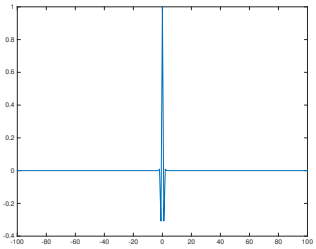

(a): $\omega_0 = 10$,$t_0 = 1$

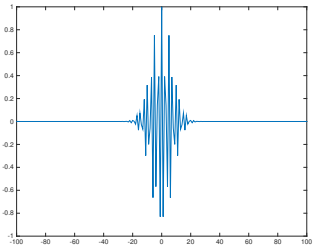

(b): $\omega_0 = 10$,$t_0 = 10$

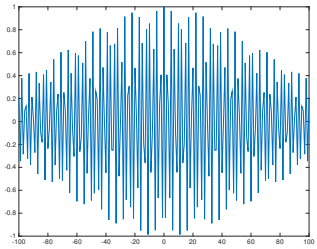

(c): $\omega_0 = 10$,$t_0 = 100$

Figure 6.14: Continuous Pulse with Different Parameters

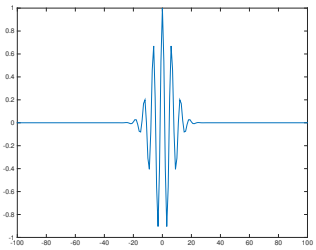

(a): $\omega_0 = 1$,$t_0 = 10$

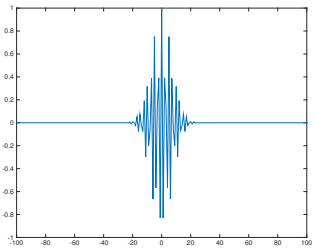

(b): $\omega_0 = 10$,$t_0 = 10$

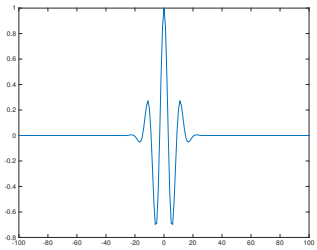

(c): $\omega_0 = 100$,$t_0 = 10$

Figure 6.15: Continuous Pulse with Different Parameters

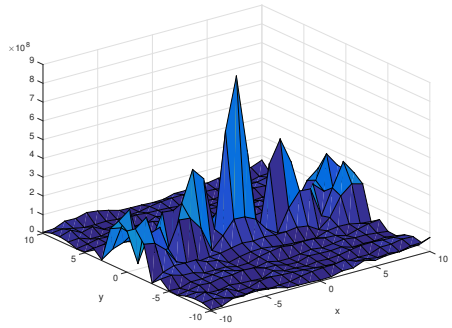

(a): 2D offset(Surface)($\omega_0 = 10$, $t_0 = 10$)

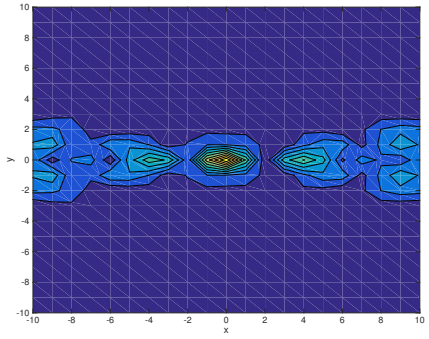

(b): 2D offset(Contour)($\omega_0 = 10$, $t_0 = 10$)

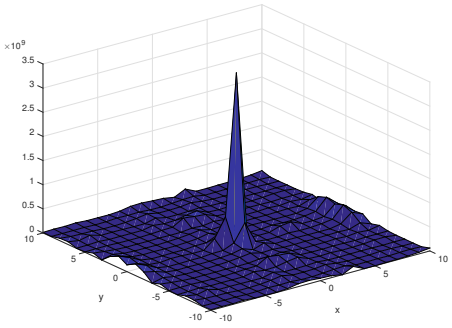

(c): 2D offset(Surface)($\omega_0 = 10$, $t_0 = 1$)

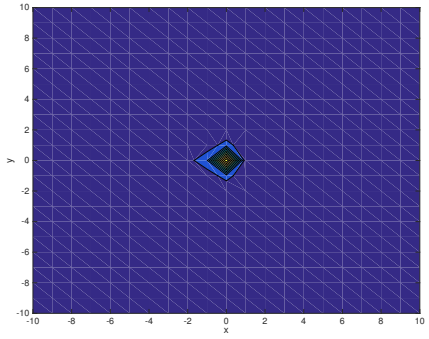

(d): 2D offset(Contour)($\omega_0 = 10$, $t_0 = 1$)

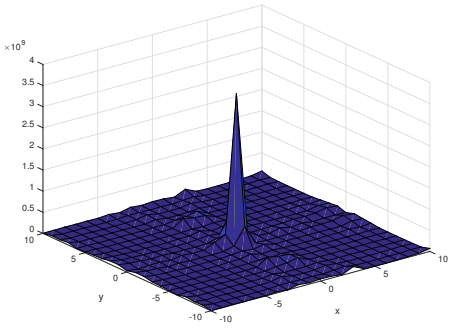

(e): 2D offset(Surface)($\omega_0 = 10$, $t_0 = 0.1$)

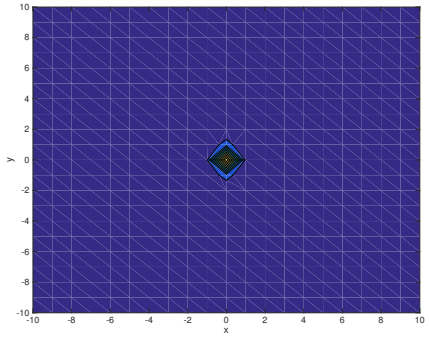

(f): 2D offset(Contour)($\omega_0 = 10$, $t_0 = 0.1$)

Figure 6.16: Imaging Function in Continuous Pulse Source with Fixed ω_0

is no relationship between ω_0 and the resolution when the value of t_0 is not small enough. In Figure 6.18, when we fix $t_0 = 0.1$, the resolution will be much better than above, and ω_0 does not influence the resolution a lot. Also, we can find that there is no difference on theses figures when t_0 is small enough.

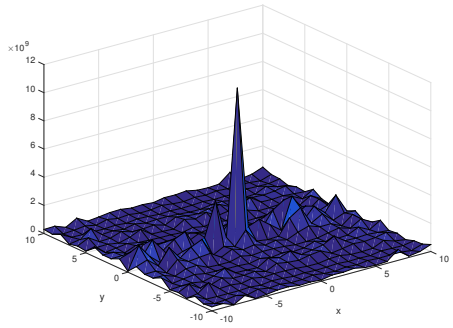

(a): 2D offset(Surface)($\omega_0 = 100$,$t_0 = 10$)

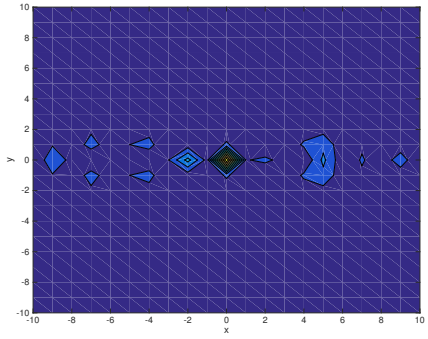

(b): 2D offset(Contour)($\omega_0 = 100$,$t_0 = 10$)

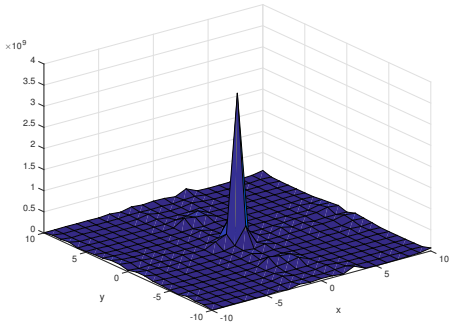

(c): 2D offset(Surface)($\omega_0 = 10$,$t_0 = 10$)

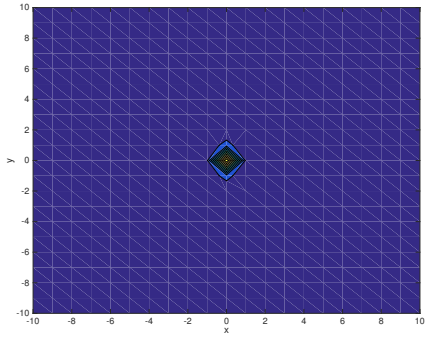

(d): 2D offset(Contour)($\omega_0 = 10$,$t_0 = 10$)

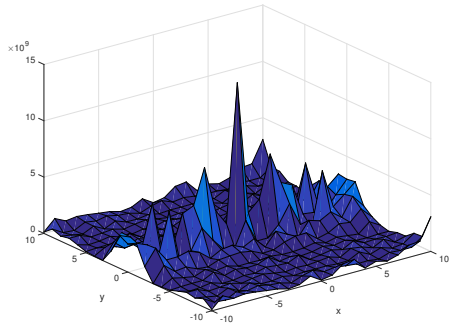

(e): 2D offset(Surface)($\omega_0 = 1$,$t_0 = 10$)

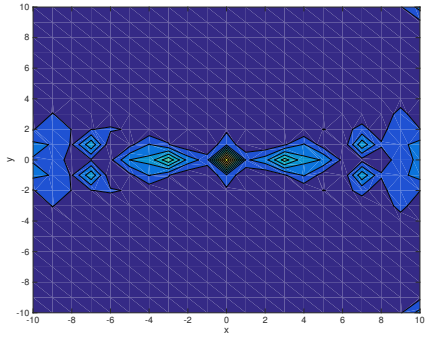

(f): 2D offset(Contour)($\omega_0 = 1$,$t_0 = 10$)

Figure 6.17: Imaging Function in Continuous Pulse Source with Fixed t_0

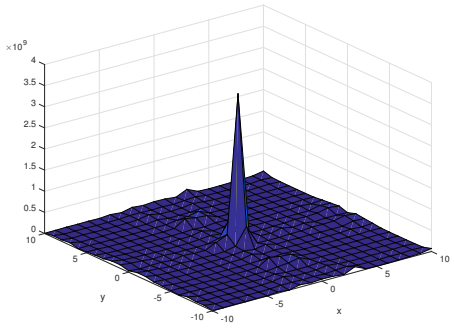

(a): 2D offset(Surface)($\omega_0 = 100$,$t_0 = 0.1$)

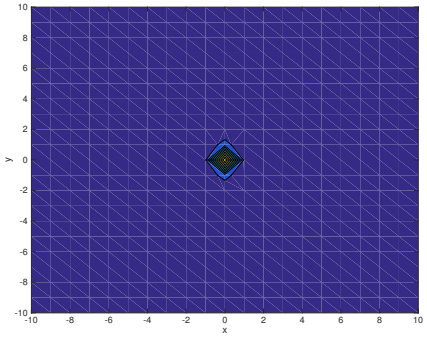

(b): 2D offset(Contour)($\omega_0 = 100$,$t_0 = 0.1$)

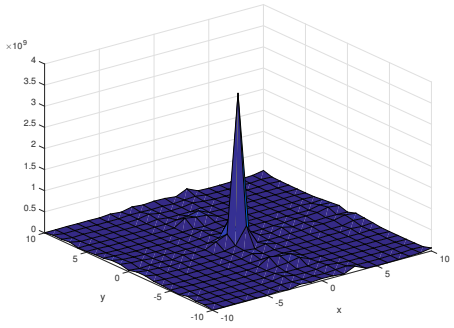

(c): 2D offset(Surface)($\omega_0 = 10$,$t_0 = 0.1$)

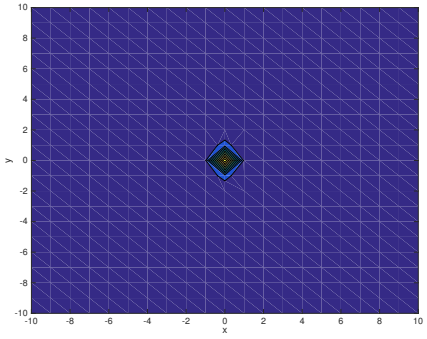

(d): 2D offset(Contour)($\omega_0 = 10$,$t_0 = 0.1$)

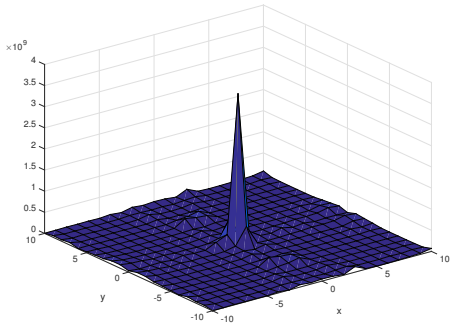

(e): 2D offset(Surface)($\omega_0 = 1$,$t_0 = 0.1$)

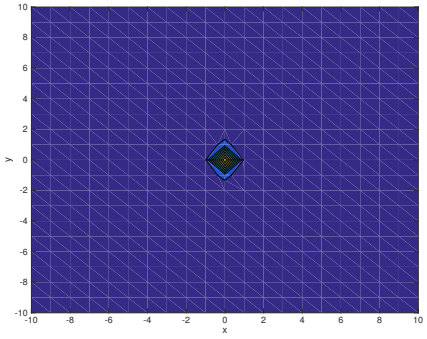

(f): 2D offset(Contour)($\omega_0 = 1$,$t_0 = 0.1$)

Figure 6.18: Imaging Function in Continuous Pulse Source with Fixed t_0

Chapter 7

Summary and Examples

In this section, we will show the main results in different cases by tables. Table 1 shows the theretical results from known source case, unknown source case, image contribution of incident waves and unknown pulse source case. Table 2 shows the main results in different ϕ, where ϕ denotes the angle between z axis and the propagation direction of the incident waves from the source to the inclusion.

If $\phi = 0$, it denotes that our source is a backlight; if $\phi = \frac{\pi}{2}$, it shows that we have a sidelight source; if $\phi = \pi$, then we have a headlight source. With different ϕ, we have different resolution and stability results as Table 2:

1. *Resolution Derivation* In Known Source Case considering P scattering component only, with a backlight, the transverse radius is Rayleigh resolution and the longitudinal radius is infinity; with a sidelight, the transverse radius is harmonic sum resolution and the longitudinal radius is broadband resolution; with a headlight, the transverse radius is Rayleigh resolution and the longitudinal radius is broadband resolution. In Known Source Case considering S scattering component only, with a backlight, the transverse radius is Rayleigh resolution and the longitudinal radius is harmonic difference resolution; with a sidelight, the transverse radius is harmonic sum resolution and the longitudinal radius is broadband resolution; with a headlight, the transverse radius is Rayleigh resolution and the longitudinal radius is harmonic sum resolution. In the other three cases, the transverse radius is Rayleigh resolution and the longitudinal radius is harmonic difference resolution no matter how ϕ changes.

2. *Stability Analysis* In Known Source Case, SNR $\geq \frac{0.83T}{\tau}$, no matter considering P component only or S component only and also it holds for different ϕ. In Unknown Source Case, SNR $\geq \frac{T}{5\tau}$ holds for different ϕ. In Image Contribution of Incident Waves, with a backlight, SNR $\sim e^{\frac{h^2}{2\tilde{l}\lambda_p}} H(\Delta x, \Delta z) \leq e^{\frac{h^2}{2\tilde{l}\lambda_p}}$; with a sidelight, SNR $\sim e^{\frac{h}{\lambda_p}} H(\Delta x, \Delta z) \leq e^{\frac{h}{\lambda_p}}$; with a headlight, SNR $\sim e^{\frac{2h}{\lambda_p}} H(\Delta x, \Delta z) \leq e^{\frac{2h}{\lambda_p}}$. Because we know that $H(\Delta x, \Delta z) = A^{-1} \int_{-A/2}^{A/2} e^{-\frac{|\Delta z + \Delta x(a/h)|}{\lambda_{p,s}}} da$ and $1 = H(0,0) = \max H(\Delta x, \Delta z)$. In addition, with a sidelight or headlight, SNR is much larger than that with a backlight in this case. In Unknown Pulse Source Case, with a backlight, SNR $\sim A^{-1}C^{-1}(\frac{h^2}{2\tilde{l}lc_p})E[I]$; with a sidelight, SNR $\sim A^{-1}C^{-1}(\frac{-h}{lc_p})E[I]$; with a headlight, SNR $\sim A^{-1}C^{-1}(\frac{-2h}{lc_p})E[I]$. Additively, with a sidelight or headlight, SNR is much larger than that with a backlight.

In Table 3, it shows the results in true values, where $c_p = 6$km/s, $c_s = 4$km/s, $\lambda_p = 0.15$km, $\lambda_p = 0.1$km, $h = 50$km, $A = 0.1$km, $\tilde{l} = 100$km, $T = 100$s, $\tau = 5$s, $\omega_0 = 10$, $t_0 = 100$, and $l = 0.01$km. In Figure 7.1, it shows the coeffient of SNR in Pulse Source case, that is, when $|\Delta t|$ is larger and larger, the coeffient $A^{-1}C^{-1}(\Delta t)$ will have a very large absolute value.

Table 7.1: Main Results in Different Cases

Cases	Resolution		Stability
	Transverse Radius	Longitudinal Radius	
Known Source	P: $\frac{\lambda_p}{\frac{A}{h}+\sin\phi}$	$\frac{\lambda_p}{\sqrt{2-2\cos\phi}}$	SNR $\geq \frac{0.83T}{\tau}$
	S: $\frac{1}{\frac{A}{h\lambda_s}+\frac{\sin\phi}{\lambda_p}}$	$\frac{\sqrt{\left(\frac{\sin\phi}{\frac{A\lambda_p}{h\lambda_s}+\sin\phi}\right)^2+1}}{\frac{1}{\lambda_s}-\frac{\cos\phi}{\lambda_p}}$	
Unknown Source	$\frac{h\bar{\lambda}_{p,s}}{A}$	$\bar{\lambda}_{p,s}$	SNR $\geq \frac{T}{5\tau}$
ICIW[a]	$\frac{h\bar{\lambda}_{p,s}}{A}$	$\bar{\lambda}_{p,s}$	SNR $\gg 1$
Pulse Source	$\frac{h\bar{\lambda}_{p,s}}{A}$	$\bar{\lambda}_{p,s}$	SNR $\gg 1$

[a] ICIW denotes image contribution of incident waves.

Table 7.2: Main Results in Different ϕ

Cases			Resolution		Stability
			Transverse	Longitudinal	
Known Source	P	$\phi = 0$	$\frac{\lambda_p h}{A}$	∞	SNR $\geq \frac{0.83T}{\tau}$
		$\phi = \frac{\pi}{2}$	$\frac{\lambda_p}{\frac{A}{h}+1}$	$\frac{\lambda_p}{\sqrt{2}}$	
		$\phi = \pi$	$\frac{\lambda_p h}{A}$	$\frac{\lambda_p}{2}$	
	S	$\phi = 0$	$\frac{\lambda_s h}{A}$	$\bar{\lambda}_{p,s}$	
		$\phi = \frac{\pi}{2}$	$\frac{h\lambda_s}{\frac{A}{h\lambda_s}+\frac{1}{\lambda_p}}$	$\frac{\sqrt{(\frac{1}{\frac{A\lambda_p}{h\lambda_s}+1})^2+1}}{\frac{1}{\lambda_s}}$	
		$\phi = \pi$	$\frac{\lambda_s h}{A}$	$\frac{\sqrt{(\frac{1}{\frac{A\lambda_p}{h\lambda_s}+1})^2+1}}{\frac{1}{\lambda_s}}$	
Unknown Source		$\phi = 0$	$\frac{h\bar{\lambda}_{p,s}}{A}$	$\bar{\lambda}_{p,s}$	SNR $\geq \frac{T}{5\tau}$
		$\phi = \frac{\pi}{2}$			
		$\phi = \pi$			
ICIW[a]		$\phi = 0$	$\frac{h\bar{\lambda}_{p,s}}{A}$	$\bar{\lambda}_{p,s}$	SNR $\sim e^{\frac{h^2}{2l\lambda_p}} H(\Delta x, \Delta z)$
		$\phi = \frac{\pi}{2}$			SNR $\sim e^{\frac{h}{\lambda_p}} H(\Delta x, \Delta z)$
		$\phi = \pi$			SNR $\sim e^{\frac{2h}{\lambda_p}} H(\Delta x, \Delta z)$
Pulse Source		$\phi = 0$	$\frac{h\bar{\lambda}_{p,s}}{A}$	$\bar{\lambda}_{p,s}$	SNR $\sim A^{-1}C^{-1}(\frac{h^2}{2\bar{l}lc_p})E[I]$
		$\phi = \frac{\pi}{2}$			SNR $\sim A^{-1}C^{-1}(\frac{-h}{lc_p})E[I]$
		$\phi = \pi$			SNR $\sim A^{-1}C^{-1}(\frac{-2h}{lc_p})E[I]$

[a] ICIW denotes image contribution of incident waves.

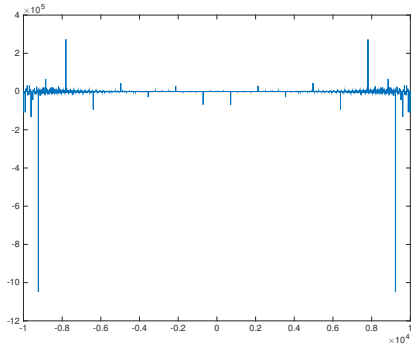

Figure 7.1: The Coefficients of SNR in Pulse Source Case with True Values

Table 7.3: Main Results in True Values

Cases			Resolution		Stability
			Trans.	Long.	
Known Source	P	$\phi = 0$	75	∞	SNR ≥ 16.6
		$\phi = \frac{\pi}{2}$	0.150	0.106	
		$\phi = \pi$	75	0.075	
	S	$\phi = 0$	50	0.3	
		$\phi = \frac{\pi}{2}$	0.150	0.141	
		$\phi = \pi$	50	0.06	
Unknown Source		$\phi = 0$	150	0.3	SNR ≥ 4
		$\phi = \frac{\pi}{2}$			
		$\phi = \pi$			
ICIW[a]		$\phi = 0$	150	0.3	SNR $\gg 1$
		$\phi = \frac{\pi}{2}$			
		$\phi = \pi$			
Pulse Source		$\phi = 0$	150	0.3	SNR $\sim 33\|E[I]\|$
		$\phi = \frac{\pi}{2}$			SNR $\sim 1.36 \times 10^9 \|E[I]\|$
		$\phi = \pi$			SNR $\sim 1.67 \times 10^{31} \|E[I]\|$

[a] ICIW denotes image contribution of incident waves.

Bibliography

[1] J. P. Fouque, J. Garnier, G. Papanicolaou, and K. Solna, *Wave Propagation and Time Reversal in Randomly Layered Media*, Stochastic Modelling and Applied Probability, 56, Springer, New York, 2007.

[2] V. A. Korneev and L. R. Johnson, *Scattering of P and S Waves by a Spherically Symmetric Inclusion*, Pure and applied geophysics, 1996, 147(4): pp. 675-718.

[3] J. Garnier, *Sensor Array Imaging in a Noisy Environment*, NIMS Lecture Note Series TP1003, National Institute for Mathematical Sciences, South Korea, 2010.

[4] J. Garnier and G. Papanicolaou, *Passive Sensor Imaging Using Cross Correlations of Noisy Signals in a Scattering Medium*, SIAM Journal on Imaging Sciences, 2009, 2(2): pp. 396-437.

[5] I.S.Reed, *On a Monent Theorem for Complex Gaussian Processes*, IRE Transactions on Information Theory, 1962, 3(8): pp. 194-195.

[6] T. L. Duvall Jr, S. M. Jefferies, J. W. Harvey, and M. A. Pomerantz, *Timedistance helioseismology*, Nature, 362 (1993), pp. 430-432.

[7] J. Rickett and J. Claerbout, *Acoustic daylight imaging via spectral factorization: Helioseismology and reservoir monitoring*, The leading edge, 1999, 18(8): 957-960.

[8] G. T. Schuster, J. Yu, J. Sheng, and J. Rickett, *Interferometric/daylight seismic imaging*, Geophysical Journal International, 2004, 157(2): 838-852.

[9] E. Larose, L. Margerin, A. Derode, B. Van Tiggelen, M. Campillo, N. Shapiro, A. Paul, L. Stehly, and M. Tanter, *Correlation of random wave fields: an interdisciplinary review*, Geophysics, 71 (2006), pp. SI11-SI21.

[10] P. Goue dard, L. Stehly, F. Brenguier, M. Campillo, Y. Colin de Verdie're, E. Larose, L. Margerin, P. Roux, F. J. Sanchez-Sesma, N. M. Shapiro, and R. L. Weaver, *Cross-correlation of random fields: mathematical approach and applications*, Geophysical Prospecting, in press (2008).

[11] N. M. Shapiro, M. Campillo, L. Stehly, and M. H. Ritzwoller, *High-resolution surface wave tomography from ambient noise*, Science, 307 (2005), pp. 1615-1618.

[12] K. G. Sabra, P. Roux, P. Gerstoft, W. A. Kuperman, M. C . Fehler, *Extracting coherent coda arrivals from cross correlations of long period seismic waves during the Mount St Helens 2004 eruption*, Geophys. Res. Lett., 33 (2006), L06313.

[13] F. Brenguier, N. M. Shapiro, M. Campillo, V. Ferrazzini, Z. Duputel, O. Coutant, and A. Nercessian, *Towards forecasting volcanic eruptions using seismic noise*, Nature Geoscience, 1 (2008), pp. 126-130.

[14] F.Brenguier,N.M.Shapiro,M.Campillo,A.Nercessian,andV.Ferrazzini,3-Dsurface wave tomography of the Piton de la Fournaise volcano using seismic noise correlations, Geophys. Res. Lett., 34 (2007), L02305.

[15] A. Curtis, P. Gerstoft, H. Sato, R. Snieder, and K. Wapenaar, *Seismic interferometry - turning noise into signal*, The Leading Edge, 25 (2006), pp. 1082-1092.

[16] J.-P. Fouque, J. Garnier, G. Papanicolaou, and K. Sølna, *Wave propagation and time reversal in randomly layered media*, Springer, New York, 2007.

[17] P. Roux, K. G. Sabra, W. A. Kuperman, and A. Roux, *Ambient noise cross correlation in free space: Theoretical approach*, J. Acoust. Soc. Am., 117 (2005), pp. 79-84.

[18] G. Mie, *Contribution on the Optics of Cloudy Media*, Special Colloidal Metal Solutions, Ann. der Physik 25 (1908), pp. 377-445 (in German).

[19] H. C. Van der hulst, *Light Scattering by Small Particles*, Wiley, New York 1957, pp.470

[20] C. F. Ying and R.Truell, *Scattering of a Plane Longitudinal Wave by a Spherical Obstacle in an Isotropically Elastic Solid*, J. Appl. Phys. 27, 1956, pp. 1086-1097.

[21] U. K. Nigul et al., *Echo-signals from Elastic Objects*, Academy of Science of Estonian SSR, 1974, pp. 345 (in Russian).

[22] V. S. Morochnik, *Scattering of Shear Elastic Waves by a Low-contrast Spherical Inclusion*, Izvestia Acad. Nauk USSR, Fizika Zemli 6, 1983, pp. 41-49 (in Russian).

[23] G. I. Petrashen, *Methods of Investigation of Wave Propagation in Media with Spherical and Cylindrical Boundaries*, Scientific Papers of Leningrad State University, Series in Mathematical Sciences, 1953, 170 (27) (in Russian).

[24] V. A. Korneev, and G. I. Petrashen, *Calculation of Diffraction Wave Fields Formed on an Elastic Sphere*, Problems of Dynamic Theory of Seismic Wave Propagation 27, 1987, pp. 26-44.

[25] V. A. Korneev and L. R. Johnson, *Scattering of Elastic Waves by a Spherical Inclusion – 1. Theory and Numerical Results*, Geophys. J. Int., 115(1993), pp. 230-250.

[26] V. A. Korneev andL. R. Johnson, *Scattering of Elastic Waves by a Spherical Inclusion– 2. Limitations of Asymptotic Solutions*, Geophys. J. Int. 115 (1993), pp. 251-263.

[27] J. Garnier, G.Papanicolaou *Resolution analysis for imaging with noise*, Inverse Problems, 2010, 26(7): 074001.

Appendices

A Introduction to Elastic Wave Equation

A.1 Motivation

Elastic wave equation has been widely used to describe wave propagation in an elastic medium, such as seismic waves in Earth and ultrasonic waves in human body. Seismic waves are waves of energy that travel through the earth, and are a result of an earthquake, explosion, or a volcano.

A.2 Elastic Wave Equation

The standard form for seismic elastic wave equation in homogeneous medium is :

$$\rho u_{tt} = (\lambda + 2\mu)\nabla\nabla \cdot u - \mu\nabla \times \nabla \times u,$$

where ρ is the density,u is the displacement for the wave, and λ,μ are Lame parameters.

We will make use of Newton's second law $F = ma$, where the mass $m = \rho dx_1 dx_2 dx_3$ and the acceleration $a = u_{tt} = \frac{\partial^2 u}{\partial t^2}$. The total force from stress field is

$$F = F_i + F_i^{body},$$

where $F_i^{body} = f_i dx_1 dx_2 dx_3$ and $F_i = \Sigma \frac{\partial \tau_{ij}}{\partial x_j} dx_1 dx_2 dx_3 = \partial_j \tau_{ij} dx_1 dx_2 dx_3$. Combining the

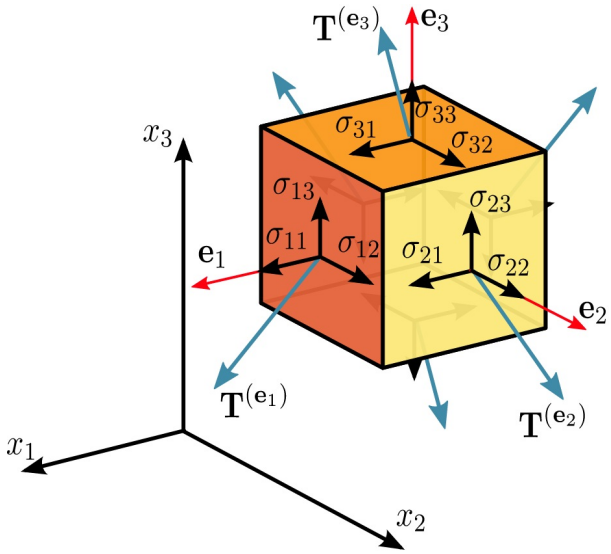

Components of Stress in Three Dimensions.

above equations, we can get the Momentum equation:

$$\rho \frac{\partial^2 u}{\partial t^2} = \frac{\partial \tau_{ij}}{\partial x_j} + f_i,$$

where τ is the stress tensor.

Definition of Stress: A measure of the internal forces acting within a deformable body. The stress at any point n an object, assumed to behave as a contimuum, is completely defined by nine component stresses: three orthogonal normal stresses and six orthognonal shear stresses. The stress tensor τ_{ij} is the Cauchy stress tensor which is a second order tensor of a linear map with nine components τ_{ij} that completely define the state of stress at a point inside a material in the deformed placement or configuration. The tensor relates a unit-length direction vector $\mathbf{n}$ to the stress vector $\mathbf{T}^{(\mathbf{n})}$ across an imaginary surface perpendicular to $\mathbf{n}$:

$$\tau = \begin{bmatrix} \tau_{11} & \tau_{12} & \tau_{13} \\ \tau_{21} & \tau_{22} & \tau_{23} \\ \tau_{31} & \tau_{32} & \tau_{33} \end{bmatrix} = \begin{bmatrix} \tau_{xx} & \tau_{xy} & \tau_{xz} \\ \tau_{yx} & \tau_{yy} & \tau_{yz} \\ \tau_{zx} & \tau_{zy} & \tau_{zz} \end{bmatrix}.$$

Definition of Strain: A local measure of relative change in the displacement field, that

is, the spatial gradients in the displacement field. Also, it related to deformation, or change in shape, of a material rather than any change in position:

$$\mathbf{e}_{ij} = \frac{1}{2}(\partial_i u_j + \partial_j u_i) = \begin{bmatrix} \frac{\partial u_1}{\partial x_1} & \frac{1}{2}(\frac{\partial u_1}{\partial x_2} + \frac{\partial u_2}{\partial x_1}) & \frac{1}{2}(\frac{\partial u_1}{\partial x_3} + \frac{\partial u_3}{\partial x_1}) \\ \frac{1}{2}(\frac{\partial u_2}{\partial x_2} + \frac{\partial u_1}{\partial x_2}) & \frac{\partial u_2}{\partial x_2} & \frac{1}{2}(\frac{\partial u_2}{\partial x_3} + \frac{\partial u_3}{\partial x_2}) \\ \frac{1}{2}(\frac{\partial u_1}{\partial x_2} + \frac{\partial u_2}{\partial x_1}) & \frac{1}{2}(\frac{\partial u_3}{\partial x_1} + \frac{\partial u_1}{\partial x_3}) & \frac{\partial u_3}{\partial x_3} \end{bmatrix}.$$

Stress and Strain are linked in elastic media by Stress-Strain or constitutive relationship. The most general linear relationship between Stress and Strain is :

$$\tau_{ij} = C_{ijkl}\mathbf{e}_{kl},$$

where $\mathbf{C}$ denotes the stiffness (or elastic coefficient), and C_{ijkl} is termed the elastic tensor.

A.3 The Seismic Wave Equation in Isotropic Medium

The material is isotropic if the properties of the solid are the same in all directions. In isotropic medium, the number of the independent parameters is reduced to two:

$$C_{ijkl} = \lambda\delta_{ij}\delta_{kl} + \mu(\delta_{il}\delta_{jk} + \delta_{ik}\delta_{jl}),$$

where λ and μ are called the Lame parameters; $\delta_{ij} = 1$ for $i = j$, $\delta_{ij} = 0$ otherwise; $\mu = \frac{\tau_{xy}}{2\mathbf{e}_{xy}}$. The stress-stain equation for an isotropic medium:

$$\tau_{ij} = \lambda\delta_{ij}\mathbf{e}_{kk} + 2\mu e_{ij} = \lambda\delta_{ij}\partial_k u_k + \mu(\partial_i u_j + \partial_j u_i).$$

Substituting the above equations in the homogeneous equation of motion:

$$\begin{aligned} \rho u_{tt} =& \partial_j[\lambda\delta_{ij}\partial_k u_k + \mu(\partial_i u_j + \partial_j u_i)] \\ =& \partial_i\lambda\partial_k u_k + \lambda\partial_i\partial_k u_k + \partial_j\mu(\partial_i u_j + \partial_j u_i) + \mu\partial_j\partial_i u_j + \mu\partial_j\partial_j u_i \\ =& \partial_i\lambda\partial_k u_k + \partial_j\mu(\partial_i u_j + \partial_j u_i) + \lambda\partial_i\partial_k u_k + \mu\partial_i\partial_j u_j + \mu\partial_j\partial_j u_i. \end{aligned}$$

Thus, we can get

$$\rho u_{tt} = \nabla\lambda(\nabla \cdot u) + \nabla\mu \cdot [\nabla u + (\nabla u)^T] + (\lambda + \mu)\nabla\nabla \cdot u + \mu\nabla^2 u.$$

By using $\nabla^2 u = \nabla\nabla \cdot u - \nabla \times \nabla \times u$, we can get

$$\rho u_{tt} = \nabla\lambda(\nabla \cdot u) + \nabla\mu \cdot [\nabla u + (\nabla u)^T] + (\lambda + 2\mu)\nabla\nabla \cdot u - \nabla \times \nabla \times u.$$

The first two terms on the involve gradient in the Lame parameters and are non-zero whenever the material is inhomogeneous. Including these factors makes the equations very complicated and difficult to solve efficiently. If velocity is only a function of depth, then the material can be modeled as a series of homogeneous layers. Within each layer, there are no gradients in the Lames parameters and so these terms go to zero. The standard form for seismic wave equation in homogeneous medium is:

$$\rho u_{tt} = (\lambda + 2\mu)\nabla\nabla \cdot u - \nabla \times \nabla \times u.$$

If ρ, λ and μ are constants, the wave equation is simplified as:

$$u_{tt} = \alpha^2\nabla\nabla \cdot u - \beta^2\nabla \times \nabla \times u,$$

where the P wave velocity $\alpha = \sqrt{\frac{\lambda+2\mu}{\rho}}$ and the S wave velocity $\beta = \sqrt{\frac{\mu}{\rho}}$.

B Model Assumptions

In our model, the typical wavelength of the propagating pulse λ_0 is comparable to the propagation distance L, while the size l of the layers is small(Here, the radius of the inclusion R is small). The typical wavelength is taken to be the pulse width times a reference propagation speed. In this homogenization regime, propagation in a random medium is asymptotically equivalent to propagation in a homogeneous effective medium obtained by averaging the density and the reciprocal of the bulk modulus. In many applications the propagation dis-

tance is large compared with the size of the pulse, and wave fluctuations build up behind it as it travels deep into the random medium. In order to model this regime, we take the propagation distance L to be lage compared to the typical wavelength λ_0, and the typical layer size l small compared to λ_0,

$$l \ll \lambda_0 \ll L.$$

In our model, that is,

$$R \ll \lambda_0 \ll \tilde{l},$$

where, $\tilde{l}$ is the distance between source and inclusion.

We refer to this scaling as the high-frequency white-noise regime. It is a particularly interesting one becuse it is a high-frequency regime with respect to the large-scae variations of the medium, $L/\lambda_0 \gg 1$, but it is a low-frequency regime with respect to the small-scale random fluctuations, $l/\lambda_0 \ll 1$. As a result, the effect of the random fluctuations takes a canonical form the white-noise regime is one of the scaling regimes that have remarkably complete asymptotic theory.

C Probabilistic Tools

C.1 The Law of Large Numbers

In probability theory, the law of large numbers (LLN) is a theorem that describes the result of performing the same experiment a large number of times. According to the law, the average of the results obtained from a large number of trials should be close to the expected value, and will tend to become closer as more trials are performed.

Two different versions of the law of large numbers are described below; they are called the strong law of large numbers, and the weak law of large numbers. Both versions of the law state that with virtual certainty the sample average $\overline{X}_n = \frac{1}{n}(X_1 + \cdots + X_n)$, converges to the expected value $\overline{X}_n \to \mu = E(X)$ for $n \to \infty$, where X_1, X_2, ... is an infinite sequence of i.i.d. Lebesgue integrable random variables with expected value $E(X_1) = E(X2) = \cdots = E(X) = \mu$. Lebesgue integrability of X_j means that the expected

value$E(X_j)$ exists according to Lebesgue integration and is finite.

An assumption of finite variance $Var(X_1) = Var(X_2) = ... = \sigma^2 < \infty$ is not necessary. Large or infinite variance will make the convergence slower, but the LLN holds anyway. This assumption is often used because it makes the proofs easier and shorter.

Weak Law

Simulation illustrating the law of large numbers. Each frame, you flip a coin that is red on one side and blue on the other, and put a dot in the corresponding column. A pie chart shows the proportion of red and blue so far. Notice that the proportion varies a lot at first, but gradually approaches 50%. The weak law of large numbers (also called Khintchine's law) states that the sample average converges in probability towards the expected value $\overline{X}_n \xrightarrow{P} \mu$ when $n \to \infty$. That is to say that for any positive number ϵ,

$$\lim_{n\to\infty} \Pr\big(|\overline{X}_n - \mu| > \varepsilon \big) = 0.$$

Interpreting this result, the weak law essentially states that for any nonzero margin specified, no matter how small, with a sufficiently large sample there will be a very high probability that the average of the observations will be close to the expected value; that is, within the margin.

Strong Law

The strong law of large numbers states that the sample average converges almost surely to the expected value $\overline{X}_n \xrightarrow{a.s.} \mu$ when $n \to \infty$. That is,

$$\Pr\Big(\lim_{n\to\infty} \overline{X}_n = \mu \Big) = 1.$$

The proof is more complex than that of the weak law. This law justifies the intuitive interpretation of the expected value of a random variable when sampled repeatedly as the "long-term average". Almost sure convergence is also called strong convergence of random variables. This version is called the strong law because random variables which converge strongly (almost surely) are guaranteed to converge weakly (in probability). The strong law implies the weak law. The strong law of large numbers can itself be seen as a special case of the pointwise ergodic theorem. Moreover, if the summands are independent but not

identically distributed, then

$$\overline{X}_n - \mathrm{E}\left[\overline{X}_n\right] \xrightarrow{a.s.} 0,$$

provided that each X_k has a finite second moment and

$$\sum_{k=1}^{\infty} \frac{1}{k^2} \mathrm{Var}[X_k] < \infty.$$

This statement is known as Kolmogorov's strong law, see e.g. Sen & Singer (1993, Theorem 2.3.10).

D The Cross Correlation

In signal processing, cross-correlation is a measure of similarity of two waveforms as a function of a time-lag applied to one of them. This is also known as a sliding dot product or sliding inner-product. It is commonly used for searching a long signal for a shorter, known feature. It has applications in pattern recognition, single particle analysis, electron tomographic, averaging, cryptanalysis, and neurophysiology.

D.1 Wave cross correlations in a homogeneous medium with random sources

Let $u(t, \mathbf{x}_1)$ and $u(t, \mathbf{x}_2)$ denote the time-dependent wave fields recorded by two sensors at $\mathbf{x}_1$ and $\mathbf{x}_2$. Their cross correlation function over the time interval $[0, T]$ with time lag τ is given by

$$C_T(\tau, \mathbf{x}_1, \mathbf{x}_2) = \frac{1}{T} \int_0^T u(t, \mathbf{x}_1) u(t + \tau, \mathbf{x}_2) dt.$$

In a homogeneous medium, if the source of the waves is a space-time stationary random field that is also delta correlated in space and time,

$$\frac{\partial}{\partial \tau} C_T(\tau, \mathbf{x}_1, \mathbf{x}_2) \simeq -[G(\tau, \mathbf{x}_1, \mathbf{x}_2) - G(-\tau, \mathbf{x}_1, \mathbf{x}_2)],$$

where G is the Green's function. This approximate equality holds for T sufficiently large and provided some limiting absorption is introduced to regularize the integral. The main point here is that the time-symmetrized Greens function can be obtained from the cross correlation if there is enough source diversity. In this case the wave field at any sensor is equipartitioned, in the sense that it is a superposition of uncorrelated plane waves of all directions. We can recover in particular the travel time $\tau(\mathbf{x}_1, \mathbf{x}_2)$ from the singular support of the cross correlation.

D.2 Wave cross correlations in a scattering medium

In the case of a spatially localized distribution of noise sources, directional diversity of the recorded fields can be enhanced if there is sufficient scattering in the medium. An ergodic cavity with a homogeneous interior is a good example: Even with a source distribution that has very limited spatial support, the reverberations of the waves in the cavity generate interior fields with high directional diversity. Multiple scattering of waves by random inhomogeneities can also lead to wave field equipartition if the transport mean free path is short compared to the distance from the sources to the sensors. The transport mean free path is the propagation distance over which wave energy transport in a scattering medium is effectively isotropic. In such a scattering medium, the inhomogeneities can be viewed as secondary sources in the vicinity of the sensors.

If in a random medium the transport mean free path is short compared to the distance between the sensors, then the cross correlation function still gives an estimate of the Green's function, which is itself random because of the medium. However, its coherent part that has information about the travel time is essentially unobservable. The travel time can be estimated in a random medium when the noise sources are spatially limited provided that (i) the transport mean free path is short compared to the distance between the sources and the sensors, and (ii) it is long compared to the distance between the sensors.

D.3 Extracting the Green's function from the cross correlation

The wave equation with noise sources. We consider the solution u of the wave equation in a d-dimensional inhomogeneous medium:

$$\frac{1}{c^2(\mathbf{x})}\frac{\partial^2 u}{\partial t^2} - \Delta_{\mathbf{x}} u = n^\epsilon(t, \mathbf{x}).$$

The term $n^\epsilon(t, \mathbf{x})$ models a random distribution of noise sources. It is a zero-mean stationary (in time) Gaussian process with autocorrelation function

$$< n^\epsilon(t_1, \mathbf{y}_1) n^\epsilon(t_2, \mathbf{y}_2) >= F^\epsilon(t_2 - t_1)\mathcal{T}(\mathbf{y}_1, \mathbf{y}_2).$$

Here, $< \cdot >$ stands for statistical average with respect to the distribution of the noise sources. The Gaussian property is assumed here so as to simplify the calculations of statistical stability. It could be replaced by a more general decorrelation or mixing property. We assume that the decoherence time of the noise sources is much smaller than typical travel times between sensors. If we denote with ϵ the ratio of these two time scales, we can then write the time correlation function F^ϵ in the form

$$F^\epsilon(t_2 - t_1) = F(\frac{t_2 - t_1}{\epsilon}),$$

where t_1 and t_2 are scaled relative to typical sensor travel times.

Statistical stability of the cross correlation function.

The stationary solution of the wave equation has the integral representation

$$\begin{aligned} u(t, \mathbf{x}) &= \int \int_{-\infty}^{t} n^\epsilon(s, \mathbf{y}) G(t - s, \mathbf{x}, \mathbf{y}) ds d\mathbf{y} \\ &= \int \int n^\epsilon(t - s, \mathbf{y}) G(s, \mathbf{x}, \mathbf{y}) ds d\mathbf{y}, \end{aligned}$$

where $G(t, \mathbf{x}, \mathbf{y})$ is the time-dependent Green's function. It is the fundamental solution of the wave equation.

$$\frac{1}{c^2(\mathbf{x})}\frac{\partial^2 G}{\partial t^2} - \Delta_{\mathbf{x}} G = \delta(t)\delta(\mathbf{x} - \mathbf{y}),$$

starting from $G(0, \mathbf{x}, \mathbf{y}) = \partial_t G(0, \mathbf{x}, \mathbf{y}) = 0$.

The empirical cross correlation of the signals recorded at $\mathbf{x}_1$ and $\mathbf{x}_2$ for an integration time T is

$$C_T(\tau, \mathbf{x}_1, \mathbf{x}_2) = \frac{1}{T} \int_0^T u(t, \mathbf{x}_1) u(t + \tau, \mathbf{x}_2) dt.$$

It is a statistically stable quantity, in the sense that for a large integration time T, C_T is independent of the realization of the noise sources.

Proposition: (a) The expectation of C_T (with respect to the distribution of the sources) is independent of T:

$$< C_T(\tau, \mathbf{x}_1, \mathbf{x}_2) >= C^{(1)}(\tau, \mathbf{x}_1, \mathbf{x}_2)$$

where $C^{(1)}$ is given by

$$C^{(1)}(\tau, \mathbf{x}_1, \mathbf{x}_2) = \int dy \int ds ds' G(s, \mathbf{x}_1, \mathbf{y}) G(\tau + s + s', \mathbf{x}_2, \mathbf{y}) F^\epsilon(s') \theta(\mathbf{y}),$$

or equivalently by

$$C^{(1)}(\tau, \mathbf{x}_1, \mathbf{x}_2) = \frac{1}{2\pi} \int dy \int d\omega \bar{\hat{G}}(\omega, \mathbf{x}_1, \mathbf{y}) \hat{G}(\omega, \mathbf{x}_2, \mathbf{y}) \hat{F}^\epsilon(s') e^{-i\omega\tau} \theta(\mathbf{y}).$$

(b) The empirical cross correlation C_T is a self-averaging quantity:

$$C_T(\tau, \mathbf{x}_1, \mathbf{x}_2) \to C^{(1)}(\tau, \mathbf{x}_1, \mathbf{x}_2), \; as \, T \to \infty,$$

in probability with respect to the distribution of the sources. More precisely, the fluctuations of C_T around its mean value $C^{(1)}$ are of order $T^{-1/2}$ for T large compared to the decoherence

time of the sources. The covariance function of C_T is:

$$
\begin{aligned}
&Cov(C_T(\tau, \mathbf{x}_1, \mathbf{x}_2), C_T(\tau + \Delta\tau, \mathbf{x}_1, \mathbf{x}_2)) \\
&\frac{1}{T^2} \int_0^T \int_0^T dt dt' \int ds ds' du du' \int d\mathbf{y}_1 d\mathbf{y}_1^{'} d\mathbf{y}_2 d\mathbf{y}_2^{'} \\
&\times G(s, \mathbf{x}_1, \mathbf{y}_1) G(u - \tau, \mathbf{x}_1, \mathbf{y}_2) G(s', \mathbf{x}_2, \mathbf{y}_1^{'}) G(u' - \tau - \Delta\tau, \mathbf{x}_2, \mathbf{y}_2^{'}) \\
&\times (< n^{\epsilon}(t - s, \mathbf{y}_1) n^{\epsilon}(t - u, \mathbf{y}_2) n^{\epsilon}(t' - s', \mathbf{y}_1^{'}) n^{\epsilon}(t' - u', \mathbf{y}_2^{'}) > \\
&- < n^{\epsilon}(t - s, \mathbf{y}_1) n^{\epsilon}(t - u, \mathbf{y}_2) >< n^{\epsilon}(t' - s', \mathbf{y}_1^{'}) n^{\epsilon}(t' - u', \mathbf{y}_2^{'}) >).
\end{aligned}
$$